NOTICE

The quality of this microform is heavily dependent upon the quality of the original thesis submitted for microfilming. Every effort has been made to ensure the highest quality of reproduction possible.

If pages are missing, contact the university which granted the degree.

Some pages may have indistinct print especially if the original pages were typed with a poor typewriter ribbon or if the university sent us an inferior photocopy.

Previously copyrighted materials (journal articles, published tests, etc.) are not filmed.

Reproduction in full or in part of this microform is governed by the Canadian Copyright Act, R.S.C. 1970, c. C-30.

AVIS

La qualité de cette microforme dépend grandement de la qualité de la thèse soumise au microfilmage. Nous avons tout fait pour assurer une qualité supérieure de reproduction.

S'il manque des pages, veuillez communiquer avec l'université qui a conféré le grade.

La qualité d'impression de certaines pages peut laisser à désirer, surtout si les pages originales ont été dactylographiées à l'aide d'un ruban usé ou si l'université nous a fait parvenir une photocopie de qualité inférieure.

Les documents qui font déjà l'objet d'un droit d'auteur (articles de revue, tests publiés, etc.) ne sont pas microfilmés.

La reproduction, même partielle, de cette microforme est soumise à la Loi canadienne sur le droit d'auteur, SRC 1970, c. C-30.

Canada

A Pulse-Width Modulated Series Resonant Converter Operated at Resonant Frequency

Jean-Pierre Vandelac

A Thesis

in

The Department

of

Electrical and Computer Engineering

Presented in Partial Fulfillment of the Requirements
for the Degree of Master of Engineering (Electrical) at
Concordia University
Montréal, Québec, Canada

August 1988

ISBN 0-315-44862-8

ABSTRACT

Jean-Pierre Vandelac

Resonant DC-DC converters are usually operated in frequency modulation to achieve regulation. This has the disadvantage of wideband frequency modulation. In this thesis an alternate regulation scheme which employs fixed-frequency Pulse-Width Modulation (PWM) is proposed. This control scheme is applied to the series loaded series resonant converter.

Analysis shows that such a converter operated at the resonant frequency has two modes of operation depending on the load. The modes are characterized by continuous or discontinuous resonant inductor current. The converter can therefore be operated as a resonant or quasi-resonant converter. Quasi-resonance is emphasized as it presents low switching stresses. When operated in a full-bridge configuration and a variation of PWM that can be described as phase-shift modulation between the two sets of switches, the converter presents even lower switching stresses.

Analytical results include VA rating and stresses on critical active and passive components as a function of input voltage variation. Small-signal frequency response of the converter is also analyzed. A 200KHz, 700W, 48Vdc output, off line converter is realized using this concept and experimental results are presented to corroborate the analysis.

ACKNOWLEDGEMENTS

I would like to thank Professor P.D. Ziogas for supervising my work during these recent years. I would like also to thank Gary Rokas, my supervisor at my place of employment, for reviewing this thesis.

J'aimerais remercier mon confrère, Paul Cmikiewicz, pour son assiduité, manifestée à plus d'une occasion, à reviser ce texte. Je remercie aussi mes confrères, Daniel Sicard et Richard D'Ulisse ainsi que mon ami Robert Douville-Toupin pour leur assistance dans la mise en page finale de ce mémoire.

Enfin, je remercie tout particulièrement ma compagne, Claudette, pour sa patience durant ces derniers mois. Sa compréhension m'a permis de mener à bien cette entreprise.

TABLE OF CONTENTS

LIST OF FIGURES

LIST OF SYMBOLS

When two symbols appear left of a definition, in upper and lower cases, the upper case variable refers to the steady state solution and the lower case symbols refers to the perturbed variable.

Δa is the large signal perturbation of variable a. δa is the small signal perturbation of variable a (3.4.1-8).

$A(t), A_l$	: System matrix (3.2.0-1), (3.2.0-3).
$\overline{A}$	: Normalized area under the resonant current waveform. (2.2.0-8).
A_{lc}	: Area under the continuous resonant current waveform from t_l to t_{l+1}.
A_{ld}	: Area under the discontinuous resonant current waveform from t_l to t_{l+1}.
$A(s)$	: Error-amplifier transfer function (3.1.0-2)
$B(t), B_l$	: Input matrix (3.2.0-1), (3.2.0-3).
$C(t), C_l$	: Output matrix (3.2.0-2), (3.2.0-3).
C_r	: Resonant capacitor.
CR_l	: Rectifier diode number l.
C_o	: Output capacitor.
D	: Steady-state duty cycle.
D, d	: Pulse train at the output of the pulse-width modulator.
$D(t), D_l$	: Transmission matrix (3.2.0-2), (3.2.0-3).
D_l	: Anti-parallel diode number l.
f_o	: Resonant frequency.
f_s	: Switching frequency.
f_l^t	: Weighting factor for natural modulation (3.4.2-17), (3.4.2-23).
$G(s)$	: Converter transfer function.
$\overline{G(s)}$	: Normalized converter transfer function.
$\overline{I}$	: Normalized current (2.2.0-7).
I_{avg}	: Average current.
I_{co}	: Steady-state output capacitor current.
I_o	: Output current.

I_{pk}	: Peak current.
I_r	: Steady-state resonant current.
$\dot{i}_t$	: Derivative of the steady-state resonant current at t=t$_t$.
$\dot{I}_{\bar{t}}$	: Derivative of the steady-state resonant current at t=t$_{\bar{t}}$.
I_{str}	: Stress current. Rms, peak or average depending on the device.
k_d	: Pole scaling factor for discontinuous mode (3.6.0-6) and Figure.
K_{dc}	: Nomalized DC gain (3.6.0-5) and (3.6.0-7)
k_t	: Input transition matrix (3.4.2-1).
K_t	: State transition matrix (3.4.2-1).
K_{pwm}	: Pulse-width modulator gain.
L_r	: Resonant inductor or resonant inductor value.
M	: Voltage transfer ratio.
m	: mth half-cycle.
n	: nth cycle.
N_s	: Number of switched states.
P_{in}	: Input Power.
P_o	: Output power.
PWM(s)	: Pulse-width modulator transfer function. (3.1.0-4)
Q	: Load parameter (2.2.0-3).
$\bar{Q}$	: Normalized load parameter (2.2.0-4).
Q_{co}	: Output capacitor resistance factor (3.3.1-4)
Q_{rt}	: Resonant tank quality factor (3.3.1-3)
R, R_e, R_o	: State reconstruction equation, (3.5.3-11), (3.5.3-14).
R_c	: Output capacitor equivalent series resistance (esr).
R_ℓ	: Load resistance.
R_{rt}	: Resistance in series with the resonant tank.
R_y, R_{ye}, R_{yo}	: Output reconstruction equation, (3.5.0-1), (3.5.4-3), (3.5.4-4).
S	: Sample data-system equation (3.5.0-1)
S_t	: Switch number t.
SW_t	: Parallel combination of a unipolar switch and of a diode connected in the reverse direction(anti-parallel diode).
t	: time
$T_{d_{pwm}}$	: Pulse-width modulator delay.
T_h	: Half-cycle period.

t_ℓ	: Switching instant. Figures 2-2 and 2-4.
t_i, t_ℓ	: Sum of the T_i's up to i-1 or up to l-1 (3.5.3-9), (3.5.3-18).
T_i	: Period of the i^{th} switched-state.
t_{ofs}	: Sampling wave offset time, Figure A-1.
TR	: Main transformer.
T_s	: Sampling period.
$\bar{V}$	: Normalized voltage. (2.2.0-6)
VA	: Volt-Ampere stress product.
V_{ab}	: Load branch voltage. Figures 2-1 and 2-3.
V_{amp}, v_{amp}	: Voltage-error amplifier output voltage.
VA_{op}	: Volt-Ampere stress at a given operating point.
VA_{rat}	: Product of the worst voltage stress by the worst current stress over the range of operation points of a converter.
V_c, v_c	: Resonant capacitor voltage.
$V_{c_{max}}$	: Maximum steady-state resonant capacitor voltage.
V_g	: Gate voltage.
V_{in}	: Input voltage.
$V_{in_{low}}$	: Minimum input voltage at which regulation is theoretically achieved for a given V_o. Normalizing factor.
V_o, v_o	: Steady-state output voltage.
V-s	: Volt-seconds product.
V_{str}	: Voltage stress.
X, x	: State vector (3.3.1-11)
$\dot{X}_{\underline{t}}$	: Derivative of the steady-state vector at $t=t\underline{t}$ (3.4.2-6).
$\dot{X}_{\bar{t}}$	: Derivative of the steady-state vector at $t=t\bar{t}$ (3.4.2-7).
y	: Output vector.
Z_{co}	: Output capacitor impedance at ω_o (3.3.1-5).
$\bar{Z}_{co}$	: Normalized output capacitance impedance (3.3.1-5).
Z_o	: Resonant tank characteristic impedance. (2.1.1-2)
β	: Switching strategy factor.
Δi_{r_j}, δi_{r_j}	: Resonant current perturbation at start of the j^{th} switched state.
$\Delta \bar{i}_{r_j}$, $\delta \bar{i}_{r_j}$	: Resonant current perturbation at start of the j^{th} switched state.
δx^*	: Sampled state perturbation.

$\Delta x_j, \delta x_j$	: State perturbation at start of the j^{th} switched-state.
$\Delta \bar{x}_j, \delta \bar{x}_j$	: State perturbation at end of the j^{th} switched state.
Φ	: Magnetic flux.
Φ_l	: Switched-state transition matrix (3.4.2-2).
Φ_{fh}	: First half-cycle transition matrix (3.5.2-7).
Φ_{sh}	: Second half-cycle transition matrix (3.5.2-5).
λ	: Magnetic flux linkage.
τ_j	: Perturbed switching instant (3.4.1-6).
ω_{po}	: Second order pole angular frequency (3.6.0-2).
ω_{p1}	: First first order pole angular frequency (3.6.0-8).
ω_{p2}	: Second first order pole angular frequency (3.6.0-8).
ω_o	: Angular resonant frequency (2.1.1-3)
ω_s	: Angular switching frequency.

CHAPTER 1: INTRODUCTION

1.1 DC-DC SERIES RESONANT CONVERTER

In the continuing search for more "efficient" power conversion schemes, increasing attention is focused on resonant or quasi-resonant, [1], power supplies . Advantages often cited include low switching losses,. (which lead to higher switching frequencies), utilization of parasitic inductance as a circuit element and lower Electro-Magnetic Interference (EMI) levels, [2], [3]. Amongst the multitude of resonant topologies, the series resonant converter introduced by Schwarz [4] stands out as a high efficiency power supply topology.

This converter can be implemented in many different embodiments. Figure 1-1a) to to 1-1d) show four of these embodiments where full-wave rectification is assumed to be achieved by a centertap secondary winding. The converters in Figures 1-1b) and 1-1c) can easily be shown to be functionally equivalent to the converter of Figure 1-1a). The embodiment of Figure 1-1a) is therefore referred to as the half-bridge implementation of the converter and the embodiment of Figure 1-1d is referred to as the full-bridge implementation.

The half-bridge implementation of the converter is operated by alternately switching S_1 and S_2 at a 50% duty ratio as illustrated in Figure 1-2. This has the effect of impressing a square wave of amplitude V_{in} across the load branch, V_{ab}, of the converter. In the full-bridge implementation, S_4 and S_3 are respectively switched synchronously with S_1 and S_2. This also impresses a square wave of amplitude V_{in} across the load branch. Regulation of the output voltage is obtained by varying the frequency of the square wave. The period, T, on Figure 1-2 is varied.

In this thesis, attention is focused on the DC-DC application of the converter. Z_L, on Figure 1-1, is therefore assumed to be a full-wave

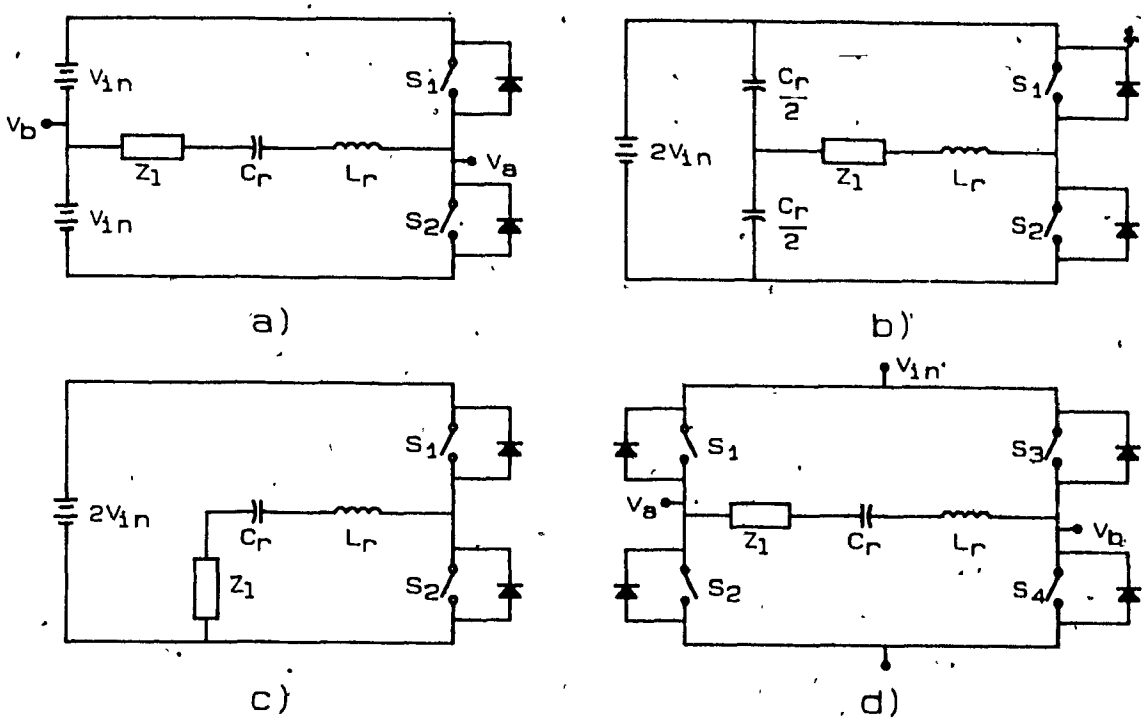

Figure 1-1: Series Resonant Converter
a) Half-bridge with split voltage input
b) Half-bridge with split resonant capacitor
c) Half-bridge with resonant capacitor DC offset
d) Full-bridge

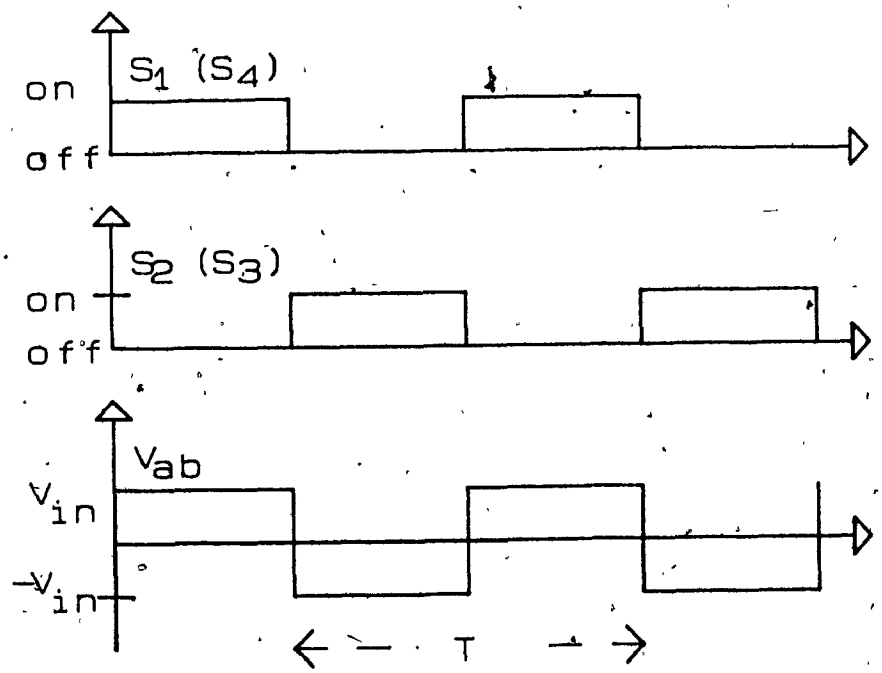

Figure 1-2: Frequency Modulation

rectifier feeding a filter capacitor in parallel with a resistive load. Frequency-modulation control of this DC-DC converter was well analyzed by Vorperian for both steady-state and small-signal behavior [5,6,7].

The current-source nature of the converter implies that the frequency band to achieve output voltage regulation over an appreciable range of loads is very large. If regulation over a wide range of input voltages is also desired, the frequency band is even larger. Therefore, optimization of the converter is difficult. For example, a series resonant converter operated above resonant frequency switches at very high frequency at low load and high input voltage. This puts severe constraints on the design of the output filter or the gate or base drive design. It also has been reported that frequency modulation control can be accompanied by entrainment problems [2]. For these reasons fixed-frequency operation may be desirable.

1.2 PULSE-WIDTH MODULATED DC-DC CONVERTERS

Half-bridge and full-bridge DC-DC converters are usually operated as "square-wave" converters. The half-bridge "square-wave" implementation is illustrated in Figure 1-3. S_1 and S_2 are switched in alternance to produce an AC voltage waveform. The voltage impressed across the primary of the transformer is rectified and filtered on the on the secondary. When S_1 or S_2 is turned on, a voltage of magnitude V_{in} is applied across the primary of the transformer. Energy is transferred from the source to the output filter inductance. During the off-time, when both S_1 or S_2 are off, the current of the output inductor shares equally between CR_1 and CR_2 and the voltage across the primary of the converter is clamped to zero. The resulting waveforms are shown in Figure 1-4. Full-bridge operation is very similar as S_4 is controlled simultaneously with S_1 and S_3 is controlled simultaneously with S_2. The commonly used term "square-wave" converter is attributed to the fact that both

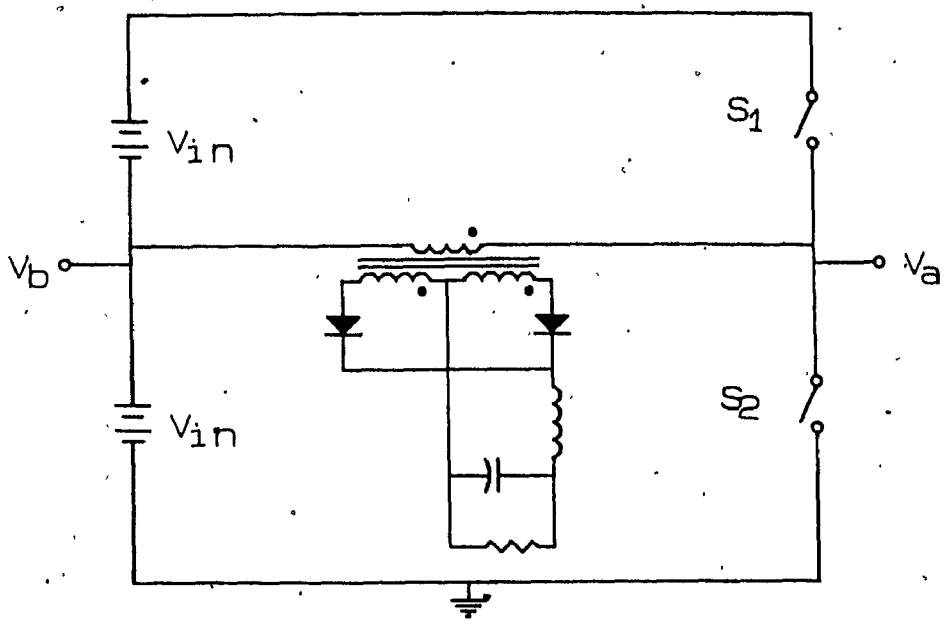

Figure 1-3: Half-bridge "Square-Wave" DC-DC converter.

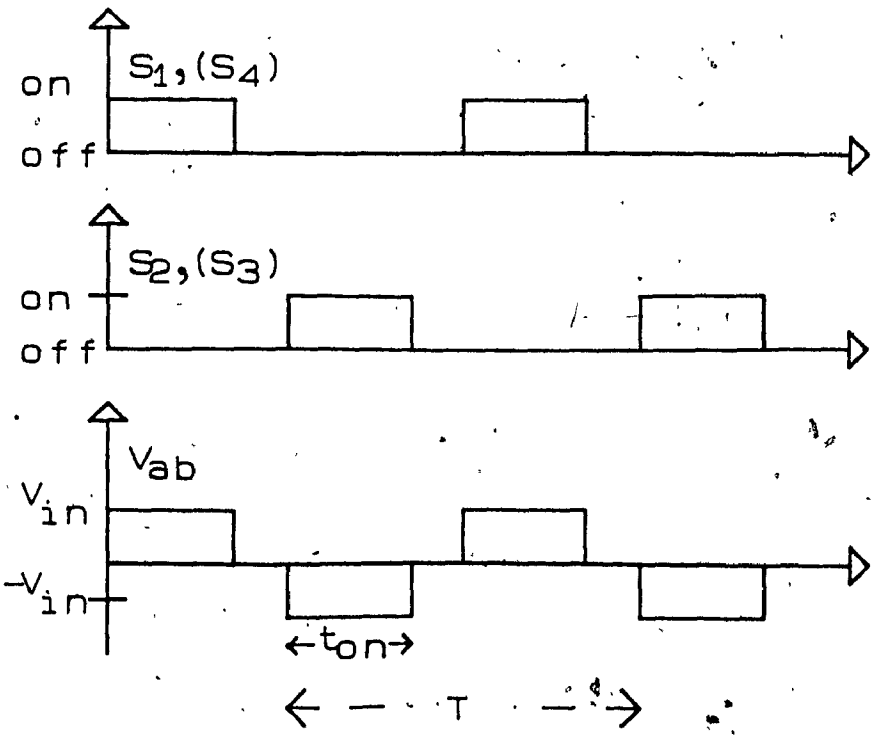

Figure 1-4: "Square-Wave" Pulse Width Modulation, PWM.

transformer current and voltage waveforms have sharp transitions or "square corners". As energy is transferred during the on-time of $S_1(S_4)$ or $S_2(S_3)$, the control of the output voltage is achieved by modulating t_{on} and by keeping a fixed period, T. This type of control scheme is referred to as fixed-frequency Pulse-Width Modulation (PWM).

In this thesis, the application of the PWM technique to the Series Resonant Converter is investigated. PWM applied to resonant converters has been known for some time, however, publications on this subject are very limited, [2], [8]. When the resonant converter is operated with a PWM control scheme, an important distinction is made between the half-bridge implementation, illustrated in Figure 1-1a), and the full-bridge implementation of Figure 1-1d). The distinction arises from the greater flexibility in the sequence the switches can be turned on and off in the full-bridge. Two possible switching strategies have been identified and are now described.

In the first strategy, the switches of the half-bridge are used in the same way as in the "square-wave" PWM converter described above. Specifically, S1 and S2 are turned on alternately, at a fixed frequency, for a controllable equal amount of time. The full-bridge implementation of the converter is functionally equivalent to the half-bridge version if S_1 and S_4 are turned on and off simultaneously and so are S_2 and S_3 as indicated in brackets in Figure 1-4.

The second switching strategy applies to the full-bridge configuration only. In this strategy the equivalent of the on-time, t_{on}, is also achieved by turning on two diagonally opposing switches (S_1 and S_4 or S_3 and S_2). The difference lies in the mechanism through which the off-time is achieved. During the off-time the load branch is clamped through two transversely opposing switches (S_1 and S_3 or S_2 and S_4). This results in the operation of S_1 and S_2 at fixed frequency and 50% duty ratio. S_3 and S_4 are operated similarly. The pulse width modulation is achieved by shifting the S_1, $\overline{S_2}$, gating signal with respect to the S_3, $\overline{S_4}$ gating signal. The switches timing diagram and

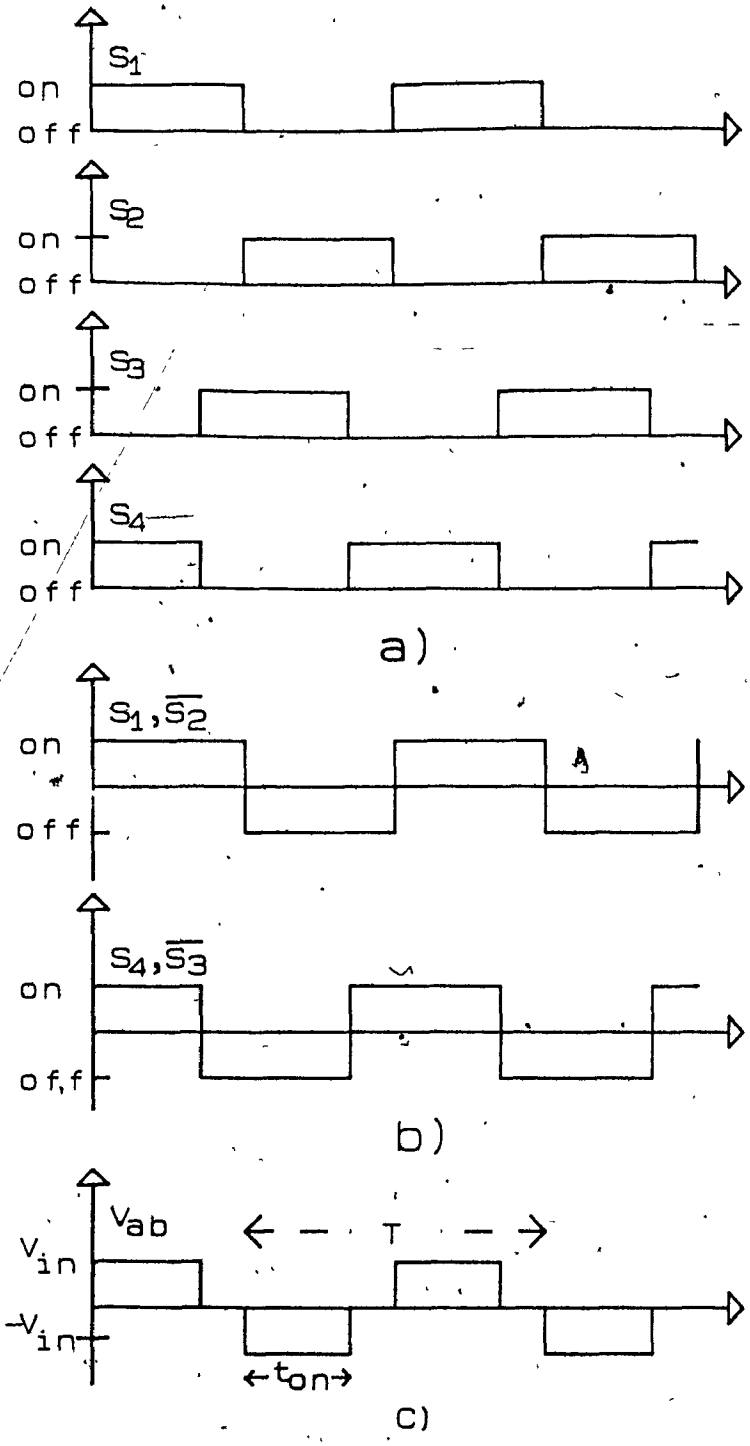

Figure 1-5: Phase Shift Pulse Width Modulation.
a) Switch sequencing
b) Gating Signals
c) Load branch voltage

the waveform resulting across the load branch, V_{ab}, are illustrated in Figure 1-5. Note the similarity of the load branch voltage with the transformer voltage of Figure 1-4.

Since, in the second switching strategy, the Pulse-Width Modulation is achieved by shifting the relative phase of two square-wave signals, this control scheme is referred to as Phase-Shift Pulse-Width Modulation (PSPWM). PSPWM is not specific to the control of the series resonant converter and is commonly used in inverter applications [9].

1.3 OPERATING FREQUENCY.

The converter is to be operated with fixed-frequency pulse-width modulation. The switching frequency can be arbitrarily set, and studies over a range of frequencies could therefore be carried out. To limit the scope of the thesis, the analysis is performed at a single switching frequency. The rationale for the selection of the switching frequency is now exposed.

It can be seen from Figure 1-5, that when t_{on} is equal to T/2, operation in PSPWM at a given frequency, is identical to the operation in frequency modulation depicted in Figure 1-2 for the same switching frequency. This is also true for PWM operation of the converter. Conclusions applicable to PWM or PSPWM operation can therefore be drawn from frequency modulation operation of the converter.

When the frequency-modulated converter is operated below resonance, the switches are naturally commutated. This is very advantageous when SCR's are used in low frequency (below 50Khz) application. However, at turn-on, the switches must commutate large currents and the parasitic capacitance of the switches are also discharged through the switches themselves. These characteristics are not very attractive. Although unimportant at low frequency, losses from parasitic capacitance discharge becomes significant at high frequency (above

50Khz) and become dominant at very high frequency (above 500Khz). In this thesis, emphasis is put on operation at high frequency. Operation at a frequency below resonant frequency is therefore not considered.

It has been reported in [3], that operation of the converter above resonant frequency yields zero-voltage switching. Zero-voltage switching, [10], is characterized as follows. The switch turns on while an anti-parallel diode carries the current in the reverse direction. The turn-on occurs with zero voltage across the switch. At turn-off the switch is rapidly turned off, while a small capacitor placed in parallel with the switch is charged by the resonant current. The resulting voltage across the switch is low during its extinction. With the availability of fast switching devices such as MOSFET's, operation above resonant frequency is therefore attractive.

As attractive as operation above resonant frequency may look, it has to be underlined that to retain zero voltage switching at all duty cycles, the operating frequency would have to be selected much above the resonant frequency. This can be seen as follows. Consider the V_{ab} on Figure 1-5 and picture its fundamental component. It is seen that the current would have to lag by a large angle for the current to be negative (or positive) at the switching instant where V_{ab} reaches V_{in} (or $-V_{in}$). Keeping this in mind two facts are underlined.

The voltage transfer ratio of the resonant converter operated in frequency modulation above resonant frequency is shown in Figure 1-6 as a function of the ratio of the switching frequency, f_s, to the resonant frequency f_o. A family of curves is given with Q as a parameter, where Q is defined as the ratio of the LC tank characteristic impedance to the load resistance. It is seen that at a given frequency, the voltage transfer ratio is dependant on the load. For example, at $f_s/f_o = 1.2$, the transfer ratio is equal to 0.22 for Q=10 and is equal to 0.72 for Q=2. With pulse-width modulation operation, these conversion ratios would therefore correspond to the maximum voltage transfer ratios (at maximum duty cycle) for these two

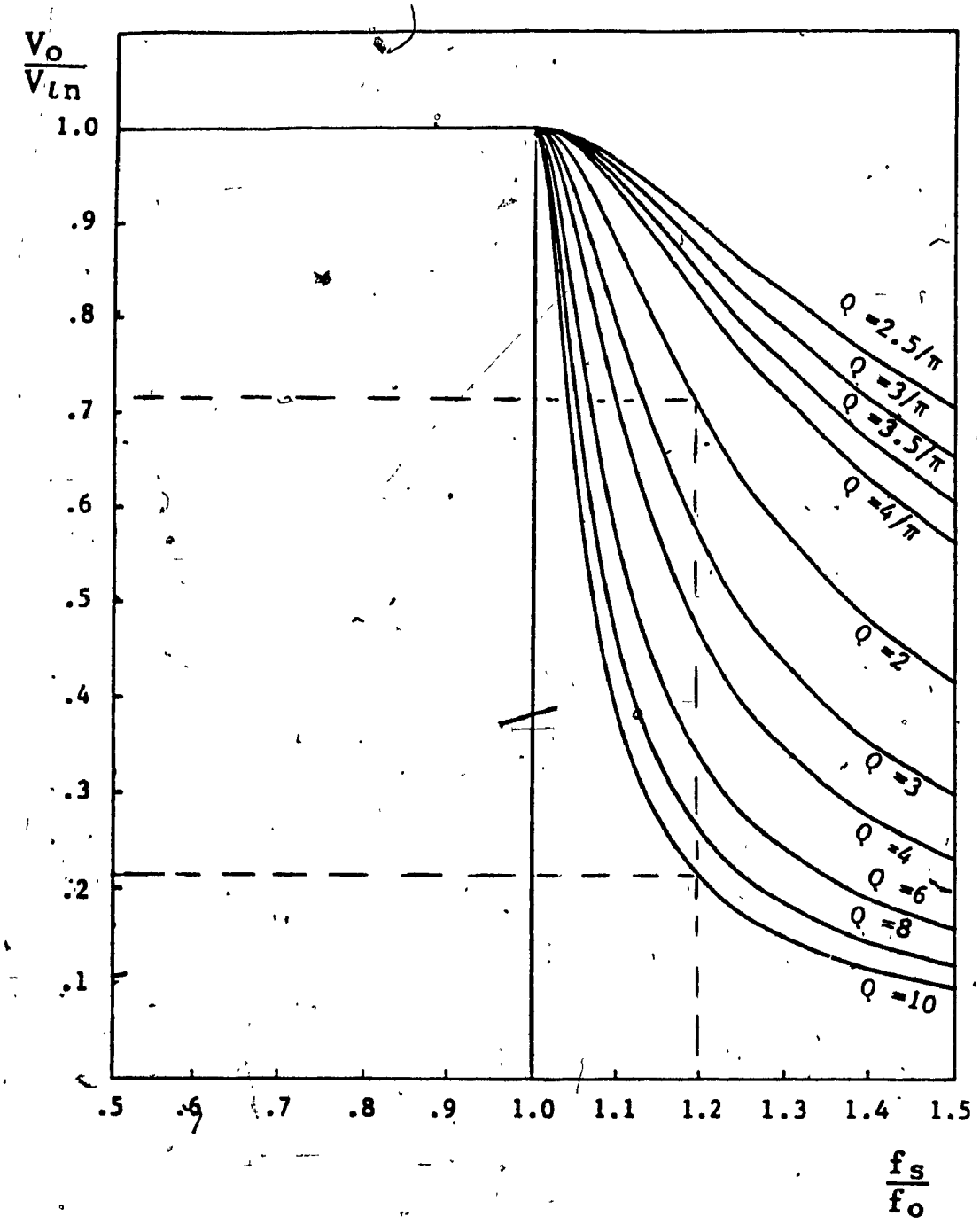

Figure 1-6: Voltage Transfer Ratio of the Series Resonant Converter Operated in Frequency Modulation Above Resonant Frequency. (Based on Fig. 3-14 in [7].)

loads. The maximum voltage transfer ratio not being the same for all loads implies that the range of voltage over which regulation could be achieved would be different for each load. This is not a desirable characteristic in DC-DC converters, which in general must operate over a wide range of output loads and a given range of input voltage. It is seen from Figure 1-6, that as the switching frequency is selected closer to resonant frequency, the maximum available transfer ratio becomes independent of load and approaches 1.

It can also be, calculated from the material given in [7] and the stress normalization procedure given in section 2.3.3 of this thesis that, for a given output power, component stresses are lower as the switching frequency approaches the resonant frequency.

For these two reasons the study is performed for a switching frequency equal to the resonant frequency.

CHAPTER 2: STEADY-STATE ANALYSIS

2.1 CIRCUIT OPERATION DESCRIPTION

When the converter is operated at resonant frequency with either PWM or PSPWM control, there are two modes of operations characterized by continuous or discontinuous resonant inductor current. The steady-state operation of the converter is now described for PWM and PSPWM control in both modes.

In the following description all inductors, capacitors and transformers are assumed to be lossless. All diodes and rectifiers have zero drop in the forward direction and no leakage current in the reverse direction. All switches are unidirectional switches with zero forward drop. The output filter time constant $R_L C_o$ is also assumed to be much larger than the switching period, so that the output filter can be modeled as a constant voltage source of amplitude V_o. To simplify notation the transformer turns ratio is taken to be 1:1:1. Generalization to an arbitrary turns ratio is trivial.

2.1.1 PWM Operation

The PWM operation of the full-bridge embodiment of the converter is similar to that of the half-bridge. For this reason the description will be restricted to the that of the half-bridge.

2.1.1.1 Discontinuous Mode with PWM

In the discontinuous mode, the resonant inductor initial current is zero. After the closure of S_1, at $t=t_0$, the current rises and CR_1 is forward biased. The current flows as indicated in Figure 2-1a) and determines the relative polarities of V_{in}, V_c and V_o. The current is therefore expressed by

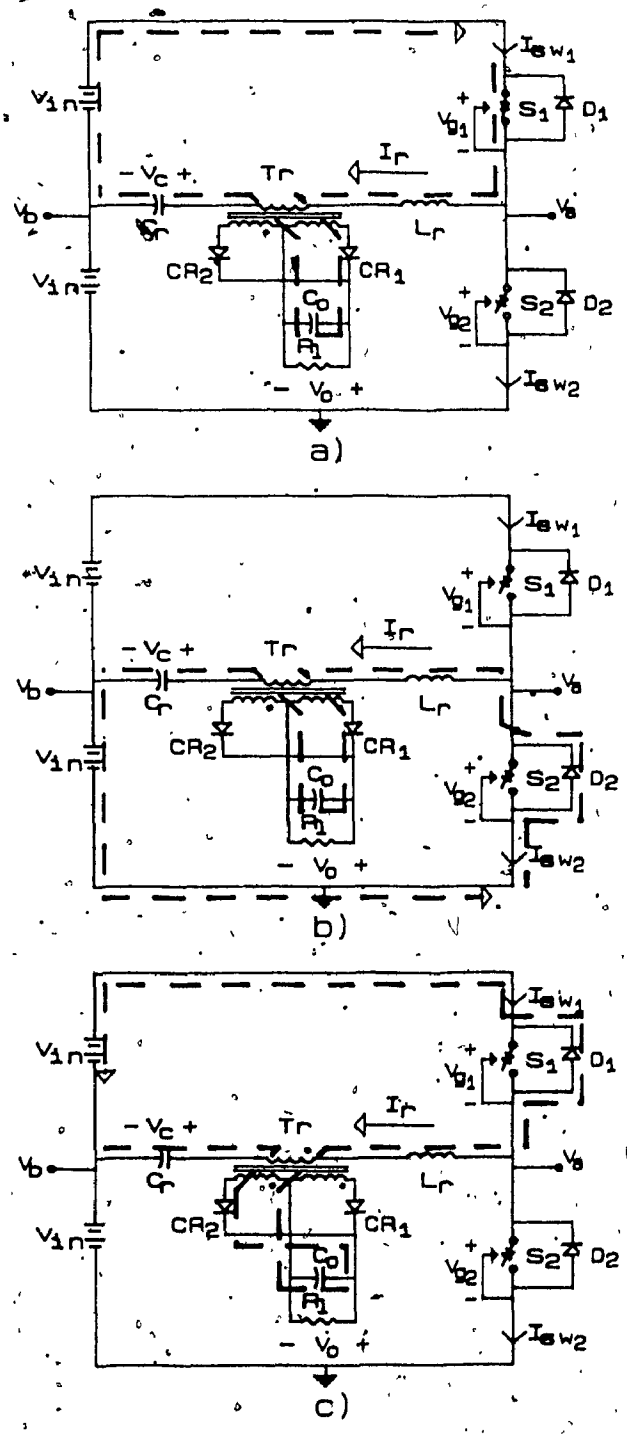

Figure 2-1: PWM Current Flow Path
a) $t_0 < t < t_1$
b) $t_1 < t < t_2$
c) $t_2 < t < T_h$

$$I_r(t) = \frac{V_{in} - V_c(t_0) - V_o}{Z_o} \sin(\omega_o t) , \qquad (2.1.1\text{-}1)$$

where

$$Z_o = (L_r / C_r)^{1/2} , \qquad (2.1.1\text{-}2)$$

$$\omega_o = 1/(L_r C_r)^{1/2} , \qquad (2.1.1\text{-}3)$$

At time $t=t_1$, when the S_1 is turned off, the inertia of the resonant inductor current forces the conduction of D_2. The current flows as indicated in Figure 2-1b). The resonant current can thereafter be expressed as

$$I_r(t) = I_r(t_1) \cos(\omega_o t - \omega_o t_1) - \frac{V_{in}+V_c(t_1)+V_o}{Z_o} \sin(\omega_o t - \omega_o t_1) . \qquad (2.1.1\text{-}4)$$

The resonant current decays until it reaches zero at $t=t_2$; D_2 turns off. The current remains at zero until S_2 is turned on at $t=t_3$. Since the current is unidirectional throughout the first half-cycle and reverses at the turn-on of S_2, the resonant capacitor voltage is maximal from t_2 to t_3.

$$V_c(t) = V_{c_{max}} \qquad t_2 \leq t \leq t_3 . \qquad (2.1.1\text{-}5)$$

From symmetry of the operation in each half-cycle it is concluded that

$$V_c(t_0) = -V_c(t_3) . \qquad (2.1.1\text{-}6)$$

The value for $V_c(t_0)$ is obtained from equations (2.1.1-5) and (2.1.1-6). Substituting in (2.1.1-1), the resonant current can be expressed as

$$I_r(t) = \frac{V_{in} + V_{c_{max}} - V_o}{Z_o} \sin(\omega_o t) , \qquad (2.1.1\text{-}7)$$

for $t_o < t < t_1$.

Note that at t_2 the voltage across C_r is positive and would naturally tend to reverse the flow of current. If reversal was to occur, the current would flow through CR_2 and D_1, as indicated in Figure 2-1c). In this circuit configuration, the output voltage V_o and V_{in} oppose V_c, discontinuous operation therefore implies that

$$V_c(t_2) = V_{c_{max}} \leq V_{in} + V_o . \qquad (2.1.1\text{-}8)$$

It is also noted that, in physical implementations of the converter, energy is stored in the transformer as magnetizing current. The magnetizing current cannot be interrupted at $t=t_2$. CR_2 is therefore forward biased at this time and the magnetizing current flows through the load. The transformer voltage reverses to $-V_o$. Consequently the voltage at the point common to S_1 and S_2, designated as V_a on Figure 2-1, is

$$V_a = V_{in} + V_{cmax} - V_o . \qquad (2.1.1\text{-}9)$$

The importance of this point will be underlined later in section 4.2.1. Selected waveforms are shown in Figure 2-2a).

2.1.1.2 Continuous Mode with PWM

In continuous mode, before S_1 turns on at $t=t_o$, the resonant current is non zero and is flowing through D_2. When S_1 turns on, D_2 is commutated and the current remains positive. The current path is illustrated in Figure 2-1a). From circuit theory, the expression for the resonant current is found to be

$$I_r(t) = I_r(t_o) \cos(\omega_o t) + \frac{V_{in} - V_c(t_o) - V_o}{Z_o} \sin(\omega_o t) . \qquad (2.1.1\text{-}10)$$

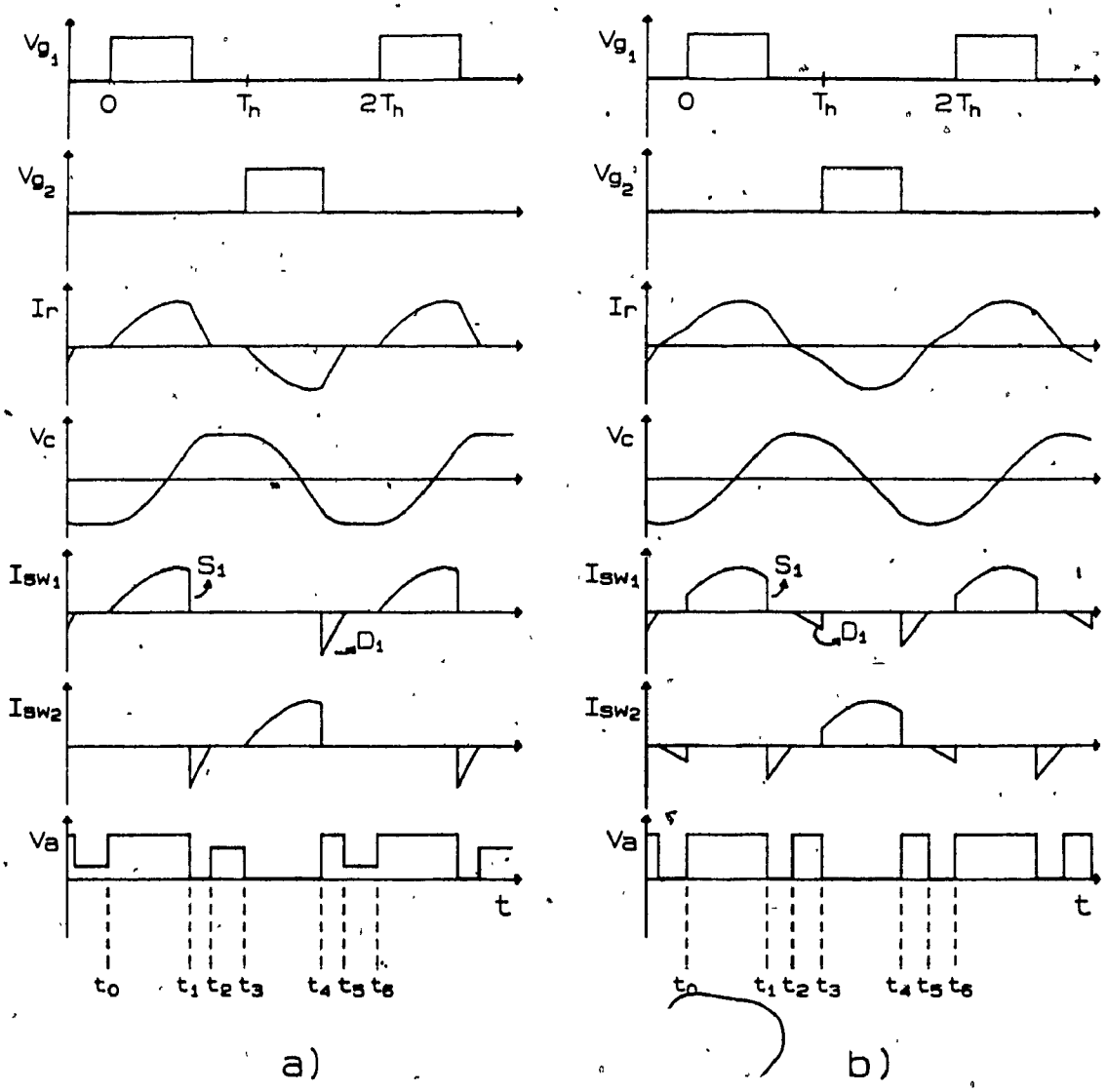

Figure 2-2: PWM Waveforms
a) Discontinuous Mode
b) Continuous Mode

At time $t=t_1$, when S_1 is turned off, the current is commutated to D_2. The current path is that of Figure 2-1b) and the resonant current is expressed by

$$I_r(t) = I_r(t_1)\cos(\omega_o t-\omega_o t_1) - \frac{V_{in}+V_c(t_1)+V_o}{Z_o}\cdot\sin(\omega_o t-\omega_o t_1) \qquad (2.1.1\text{-}11)$$

At $t=t_2$, when the current crosses zero, the capacitor voltage is maximum and larger than $V_{in}+V_o$. The current therefore rings back through D_1 as illustrated by the resonant current path of Figure 2-1c). Recalling that $I_r(t_2)$ is zero, the initial value of current is zero and the expression for the current has only a sinusoidal term.

$$I_r(t) = \frac{V_{in}-V_{c_{max}}+V_o}{Z_o}\sin(\omega_o t-\omega_o t_2) \qquad (2.1.1\text{-}12)$$

The next half-cycle is symmetrical and starts at the turn-on of S_2. Typical waveforms are shown in Figure 2-2b).

2.1.2 PSPWM Operation

2.1.2.1 Discontinuous Mode with PSPWM

As for switching operation in PWM, the initial resonant current is zero and the initial resonant capacitor voltage is maximum. S_4 is already on when S_1 is turned on at $t=t_o$; the resonant current increases and CR_1 is forward biased. The current flows as indicated in Figure 2-3a) and determines the relative polarities of V_{in}, V_c and V_o. From circuit theory, the current is found to be expressed by

$$I_r(t) = \frac{V_{in}+V_{c_{max}}-V_o}{Z_o}\sin(\omega_o t) \qquad (2.1.2\text{-}1)$$

At time $t=t_1$, when S_4 is turned off, the inertia of the resonant inductor current forces the conduction of D_3. The current flows as indicated in Figure 2-3b). The resonant current can thereafter be expressed as

$$I_r(t) = I_r(t_1)\cos(\omega_o t-\omega_o t_1) - \frac{V_c(t_1)+V_o}{Z_o}\sin(\omega_o t-\omega_o t_1) , \qquad (2.1.2-2)$$

At time $t=t_2$, when the current crosses zero, V_c is maximum. In this case a reversal of the current would imply a current flow as indicated in Figure 2-3c). The condition for discontinuous conduction in PSPWM operation is therefore

$$V_c(t_2) = V_{c_{max}} \leq V_o , \qquad (2.1.2-3)$$

Selected waveforms are shown in Figure 2-4a).

2.1.2.2 Continuous Mode with PSPWM

In continuous mode, before S_1 turns on at $t=t_o$, the resonant is non zero and is flowing in the positive direction through D_2 and S_4. When S_1 turns on, D_2 is commutated and the current remains positive. The current path is illustrated in Figure 2-3a). From circuit theory the expression for the resonant current is found to be

$$I_r(t) = I_r(t_o)\cos(\omega_o t) + \frac{V_{in}-V_c(t_o)-V_o}{Z_o}\sin(\omega_o t) . \qquad (2.1.2-4)$$

At time $t=t_1$, when S_4 is turned off, the current is commutated and flows through S_1 and D_3. The current path is that of Figure 2-3b) and the resonant current is expressed by

$$I_r(t) = I_r(t_1)\cos(\omega_o t-\omega_o t_1) - \frac{V_c(t_1)+V_o}{Z_o}\sin(\omega_o t-\omega_o t_1) . \qquad (2.1.2-5)$$

At time $t=t_2$, when the current crosses zero, V_c is maximum and larger than V_o. The current therefore reverses and flows through S_3 and D_1.

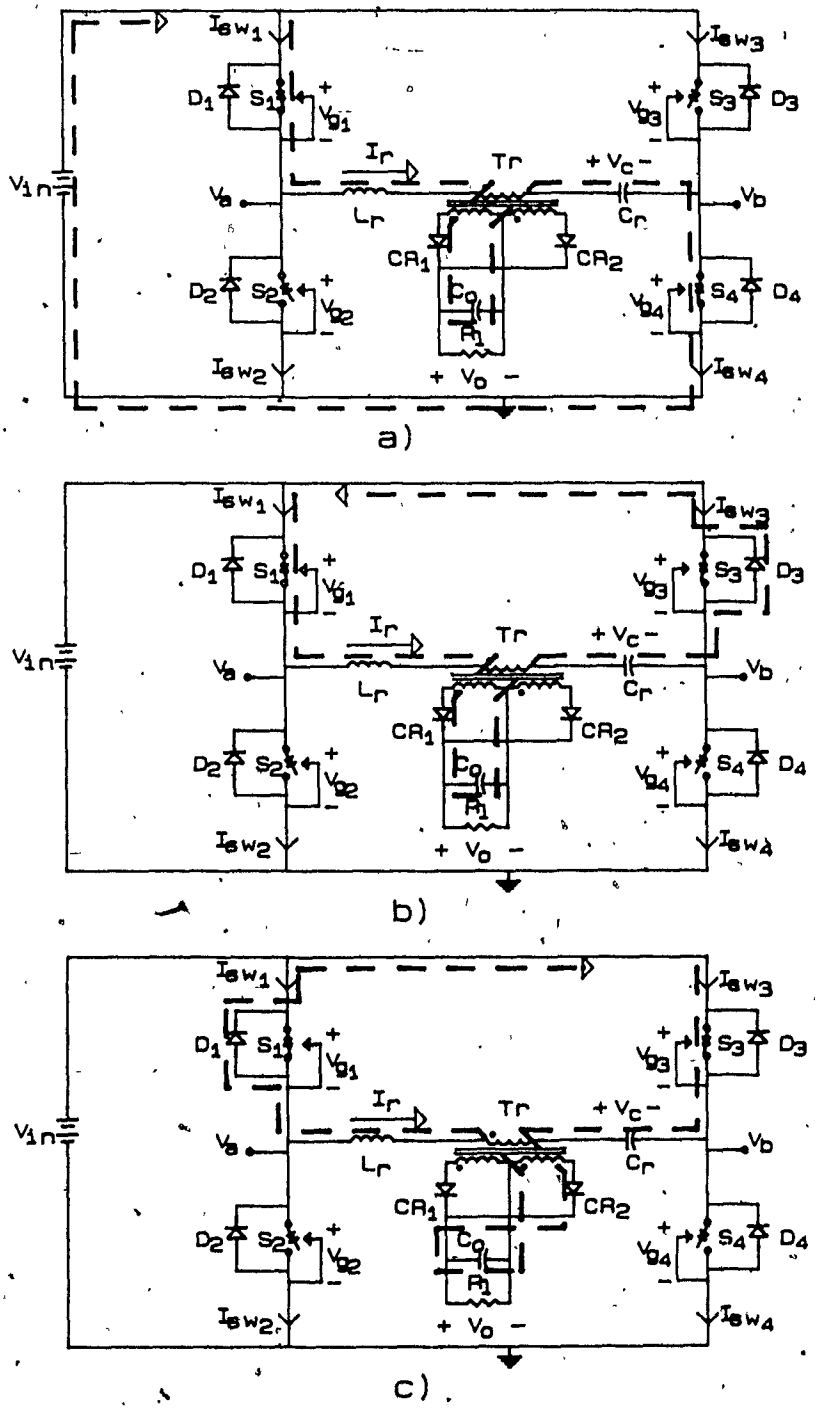

Figure 2-3: PSPWM Current Flow Path
a) $t_o < t < t_1$,
b) $t_1 < t < t_2$
c) $t_2 < t < T_h$

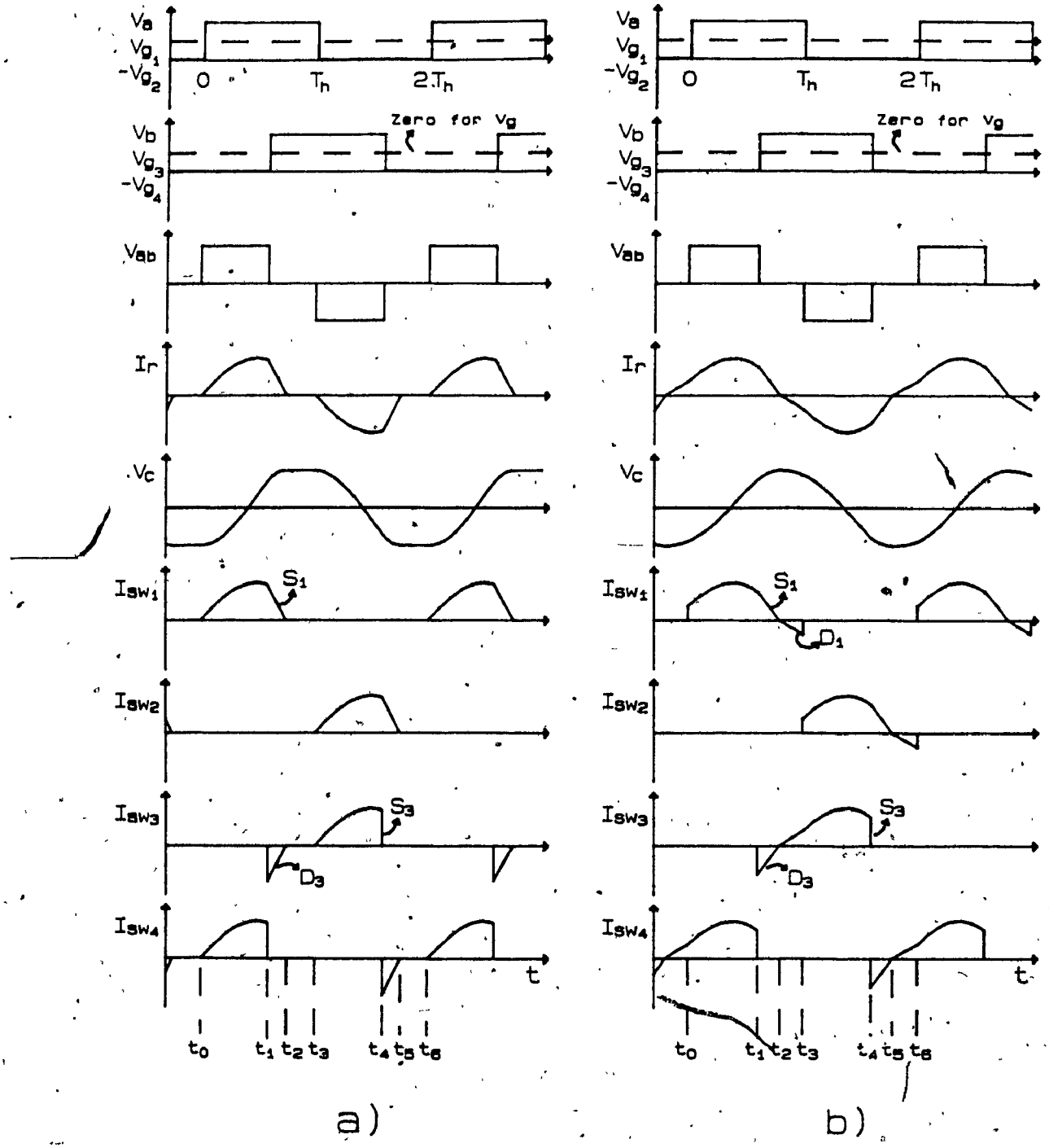

Figure 2-4: PSPWM Waveforms
a) Discontinuous Mode
b) Continuous Mode

as illustrated by the resonant current path of Figure 2-3c). Since $I_r(t_2)$ is zero, the expression for the current has only a sinusoidal term.

$$I_r(t) = \frac{-V_{c_{max}}+V_o}{Z_o} \sin(\omega_o t-\omega_o t_2) \qquad (2.1.2\text{-}6)$$

The next half-cycle is symmetrical and starts at the turn-on of S_2. Typical waveforms are shown in Figure 2-4b).

2.2 STEADY-STATE TRAJECTORY

The preceding section describes the operation of the converter. In this section, equations that describe the steady state trajectories of the resonant current and resonant voltage are derived. The voltage transfer ratio and the boundary between the conduction modes are also determined.

The equations are a function of three quantities: the load, the output voltage and the on-time. Any two of these quantities can be selected as parameters the third one becoming the variable to be solved for numerically. This is performed for both switching strategies. The analysis is given for $t_o < t < T_h$, where T_h is the half-cycle period. Resonant current and voltage for the second half-cycle are simply obtained from

$$I_r(t) = -I_r(t-T_h) , \qquad (2.2.0-1)$$

$$V_c(t) = -V_c(t-T_h) . \qquad (2.2.0-2)$$

Useful to the analysis are the following definitions: the load parameter, analogous to the quality factor of a series resonant tank,

$$Q \equiv \frac{Z_o}{R_\ell} , \qquad (2.2.0-3)$$

the normalized load parameter,

$$\bar{Q} \equiv Q \cdot \frac{\omega_o T_h}{2} , \qquad (2.2.0-4)$$

and the steady state voltage transfer ratio,

$$M \equiv \frac{V_o}{V_{in}} . \qquad (2.2.0-5)$$

It is also convenient to normalize voltages to V_{ln} (units in volts) and to normalize currents to V_{ln}/Z_o (units in amps).

$$V(t) = \overline{V(t)} \cdot V_{ln} \qquad (2.2.0\text{-}6)$$

$$I(t) = \overline{I(t)} \cdot \frac{V_{ln}}{Z_o} \qquad (2.2.0\text{-}7)$$

$\overline{V(t)}$ and $\overline{I(t)}$ are dimensionless variables which yield the actual voltage and current once multiplied by the proper scaling factor.

In section 2.3.5, normalization of the integral of the current is also used. The area, A, under the current waveform is therefore normalized as follows

$$A = \overline{A} \cdot \frac{V_{ln}}{\omega_o \cdot Z_o} . \qquad (2.2.0\text{-}8)$$

It can be noticed, from the discussion of section 2.1, that the only difference between the PWM and PSPWM operations is the voltage impressed across the load branch during the off-time, $t_1 < t < t_3$. In PSPWM operation the voltage across the load branch is always zero. Comparison of (2.1.1-4), (2.1.1-11), (2.1.1-12) to (2.1.2-2), (2.1.2-5), (2.1.2-6) reveals that these expressions are identical except for a missing term of magnitude V_{ln} in the set of equations pertaining to PSPWM. Multiplying the voltage impressed across the load branch in PWM operation during the off-time by the factor

$$\beta \equiv \begin{cases} 1 & \text{for PWM operation} \\ 0 & \text{for PSPWM operation} \end{cases} , \qquad (2.2.0\text{-}9)$$

allows the analysis of both switching strategies with a single set of equations.

2.2.1 Discontinuous Mode

It is seen, from the discussion in sections 2.1.1.1 and 2.1.2.1, that the resonant current is unidirectional during a half-cycle and that the capacitor voltage varies from $-V_{c_{max}}$ to $V_{c_{max}}$. The capacitor voltage swing during a half-cycle is therefore $2 \cdot V_{c_{max}}$. From that fact, a very useful relationship between the output voltage and the maximum capacitor voltage is derived. Let

$$A_{od} = \int_{t_o}^{t_1} I_r(t) \; \partial t \qquad (2.2.1\text{-}1)$$

and

$$A_{1d} = \int_{t_1}^{t_2} I_r(t) \; \partial t \; . \qquad (2.2.1\text{-}2)$$

Since the voltage change on the capacitor is the integral of the current,

$$2 \cdot V_{c_{max}} = \frac{1}{C_r} \int_{t_o}^{t_2} I_r(t) \cdot \partial t = \frac{A_{od}+A_{1d}}{C_r} \; . \qquad (2.2.1\text{-}3)$$

The output voltage is equal to the average load current multiplied by the load resistance.

$$V_o = \frac{R_\ell}{T_h} \left(A_{od} + A_{1d} \right) \qquad (2.2.1\text{-}4)$$

Dividing equation 2.2.1-3 by equation 2.2.1-4 yields

$$\frac{V_{c_{max}}}{V_o} = \frac{T_h}{2R_\ell C_r} = \frac{\omega_o T_h}{2R_\ell \omega_o C_r} = \overline{Q} \; , \qquad (2.2.1\text{-}5)$$

or

$$V_{c_{max}} = M\overline{Q} \cdot V_{in} \; . \qquad (2.2.1\text{-}6)$$

Using that relationship and the definition for β, the expressions for the resonant current and voltage can be derived for each of the three time intervals of the first half-cycle.

$t_o < t < t_1$

Substituting (2.2.1-6) into (2.1.1-7) and (2.1.2-1) the resonant current is found to be

$$I_r(t) = (1+M\overline{Q}-M) \cdot \sin(\omega_o t) \cdot \frac{V_{in}}{Z_o} \quad (2.2.1\text{-}7)$$

Integrating (2.2.1-7)

$$V_c(t) = V_c(t_o) + \frac{1}{C_r} \int_{t_o=0}^{t} (1+M\overline{Q}-M) \cdot \sin(\omega_o t) \cdot \frac{V_{in}}{Z_o} \, \partial t$$

$$= V_c(t_o) + \frac{1}{C_r\omega_o} \int_{w_o t_o=0}^{w_o t} (1+M\overline{Q}-M) \cdot \sin(\omega_o t) \cdot \frac{V_{in}}{Z_o} \, \partial\omega_o t \quad (2.2.1\text{-}8)$$

It is easily shown from (2.1.1-2) and (2.1.1-3) that

$$\frac{1}{C_r\omega_o} = Z_o \quad (2.2.1\text{-}9)$$

The initial value on the resonant capacitor is $-V_{c_{max}}$, substitution of (2.2.1-6) and (2.2.1-9) into (2.2.1-8) results in

$$V_c(t) = [\, -M\overline{Q} + (1+M\overline{Q}-M) \cdot (\, 1-\cos(\omega_o t) \,) \,] \cdot V_{in} \quad (2.2.1\text{-}10)$$

$t_1 < t < t_2$

Normalizing (2.1.1-4) and (2.1.2-2) yields

$$I_r(t) = \left[\overline{I_r(t_1)} \cos(\omega_o t-\omega_o t_1) - (\beta+\overline{V_c(t_1)}+M) \cdot \sin(\omega_o t-\omega_o t_1) \right] \cdot \frac{V_{in}}{Z_o} , \quad (2.2.1\text{-}11)$$

where $\overline{I_r(t_1)}$ and $\overline{V_c(t_1)}$ are obtained by first substituting $\omega_o t_1$ for $\omega_o t$ into (2.2.1-7) and (2.2.1-10), and then normalizing according to the definitions of (2.2.0-6) and (2.2.0-7). Integrating (2.2.1-11) and adding the capacitor voltage initial condition results in

$$V_c(t) = \left[\overline{V_c(t_1)} + \overline{I_r(t_1)} \sin(\omega_o t-\omega_o t_1) - (\beta+\overline{V_c(t_1)}+M) \cdot (1 - \cos(\omega_o t-\omega_o t_1)) \right] \cdot V_{in} . \quad (2.2.1\text{-}12)$$

$t_2 < t < t_3 = T_h$

$$I_r(t) = 0 \quad (2.2.1\text{-}13)$$

$$V_c(t) = MQ \cdot V_{in} \quad (2.2.1\text{-}14)$$

The equations describing the resonant current and voltage trajectories contain an unknown, t_2, the time at which conduction stops. Substituting for $\overline{I_r(t_1)}$ and $\overline{V_c(t_1)}$ into (2.2.1-11)

$$I_r(t) = \left[(1+MQ-M) \cdot \sin(\omega_o t_1) \cdot \cos(\omega_o t-\omega_o t_1) - \{ \beta +1 - (1+MQ-M) \cdot \cos(\omega_o t_1) \} \cdot \sin(\omega_o t-\omega_o t_1) \right] \cdot \frac{V_{in}}{Z_o} . \quad (2.2.1\text{-}15)$$

t_2 is found by equating (2.2.1-15) to zero with $\omega_o t=\omega_o t_2$. Setting $\omega_o t_2$ in evidence:

$$\omega_o t_2 = \omega_o t_1 + \tan^{-1}\left[\frac{(1+M\bar{Q}-M)\cdot\sin(\omega_o t_1)}{\beta + 1 - (1+M\bar{Q}-M)\cdot\cos(\omega_o t_1)} \right] \qquad (2.2.1\text{-}16)$$

To find the equation that will allow to find M, $\bar{Q}$ or $\omega_o t_1$ as a function of the two other quantities, the principle of conservation of energy is used. Letting P_o be the average output power and P_{in} be the average input power, these quantities are given by

$$P_{in} = \frac{V_{in}}{T_h}\left[\int_{to}^{t_1} I_r(t)\,\partial t - \beta\cdot\int_{t_1}^{t_2} I_r(t)\,\partial t \right]$$

$$\frac{V_{in}}{T_h}\cdot(A_{od} - \beta A_{1d}) \qquad (2.2.1\text{-}17)$$

and

$$P_o = \frac{V_o}{T_h}\int_{to}^{Th} I_r(t)\,\partial t$$

$$= \frac{V_o}{T_h}(A_{od} + A_{1d}) \qquad (2.2.1\text{-}18)$$

The assumptions outlined in section 2.1 implies that the converter is lossless. Equating P_o to P_{in} results in

$$M = \frac{V_o}{V_{in}} = \frac{A_{od}-\beta A_{1d}}{A_{od}+A_{1d}} \qquad (2.2.1\text{-}19)$$

A_{od} is found by integrating (2.2.1-7) from t_o to t_1.

$$A_{od} = (1+M\bar{Q}-M)\cdot(1-\cos(\omega_o t_1)) \cdot \frac{V_{in}}{\omega_o \cdot Z_o} \qquad (2.2.1\text{-}20)$$

A_{1d} is found by integrating (2.1.1-11) from t_1 to t_2 and substituting for $I_r(t_1)$ and $V_c(t_1)$.

$$A_{1d} = \left[(1+M\bar{Q}-M)\cdot(\cos(\omega_o t_1) - \cos(\omega_o t_2)) - (\beta+1)\cdot\{1-\cos(\omega_o t_2-\omega_o t_1)\} \right] \cdot \frac{V_{in}}{\omega_o\cdot Z_o}$$

$$(2.2.1\text{-}21)$$

Substituting (2.2.1-20) and (2.2.1-21) into (2.2.1-19) yields

$$(1+M\bar{Q}-M)\cdot\left[\frac{M}{\beta}-1+(\beta+1)\cdot\cos(\omega_o t_1)-(M+\beta)\cdot\cos(\omega_o t_2)\right]$$

$$-(\beta+1)\cdot(M+\beta)\cdot\{1-\cos(\omega_o t_2-\omega_o t_1)\}=0 \quad . \qquad (2.2.1\text{-}22)$$

Since t_2 is a function of M, $\bar{Q}$ and $\omega_o t_1$ equation (2.2.1-22) is an implicit equation of the quantities M, $\bar{Q}$ and $\omega_o t_1$ which can be solved for by setting any two of these quantities as parameters.

The description of the resonant current and voltage steady state trajectory in discontinuous mode is complete.

2.2.2 Continuous Mode

As for the discontinuous conduction case, a relationship between the output voltage and the maximum capacitor voltage can easily be derived. Let,

$$A_{oc}=\int_{t_o}^{t_1} I_r(t)\ \partial t \qquad (2.2.2\text{-}1)$$

$$A_{1c}=\int_{t_1}^{t_2} I_r(t)\ \partial t \qquad (2.2.2\text{-}2)$$

$$A_{2c}=\int_{t_2-T_h}^{t_o} I_r(t)\ \partial t=\int_{t_2}^{T_h} -I_r(t)\ \partial t \qquad (2.2.2\text{-}3)$$

Referring to Figures 2.1-2b) and 2.1-4b), it is seen that the current is zero at $t=t_2-T_h$ and at t_2. During this interval, the current is positive and the capacitor voltage varies from $-V_{c_{max}}$ to $+V_{c_{max}}$. Since the voltage change on the capacitor is the integral of the current,

$$2 \cdot V_{cmax} = \frac{1}{C_r} \int_{t_2 - T_h}^{t_2} I_r(t)\, \partial t = \frac{A_{oc} + A_{1c} + A_{2c}}{C_r} \quad (2.2.2\text{-}4)$$

The output voltage is equal to the average rectified resonant current multiplied by the load resistance.

$$V_o = \frac{R_\ell}{T_h} \left(A_{oc} + A_{1c} + A_{2c} \right) \quad (2.2.2\text{-}5)$$

Dividing equation (2.2.2-4) by equation (2.2.2-5) the relation sought is

$$\overline{V_{cmax}} = M\overline{Q} \; . \quad (2.2.2\text{-}6)$$

This is the same expression as obtained for the discontinuous case. Using that relationship the expressions for the resonant current and capacitor voltage are derived for each of the three periods of the first half-cycle.

$t_o < t < t_1$

Normalizing (2.1.1-10) and (2.1.2-4) yields

$$I_r(t) = \left[\overline{I_r(t_o)} \cdot \cos(\omega_o t) + (1 - \overline{V_c(t_o)} - M) \cdot \sin(\omega_o t) \right] \cdot \frac{V_{\ell n}}{Z_o} \; . \quad (2.2.2\text{-}7)$$

Integrating (2.2.2-7) yields the resonant capacitor voltage

$$V_c(t) = \left[\overline{V_c(t_o)} + \overline{I_r(t_o)} \cdot \sin(\omega_o t) + (1 - \overline{V_c(t_o)} - M) \cdot (1 - \cos(\omega_o t)) \right] \cdot V_{\ell n} \; . \quad (2.2.2\text{-}8)$$

$t_1 < t < t_2$

Normalizing (2.1.1-11) and (2.1.2-5), the current is found to be

$$I_r(t) = \left[\overline{I_r(t_1)} \cos(\omega_o t-\omega_o t_1) - (\beta+\overline{V_c(t_1)}+M) \cdot \sin(\omega_o t-\omega_o t_1) \right] \cdot \frac{V_{in}}{Z_o} .$$

(2.2.2-9)

where $\overline{I_r(t_1)}$ and $\overline{V_c(t_1)}$ are obtained from (2.2.2-7) and (2.2.2-8) by substituting $\omega_o t_1$ for $\omega_o t$. Integrating the current,

$$V_c(t) = \left[\overline{V_c(t_1)} + \overline{I_r(t_1)} \sin(\omega_o t-\omega_o t_1) - (\beta+\overline{V_c(t_1)}+M) \cdot (1 - \cos(\omega_o t-\omega_o t_1)) \right] \cdot V_{in} . \quad (2.2.2-10)$$

$$t_2 < t < t_3 = T_h$$

Recalling (2.2.2-6) which states that $\overline{V_{c_{max}}} = M\bar{Q}$ and normalizing equations (2.1.1-12) and (2.1.2-6) the current is

$$I_r(t) = (\beta-M\bar{Q}+M) \cdot \sin(\omega_o t-\omega_o t_2) \cdot \frac{V_{in}}{Z_o} . \quad (2.2.2-11)$$

The resonant capacitor voltage is obtained by integrating the current.

$$V_c(t) = \left[M\bar{Q} + (\beta-M\bar{Q}+M) \cdot (1 - \cos(\omega_o t-\omega_o t_2)) \right] \cdot V_{in} \quad (2.2.2-12)$$

The equations describing the resonant current and voltage trajectories contain two more unknowns than the discontinuous mode equations: the initial resonant current, $I_r(t_o)$ and the initial resonant capacitor voltage, $V_c(t_o)$. From boundary conditions and assuming t_2 to be known, $\overline{I_r(t_o)}$, $\overline{V_c(t_o)}$ and a relation between M, $\bar{Q}$ and $\omega_o t_1$ are obtained. The first two boundary condition fall from half-cycle periodicity.

$$I_r(T_h) = -I_r(t_o) \quad (2.2.2-13)$$

$$V_c(T_h) = -V_c(t_o) \quad (2.2.2-14)$$

The third boundary condition is obtained from the definition of t_2.

$$I_r(t_2) = 0 \qquad (2.2.2\text{-}15)$$

Substituting for $\overline{I_r(t_1)}$ and $\overline{V_c(t_1)}$ into (2.2.2-9), the expression for $I_r(t)$ for $t_1 < t < t_2$ becomes

$$I_r(t) = \Big[\{(\overline{I_r(t_0)}\cdot\cos(\omega_o t_1)+(1-\overline{V_c(t_0)}-M)\cdot\sin(\omega_o t_1)\} \cos(\omega_o t-\omega_o t_1) - \{\beta+\overline{V_c(t_0)}+\overline{I_r(t_0)}\sin(\omega_o t_1)+(1-\overline{V_c(t_0)}-M)\cdot(1-\cos(\omega_o t_1)+M\} \cdot \sin(\omega_o t-\omega_o t_1) \Big] \cdot \frac{V_{in}}{Z_o} \qquad (2.2.2\text{-}16)$$

Substituting (2.2.2-11) into (2.2.2-13), (2.2.2-12) into (2.2.2-14) and (2.2.2-16) into (2.2.2-15) yields, after some manipulations,

$$\begin{bmatrix} 1 & 0 & (1-\overline{Q})\cdot\sin(\omega_o T_h-\omega_o t_2) \\ 0 & 1 & \overline{Q} + (1-\overline{Q})\cdot\{1-\cos(\omega_o T_h-\omega_o t_2)\} \\ \cos(\omega_o t_2) & -\sin(\omega_o t_2) & -\sin(\omega_o t_2) \end{bmatrix} \cdot \begin{bmatrix} \overline{i_r(t_0)} \\ \overline{V_c(t_0)} \\ M \end{bmatrix}$$

$$= \begin{bmatrix} -\beta\cdot\sin(\omega_o T_h-\omega_o t_2) \\ -\beta\cdot\{1-\cos(\omega_o T_h-\omega_o t_2)\} \\ (\beta+1)\cdot\sin(\omega_o t_2-\omega_o t_1)-\sin(\omega_o t_2) \end{bmatrix} . \qquad (2.2.2\text{-}17)$$

The solution to (2.2.2-17) is

$$I_r(t_o) = -(\beta-M\overline{Q}+M) \cdot \sin(\omega_o T_h-\omega_o t_2) \cdot \frac{V_{in}}{Z_o} , \qquad (2.2.2\text{-}18)$$

$$V_c(t_o) = \Big[-\beta - M + (\beta-M\overline{Q}+M)\cdot\cos(\omega_o T_h-\omega_o t_2) \Big] \cdot V_{in} , \qquad (2.2.2\text{-}19)$$

$$M = \frac{(\beta+1)\cdot\{\sin(\omega_o t_2-\omega_o t_1) - \sin(\omega_o t_2)\} + \beta\cdot\sin(\omega_o T_h)}{(Q-1)\cdot\sin(\omega_o T_h)} \quad . \qquad (2.2.2\text{-}20)$$

In order to find t_2, the principle of conservation of energy is used. Let P_o be the average output power and P_{in} be the average input power. These quantities are found to be

$$P_{in} = \frac{V_{in}}{T_h}\left[\int_{t_o}^{t_1} I_r(t)\,\partial t - \beta\int_{t_1}^{t_2} i_r(t)\,\partial t - \beta\int_{t_2}^{T_h} |I_r(t)|\,\partial t\right]$$

$$= \frac{V_{in}}{T_h}\cdot\left[A_{oc} - \beta(A_{1c}+A_{2c})\right] \qquad (2.2.2\text{-}21)$$

and

$$P_o = \frac{V_o}{T_h}\cdot\int_{t_o}^{T_h} |I_r(t)|\,\partial t$$

$$= \frac{V_o}{T_h}\left(A_{oc} + A_{1c} + A_{2c}\right) \qquad (2.2.2\text{-}22)$$

Letting P_o be equal to P_{in} yields

$$(M-1)\cdot A_{oc} + (M+\beta)\cdot(A_{1c}+A_{2c}) = 0 \quad . \qquad (2.2.2\text{-}23)$$

A_{oc} A_{1c} and A_{2c} are found by integrating 2.2.2-7, 2.2.2-16 and 2.2.2-11 over the periods where they apply.

$$A_{oc} = \left[\overline{I_r(t_o)}\cdot\sin(\omega_o t_1) + (1-\overline{V_c(t_o)}-M)\cdot(1-\cos(\omega_o t_1))\right]\cdot\frac{V_{in}}{\omega_o\cdot Z_o}$$

$$= \left[-(\beta-MQ+M)\cdot[\cos(\omega_o T_h-\omega_o t_2)-\cos(\omega_o T_h-\omega_o t_2+\omega_o t_1)] + (1+\beta)\cdot(1-\cos(\omega_o t_1))\right]\cdot\frac{V_{in}}{\omega_o\cdot Z_o}$$

$$(2.2.2\text{-}24)$$

$$A_{1c} = \Big[\overline{I_r(t_0)} \cdot (\sin(\omega_o t_2)-\sin(\omega_o t_1)) + (1-\overline{V_c(t_0)}-M) (\cos(\omega_o t_1)-\cos(\omega_o t_2)) - (1+\beta) (1 - \cos(\omega_o t_2-\omega_o t_1)) \Big] \cdot \frac{V_{in}}{\omega_o \cdot Z_o}$$

$$= \Big[-(\beta-M\bar{Q}+M)\cdot(-\cos(\omega_o T_h)+\cos(\omega_o T_h-\omega_o t_2+\omega_o t_1) -(1+\beta)\cdot(1-\cos(\omega_o t_2-\omega_o t_1) - \cos(\omega_o t_1) + \cos(\omega_o t_2) \Big] \cdot \frac{V_{in}}{\omega_o \cdot Z_o} \quad (2.2.2\text{-}25)$$

$$A_{2c} = - (\beta-M\bar{Q}+M) \cdot (1-\cos(\omega_o T_h-\omega_o t_2)) \cdot \frac{V_{in}}{\omega_o \cdot Z_o} \quad (2.2.2\text{-}26)$$

Substitution of (2.2.2-24) to (2.2.2-26) shows that (2.2.2-23) is an implicit function of the single variable $\omega_o t_2$ with parameters $\omega_o t_1$ and $\bar{Q}$ and M. Setting any two of $\omega_o t_1$, $\bar{Q}$, or M, equations (2.2.2-20) and (2.2.2-26) can be solved for as a set of two equations with two unknowns. The actual algorithm used is illustrated in Figure 2-5, where the subsequent guesses are computed using a root solving routine like the secant method. [11].

Although the solution is complete one fact is worth noting. The analysis is performed for a switching frequency equal to the resonant frequency. At the resonant frequency $\omega_o T_h$ is equal to π. It is seen that the denominator of (2.2.2-20) tends to zero as the switching frequency tends to the resonant frequency. For a solution to exist the numerator must also tends to zero and a finite limit must exist. This can be numerically verified to be the case by repeatedly carrying out the algorithm described by Figure 2-5 and letting $\omega_o T_h$ tend to π from the left or right limit. For the numerator to tend to zero, the term $\sin(\omega_o t_2-\omega_o t_1)-\sin(\omega_o t_2)$ must also tend to zero as the switching frequency approaches the resonant frequency. In the description given above, t_1 is smaller than t_2 and each interval t_1 and t_2 must repeat

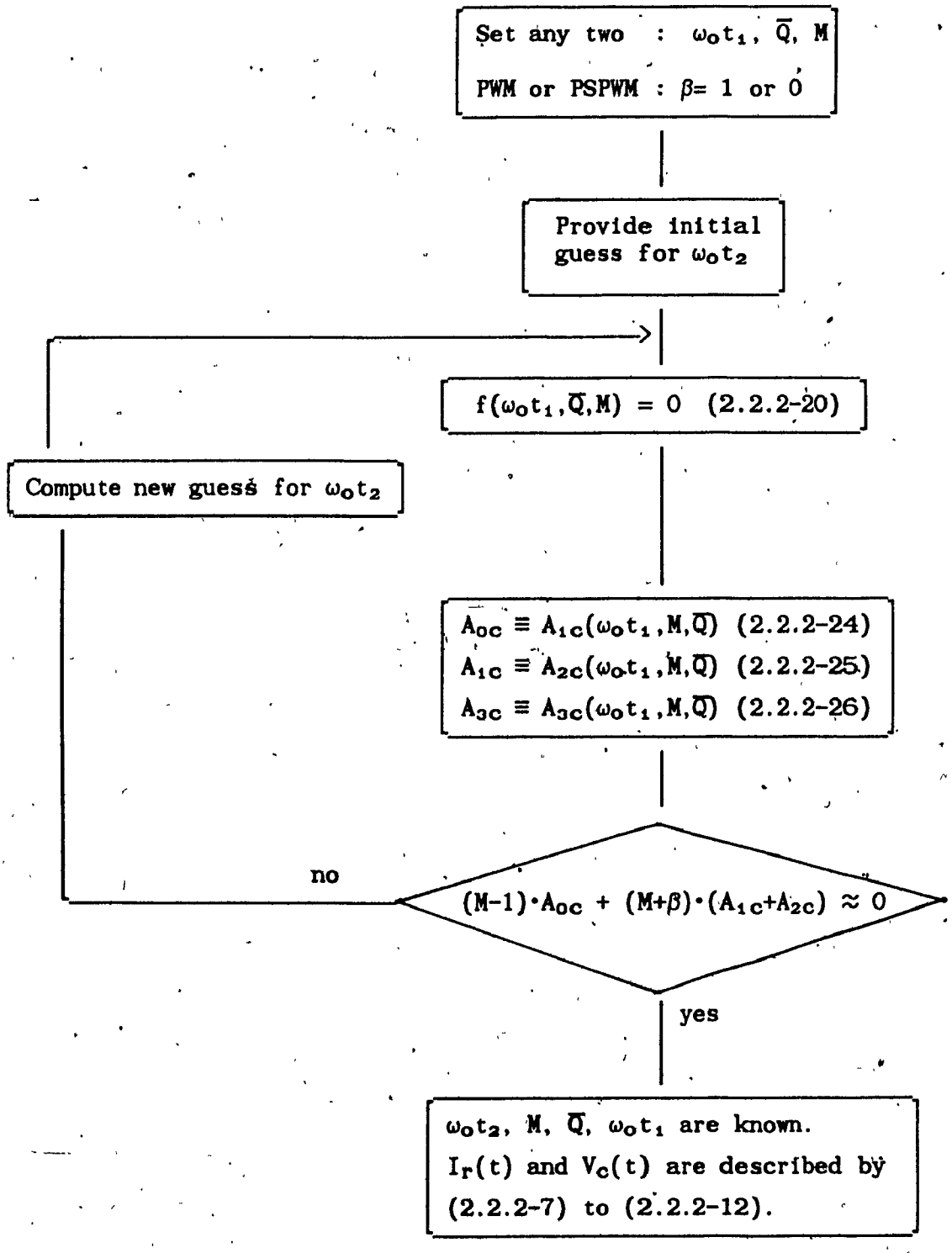

Figure 2-5: Flowchart for the Determination of the Steady State in Continuous Conduction.

twice per cycle. This implies that:

$$0 < \omega_o t_1 \leq \omega_o t_2 \leq \pi. \qquad (2.2.2\text{-}27)$$

At resonance $\sin(\omega_o t_2 - \omega_o t_1)$ must be equal to $\sin(\omega_o t_1)$. A graphical solution for which respects the condition imposed by (2.2.2-27) is given in Figure 2-6. For the two sine functions to be equal the angles between the x axis and the two hypotenuses must be equal. This implies that

$$\omega_o t_2 = \frac{\pi}{2} + \frac{\omega_o t_1}{2} \qquad (2.2.2\text{-}28)$$

This can be used as an initial guess when the algorithm of Figure 2-5 is performed with $\omega_o T_h$ approaching π.

2.2.3 Mode Boundary and Voltage Transfer Ratio

It is seen from (2.1.1-8), (2.1.2-3) and (2.2.0-9) that the conditions for continuous conduction is

$$V_c(t_2) = V_{c_{max}} > V_o + \beta V_{in} \qquad (2.2.3\text{-}1)$$

This is

$$M\overline{Q} > M + \beta \qquad (2.2.3\text{-}2)$$

For PSPWM operation, this equation reduces to

$$\overline{Q} > 1 \qquad (2.2.3\text{-}3)$$

and the boundary between discontinuous conduction and continuous conduction is expressed explicitly as a function of the load only.

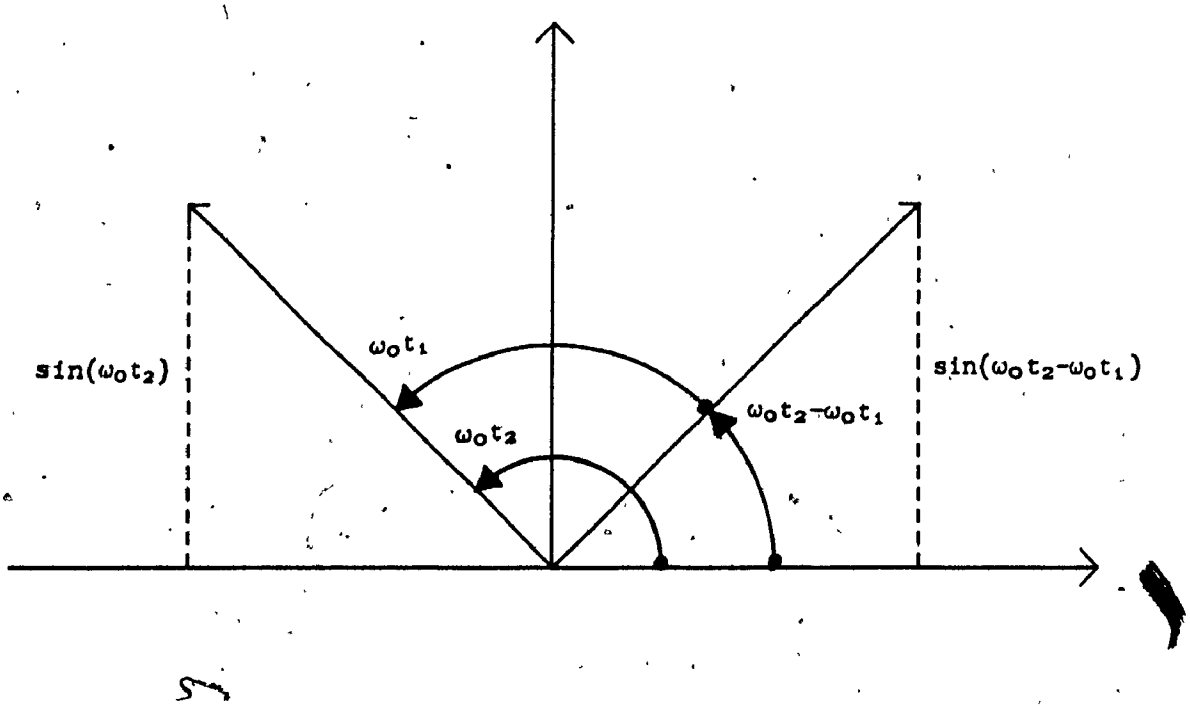

Figure 2-6: Trigonometric Solution for $\omega_o t_2$.

For PWM control the the expression is

$$M\bar{Q} > M + 1 \qquad (2.2.3\text{-}4)$$

For any given transfer ratio M , it is seen that boundary between the discontinuous and continuous mode is a function of the load only. Setting M and $\bar{Q}$ the mode of conduction is readily determined. $\omega_o t_1$ can be then be found.

Defining the duty cycle,

$$D \equiv \frac{\omega_o t_1}{\omega_o T_h} \qquad (2.2.3\text{-}5)$$

the mode boundaries are illustrated in thick lines in Figure 2-7. Voltage transfer ratio is also illustrated for various values of $\bar{Q}$ as $\omega_o T_h$ tends to π.[1] For operation in discontinuous mode the voltage transfer ratio is load dependent. In continuous conduction the voltage transfer ratio is load independent. This is: for a given duty cycle, the computed voltage transfer ratio M is identical for any $\bar{Q}$ which satisfies (2.2.3-2). So the boundary between continuous and discontinuous mode also illustrates the transfer voltage ratio in continuous mode. This property is strikingly similar to that of "square-wave" PWM converters for which the transfer ratio is load dependant for discontinuous filter inductor current and load independent for continuous filter inductor current.

[1]The voltage transfer ratio was computed for $\omega_o T_h = 0.9999\pi$.

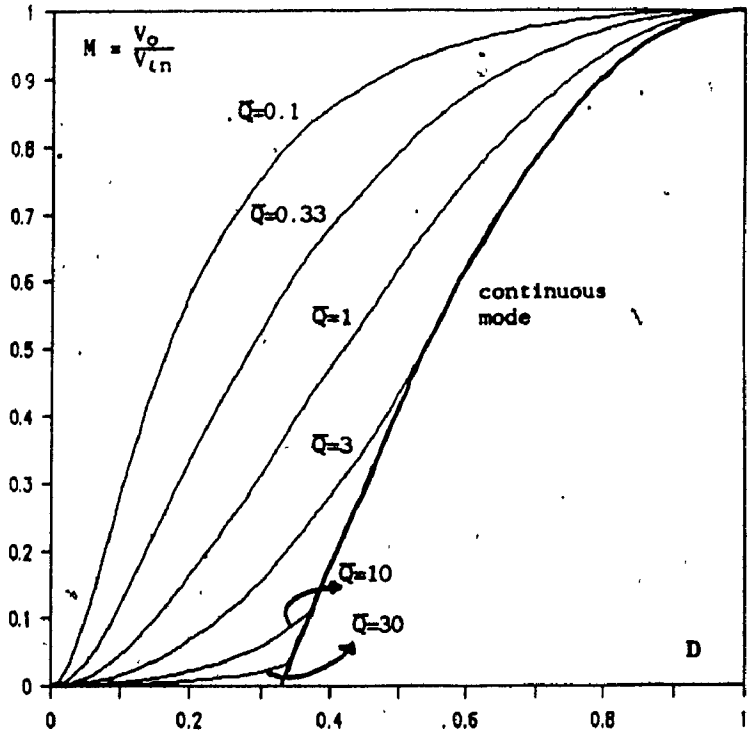

a)

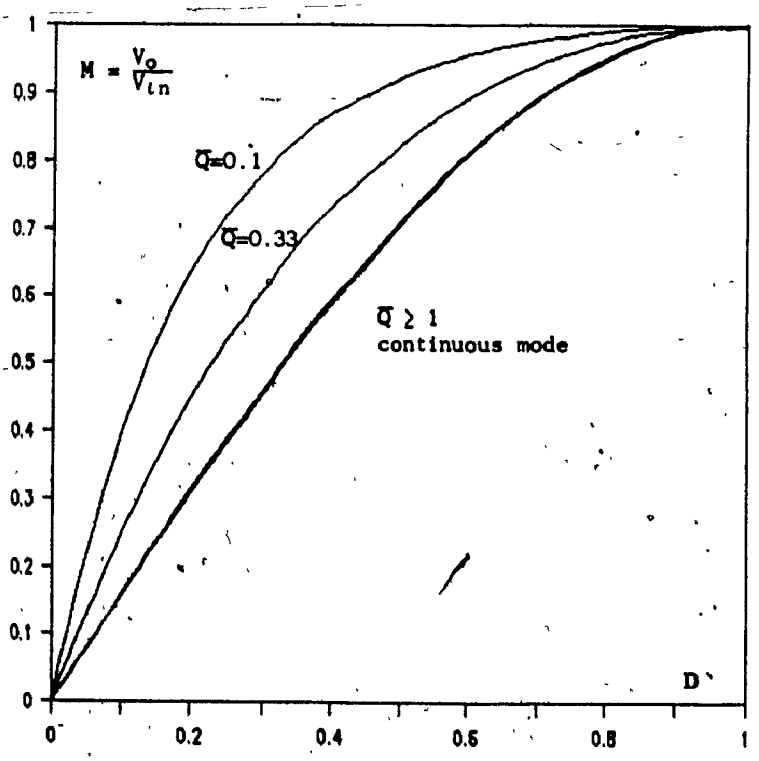

b)

Figure 2-7: Voltage Transfer Ratio
a). PWM
b) PSMSPW

2.3 STEADY-STATE COMPONENT STRESSES

2.3.1 Volt-Ampere Product

Rating of electric power system components is usually expressed in terms of a Volt-Ampere product or VA rating. For the study of the converter, this practice is very convenient as it allows to quantify the stress on the components in terms of output power independently of the input voltage, output voltage, or output current. The stress can be expressed as

$$VA_{op} = y \cdot P_o \ , \qquad (2.3.1\text{-}1)$$

where P_o is the output power and y is a real number. This representation is useful to compare the stress imposed on the components for different designs of same output powers. In particular this formulation is useful to select the optimal operating point $(M,\overline{Q})$ of the converter.

As useful as this representation may be, actual components must be selected according to the actual current and voltage stress. Converters are often required to operate over a various range of input voltage and output load. The worst operating point $VA_{op_{max}}$, may not be equal to the the product of the worst current stress by the worst voltage stress. For these reasons the VA rating is defined as

$$VA_{rat} = \text{Worst current stress} \cdot \text{Worst voltage stress} \ . \qquad (2.3.1\text{-}2)$$

2.3.2 Device Stress Description

The Volt-Ampere characterization of power system components is generally given in terms of RMS current and voltage. In switch-mode applications, where current and voltage are generally not sinusoidal, the relation between RMS, peak, and average quantities is not readily determined. A discussion on the selection of the quantities used in this thesis to obtain a Volt-Ampere product is now given.

2.3.2.1 Input Bus and Capacitors

The input bus stress is characterized as if the input bus was a capacitor fed by a current source of amplitude equal to the average current drawn by the converter.

Capacitor voltage ratings are generally given in terms of maximum instantaneous voltage. The maximum instantaneous voltage is used to characterize the capacitors voltage stress.

Current stress will result in heating of the capacitors, therefore RMS current is selected to describe current stress. Maximum $\partial V/\partial t$ is also sometimes specified for certain types of capacitors [12]. This is relevant for the resonant capacitor.

$$I_{pk} = \frac{1}{C_r} \cdot \frac{\partial V_{max}}{\partial t} \qquad (2.3.2\text{-}1)$$

is also calculated to be considered separately.

2.3.2.2 Switch

Switch voltage rating is generally given in terms of instantaneous voltage. The maximum instantaneous voltage is used to characterize the switch voltage stress.

Current handling capability of devices can be specified in many different ways. Maximum instantaneous current is one of the parameters given in data sheets. But most critical is the thermal stress of the device. To implement the switches, several types of device can be used. Presently the most commonly used type of devices which have turn-off capability are the MOSFET and the bipolar transistor. The MOSFET "on" characteristic is that of a resistor, while the characteristic of the bipolar transistor is that of a constant voltage source in series with a resistance. The bipolar transistor power dissipation is therefore dependant on both the average current and the RMS current. One possible current stress characterization to use in the VA product would be

$$I_{str} = (I_{avg} \cdot I_{rms})^{1/2} \quad (2.3.2\text{-}2)$$

However, since both types of devices exhibit a resistive drop, the RMS current is used for the VA product.

2.3.2.3 Diodes and Rectifiers

The voltage rating of diodes is given in terms of instantaneous voltage. Therefore, the maximum instantaneous voltage is used to characterize the diode voltage stress.

Diode "on" characteristic is that of a constant voltage source. Current stress is therefore expressed in terms of average current.

One very convenient method to calculate conduction power dissipation in a diode is to multiply the forward drop of the diode at the maximum instantaneous current by the average current.

$$P_{diss} = V_f(I_{pk}) \cdot I_{avg} \quad (2.3.2\text{-}3)$$

This procedure yields a reasonable evaluation of the power dissipation provided that $V_f(I_{pk})$ is not evaluated in or above the resistive knee

of the V_f–I_f curve illustrated in Figure 2.8. If the $V_f(I_{pk})$ falls into or above this knee the estimate of (2.3.2-3) will be too conservative.

2.3.2.4 Transformer and Inductor

The size of magnetic components is dictated by the flux handling requirement and by the limit on power dissipation. Power dissipation is affected by both the flux swing and the RMS current flowing in the windings.

To determine the voltage stress, consider Lenz law.

$$V = \frac{\partial \Phi}{\partial t} \qquad (2.3.2\text{-}4)$$

It is seen that the flux swing is not expressed in terms Volts but rather in terms of volt-seconds. For this reason the VA product is replaced by a Volt-Ampere-Second product for magnetic components.

The current stress is expressed in terms of RMS current.

2.3.3 Component Stress Normalization

To this point the voltages have been normalized to the input voltage V_{in} and the currents have been normalized to V_{in}/Z_o. For a converter which operates over a given input voltage range a further step of normalization is required. Also, since the characteristic impedance, Z_o, is a design parameter, normalizing to this quantity is meaningless until the design is complete.

Taking into account the case where the converter is to be operated over a range of input voltages, the voltage stress is normalized to a reference input voltage.

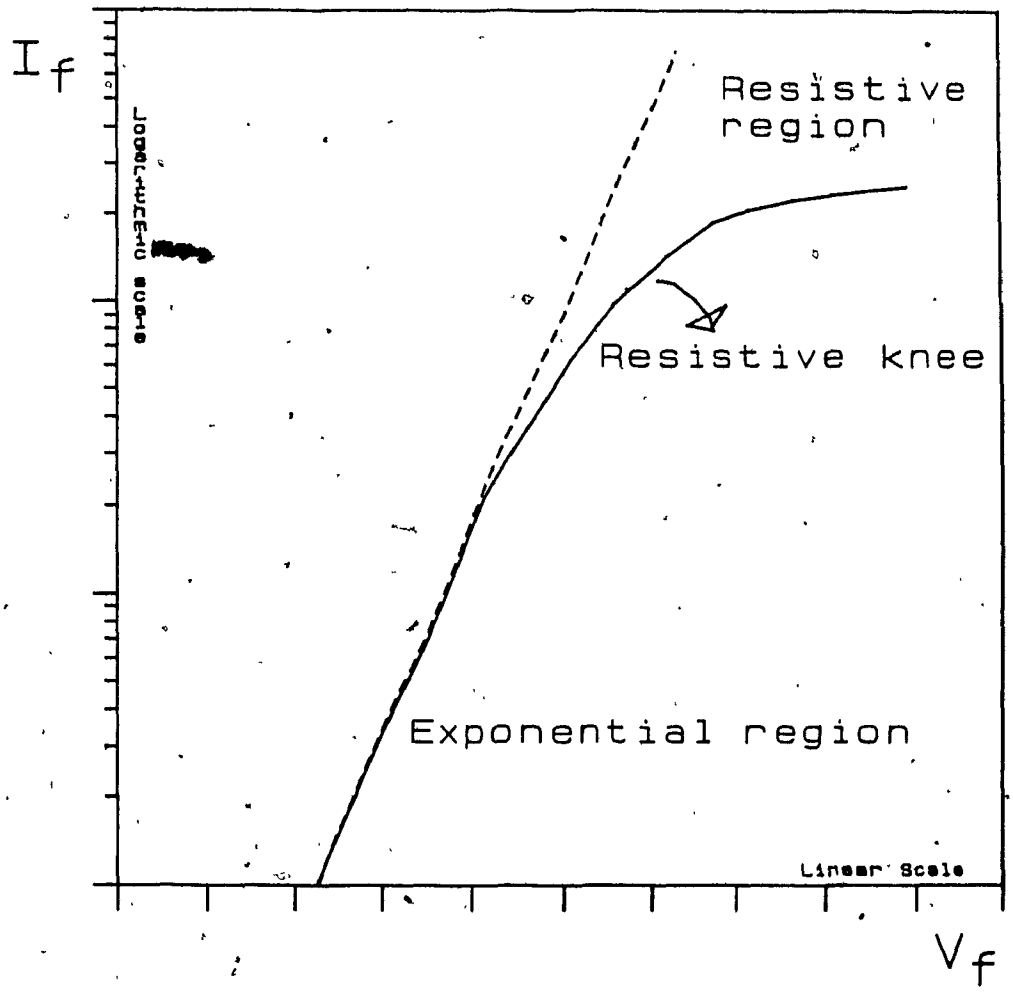

Figure 2-8: Typical Power Diode Forward Drop Characteristic.

$$V = \bar{V} \cdot \frac{V_{in}}{V_{in_{ref}}} \cdot V_{in_{ref}} \qquad (2.3.3\text{-}1)$$

For any given output voltage

$$V_o = M \cdot V_{in} = M_{ref} \cdot V_{in_{ref}} , \qquad (2.3.3\text{-}2)$$

and (2.3.3-1) can be rewritten

$$V = \bar{V} \cdot \frac{M_{ref}}{M} \cdot V_{in_{ref}} . \qquad (2.3.3\text{-}3)$$

M_{ref} can be arbitrarily chosen, but selecting M_{ref} as the largest possible value achievable over the entire control range provides a common reference point irrespective of the value of M selected to operate at any given input output voltage combination. For the converter under study, it has been seen that the maximum value for M is 1 for any value of $\bar{Q}$. Substituting in (2.3.3-3) yields,

$$V = \bar{V} \cdot \frac{1}{M} \cdot V_{in_{low}} , \qquad (2.3.3\text{-}4)$$

where $V_{in_{low}}$ is the minimum input voltage at which regulation is theoretically possible for a given output voltage. Note that, since for the converter under study M_{ref} is equal to 1, $V_{in_{low}}$ is equal to the output voltage reflected to the primary side of the transformer.

The normalization for the current can be made independent from Z_o by realizing that the output power is

$$P_o = \frac{V_o^2}{R_\ell} = \frac{M^2 V_{in}^2 Q}{Z_o} . \qquad (2.3.3\text{-}5)$$

Z_o can be substituted for into (2.2.0-7); the normalized current expression.

$$I = \bar{I} \cdot \frac{V_{in}}{Z_o}$$

$$= \bar{I} \cdot \frac{1}{M^2 Q} \cdot \frac{P_o}{V_{in}}$$

$$= \bar{I} \cdot \frac{1}{MQ} \cdot \frac{P_o}{V_{in_{low}}} \quad (2.3.3\text{-}6)$$

(2.3.3-4) and (2.3.3-6) are convenient to compute stresses using the mathematical description of the trajectories of the resonant voltage and current. These normalizations nevertheless seem abstract. Realizing that

$$I_o = \frac{V_o}{R_\ell} = MQ \frac{V_{in}}{Z_o} , \quad (2.3.3\text{-}7)$$

substituting for MQ into (2.3.3-6), multiplying the numerator and denominator of both (2.3.3-4) and (2.3.3-6) by V_{in} yields:

$$V = \frac{V}{V_o} \cdot V_{in_{low}} , \quad (2.3.3\text{-}8)$$

$$I = \frac{I}{I_o} \cdot \frac{P_o}{V_{in_{low}}} . \quad (2.3.3\text{-}9)$$

Multiplying the voltage across a device by the current through it at a given operating point gives

$$VA_{op} = \frac{V}{V_o} \cdot \frac{I}{I_o} \cdot P_o . \quad (2.3.3\text{-}10)$$

Therefore the normalizations of (2.3.3-4) and (2.3.3-5) are, in fact, simple normalizations to the output voltage and current.

2.3.4 Peak and RMS Resonant Current

Peak and RMS value of the resonant current are very useful in calculating component stresses.

2.3.4.1 $I_{r_{rms}}$

The rms value of the resonant current can be calculated on a half-cycle basis.

$$I_{r_{rms}}^2 = \frac{1}{T_h}\int_0^{T_h} I_r^2(t)\,\partial t$$

$$= \frac{1}{T_h}\int_{t_o}^{t_1} I_r^2(t)\,\partial t + \frac{1}{T_h}\int_{t_1}^{t_2} I_r^2(t)\,\partial t + \frac{1}{T_h}\int_{t_2}^{T_h} I_r^2(t)\,\partial t$$

$$\triangleq I_{rms_o}^2 + I_{rms_1}^2 + I_{rms_2}^2 \qquad (2.3.4\text{-}1)$$

Integrating it is found that

$$I_{rms_o}^2 = \frac{1}{2\omega_o T_h}\left[\overline{I_r(t_o)}^2\left[\omega_o t_1 + \frac{\sin(2\omega_o t_1)}{2}\right] + (1-\overline{V_c(t_o)}-M)^2\cdot\left[\omega_o t_1 - \frac{\sin(2\omega_o t_1)}{2}\right] + 2\cdot\overline{I_r(t_o)}\cdot(1-\overline{V_c(t_o)}-M)\cdot\sin^2(\omega_o t_1)\right]\cdot\left[\frac{1}{MQ}\cdot\frac{P_o}{V_{in_{low}}}\right]^2 \qquad (2.3.4\text{-}2)$$

and that

$$I^2_{rms_1} = \frac{1}{2\omega_o T_h}\left[\overline{I_r(t_1)}^2\left[\omega_o t_2-\omega_o t_1 + \frac{\sin[2(\omega_o t_2-\omega_o t_1)]}{2}\right] + \right.$$

$$+ (\beta+\overline{V_c(t_1)}+M)^2\cdot\left[\omega_o t_2-\omega_o t_1 - \frac{\sin[2(\omega_o t_2-\omega_o t_1)]}{2}\right] +$$

$$\left. - 2\cdot\overline{I_r(t_1)}\cdot(\beta+\overline{V_c(t_1)}+M)\cdot\sin^2(\omega_o t_2-\omega_o t_1)\right]\cdot\left[\frac{1}{MQ}\cdot\frac{P_o}{V_{in_{low}}}\right]^2 .$$

(2.3.4-3)

In discontinuous mode, the current is zero from t_2 to T_h and

$$I_{rms_2} = 0 . \qquad (2.3.4\text{-}4a)$$

In continuous mode

$$I^2_{rms_2} = \frac{1}{2\omega_o T_h}\left[(\beta-M\overline{Q}+M)^2\cdot\left[\omega_o T_h-\omega_o t_2-\frac{\sin[2(\omega_o T_h-\omega_o t_2)]}{2}\right]\right]\cdot\left[\frac{1}{MQ}\cdot\frac{P_o}{V_{in_{low}}}\right]^2 .$$

(2.3.4-4b)

Note that in discontinuous mode $\overline{I_r(t_o)}$ is zero and $\overline{V_c(t_o)}= -M\overline{Q}$, (2.3.4-2) reduces to

$$I^2_{rms_o} = \frac{1}{2\omega_o T_h}\left[(1+M\overline{Q}-M)^2\cdot\left[\omega_o t_1 - \frac{\sin(2\omega_o t_1)}{2}\right]\right]\cdot\left[\frac{1}{MQ}\cdot\frac{P_o}{V_{in_{low}}}\right]^2 .$$

(2.3.4-5)

2.3.4.2 $I_{r_{pk}}$

The maximum instantaneous value of the current occurs in the interval $t_o < t \leq t_1$. Taking the derivative of (2.2.2-7) and equating to zero yields

$$-\overline{I_r(t_o)}\cdot\sin(\omega_o t_{max}) + (1-\overline{V_c(t_o)}-M)\cdot\cos(\omega_o t_{max}) = 0 \quad . \qquad (2.3.4\text{-}6)$$

This is satisfied for

$$\omega_o t_{max} = \tan^{-1}\left[\frac{1-\overline{V_c(t_o)}-M}{\overline{I_r(t_o)}}\right] ; \qquad (2.3.4\text{-}7)$$

The maximum current is found from

$$I_{r_{pk}} = \overline{I_r(t_o)}\cdot\cos(\omega_o t_{pk}) + (1-\overline{V_c(t_o)}-M)\cdot\sin(\omega_o t_{pk}) \cdot \frac{1}{MQ}\cdot\frac{P_o}{V_{in_{low}}} , \qquad (2.3.4\text{-}8)$$

where

$$\omega_o t_{pk} = \begin{cases} \omega_o t_1 & \text{for } \omega_o t_1 < \omega_o t_{max} \\ \omega_o t_{max} & \text{for } \omega_o t_1 \geq \omega_o t_{max} \end{cases} \qquad (2.3.4\text{-}9)$$

Note that in discontinuous mode $I_r(t_o)=0$, $\overline{V_c(t_o)}=-MQ$. (2.3.4-7) and (2.3.4-8) reduce to

$$\omega_o t_{max} = \frac{\pi}{2} \qquad (2.3.4\text{-}10)$$

and

$$I_{r_{pk}} = (1+MQ-M)\cdot\sin(\omega_o t_{pk}) \cdot \frac{1}{MQ}\cdot\frac{P_o}{V_{in_{low}}} . \qquad (2.3.4\text{-}11)$$

2.3.5 Device Stress Calculations

Component and bus stresses are given for the full-bridge implementation only. The stress for the various half-bridge implementations of Figure 1-1 can be derived from the full-bridge results in a straightforward manner.

2.3.5.1 Input Bus Stress

The input bus voltage is

$$V_{str} = V_{in} = \frac{1}{M} \cdot V_{in_{low}} \qquad (2.3.5\text{-}1)$$

In PWM the current stress is given by

$$I_{str} = I_{r_{rms}} , \qquad (2.3.5\text{-}2)$$

where $I_{r_{rms}}$ is given by (2.3.4-1). For PSPWM operation

$$I_{str} = I_{rms_o} , \qquad (2.3.5\text{-}3)$$

where I_{rms_o} is given by (2.3.4-2).

2.3.5.2 Switch Stress

The maximum voltage any switch must block is equal to the bus voltage.

$$V_{str} = \frac{1}{M} \cdot V_{in_{low}} \qquad (2.3.5\text{-}4)$$

Current stress however differs depending on the control scheme or on the mode.

For PWM operation in either continuous or discontinuous conduction mode, S_1 and S_4 conduct from t_o to t_1. S_2 and S_3 conduct from t_3 to t_4. The current stress for any of the switches is therefore

$$I_{str_{s\ell}} = \frac{I_{rms_o}}{2^{1/2}} , \qquad (2.3.5\text{-}5)$$

where I_{rms_o} is given by (2.3.4-2).

In PSPWM discontinuous mode S_1 conducts from t_o to t_2 and S_2 conducts from t_3 to t_5. The current stress is

$$I^2_{str_{s1}} = I^2_{str_{s2}} = \frac{I^2_{rms_o} + I^2_{rms_1}}{2} . \qquad (2.3.5\text{-}6)$$

S_4 and S_3 conduct from t_o to t_1 and t_3 to t_4 respectively. The current stress for these switches is

$$I^2_{str_{s3}} = I^2_{str_{s4}} = \frac{I^2_{rms_o}}{2} . \qquad (2.3.5\text{-}7)$$

In PSPWM continuous mode S_1 and S_2 also conduct from t_o to t_2 and t_3 to t_5 and

$$I^2_{str_{s1}} = I^2_{str_{s2}} = \frac{I^2_{rms_o} + I^2_{rms_1}}{2} . \qquad (2.3.5\text{-}8)$$

S_3 and S_4 conduct from t_5 to t_1 and t_2 to t_4 respectively.

$$I^2_{str_{s3}} = I^2_{str_{s4}} = \frac{I^2_{rms_o} + I^2_{rms_2}}{2} \qquad (2.3.5\text{-}9)$$

2.3.5.3 Anti-parallel Diode Stress

The maximum voltage any anti-parallel diode must block is equal to the bus voltage.

$$V_{str} = \frac{1}{M} \cdot V_{in_{low}} \qquad (2.3.5\text{-}10)$$

The diode average current depends on the switching strategy and on the conduction mode. The average currents are given in terms of A_{1d}, A_{1c} and A_{2c} which are given by (2.2.1-21), (2.2.2-25) and (2.2.2-26). The normalization defined by (2.2.0-8) is used.

In PWM discontinuous mode D_1 and D_4 conducts from t_4 to t_6, D_2 and D_3 conducts from t_1 to t_2. The average current per diode is therefore,

$$I_{str_{dt}} = \frac{\overline{A_{1d}}}{2\pi} \cdot \frac{1}{MQ} \cdot \frac{P_o}{V_{in_{low}}} . \qquad (2.3.5\text{-}11)$$

In PWM continuous mode, D_1 and D_4 conduct from t_4 to t_5 and from t_2 to t_3, while D_2 and D_3 conduct from t_1 to t_2 and from t_5 to t_6. The average current per diode is given by

$$I_{str_{dt}} = \frac{\overline{A_{1c}}+\overline{A_{2c}}}{2\pi} \cdot \frac{1}{MQ} \cdot \frac{P_o}{V_{in_{low}}} . \qquad (2.3.5\text{-}12)$$

In PSPWM discontinuous mode, D_1 and D_2 never conduct.

$$I_{str_{d1}} = I_{str_{d2}} = 0 \qquad (2.3.5\text{-}13)$$

D_3 and D_4 conduct from t_1 to t_2 and t_4 to t_5 respectively. The current stress is therefore

$$I_{str_{d3}} = I_{str_{d4}} = \frac{\overline{A_{1d}}}{2\pi} \cdot \frac{1}{MQ} \cdot \frac{P_o}{V_{in_{low}}} . \qquad (2.3.5\text{-}14)$$

In PSPWM continuous mode, D_1 and D_2 conduct from t_5 to t_6 and t_2 to t_3 respectively. The current stress is

$$I_{str_{d1}} = I_{str_{d2}} = \frac{\overline{A_{2c}}}{2\pi} \cdot \frac{1}{MQ} \cdot \frac{P_o}{V_{in_{low}}} . \qquad (2.3.5\text{-}15)$$

D_3 and D_4 conduct from t_1 to t_2 and t_4 to t_5 respectively. The current stress is

$$I_{str_{d3}} = I_{str_{d4}} = \frac{\overline{A_{ic}}}{2\pi} \cdot \frac{1}{MQ} \cdot \frac{P_o}{V_{in_{low}}} . \qquad (2.3.5\text{-}16)$$

Since the diodes can have more than one conduction interval, evaluation of the diode forward voltage is simplified by considering its voltage drop at the peak resonant current (2.3.4-8).

2.3.5.4 Resonant Inductor Stress

The volt-second stress on the inductor is found as follows. Lenz law states that:

$$V_{\ell r} = \frac{\partial \lambda_{\ell r}(t)}{\partial t} \qquad (2.3.5\text{-}17)$$

where $V_{\ell r}$ is the voltage across the inductor and $\lambda_{\ell r}$ is the flux linkage of the inductor. Integrating (2.3.5-17), the Volt-seconds are found to be

$$V\text{-}s = \int_{t_a}^{t_b} V_{\ell r}(t) \cdot \partial t = \int_{\lambda_{\ell r}(t_a)}^{\lambda_{\ell r}(t_b)} \partial \lambda_{\ell r} = \lambda_{\ell r}(t_b) - \lambda_{\ell r}(t_a) , \qquad (2.3.5\text{-}18)$$

where $\lambda_{\ell r}(t_b)$ is the maximum flux linkage during the cycle and $\lambda_{\ell r}(t_a)$ is the minimum flux linkage. The flux linkage for linear inductors is defined as, [13],

$$\lambda = L \cdot I \qquad (2.3.5\text{-}19)$$

Consequently

$$\lambda_{\ell r}(t_a) = L_r \cdot (-I_{r_{pk}}) \qquad (2.3.5\text{-}20)$$

and

$$\lambda_{\ell r}(t_b) = L_r \cdot (+I_{r_{pk}}) \qquad (2.3.5\text{-}21)$$

The volt-second stress during a cycle is

$$V\text{-}s_{str} = \frac{\omega_o}{\omega_o} L_r \; 2 \cdot \overline{I_{r_{pk}}} \cdot \frac{V_{in}}{Z_o}$$

$$= 2 \cdot \overline{I_{r_{pk}}} \cdot \frac{1}{M} \frac{V_{in_{low}}}{\omega_o} \qquad (2.3.5\text{-}22)$$

The current circulating in the inductor is the resonant current. Therefore, the current stress is

$$I_{str} = I_{r_{rms}} \qquad (2.3.5\text{-}23)$$

2.3.5.5 Resonant Capacitor Stress

The maximum instantaneous voltage across the resonant capacitor has been found to be

$$V_{c_{max}} = MQ \cdot V_{in} = Q \cdot V_{in_{low}} \qquad (2.3.5\text{-}24)$$

The current circulating through the resonant capacitor is the resonant current. Therefore, the current stress is

$$I_{str} = I_{r_{rms}} \qquad (2.3.5\text{-}25)$$

The maximum instantaneous current for $\partial V/\partial t$ calculations is

$$I_{cr_{pk}} = I_{r_{pk}} \qquad (2.3.5\text{-}26)$$

2.3.5.6 Transformer Stress

The transformer Volt-second stress depends on the switching strategy and on the conduction mode.

In PWM discontinuous mode the voltage impressed across the transformer during conduction is equal to the output voltage. At t_2, the magnetizing current must still flow. The current flows trough the output rectifier and the transformer voltage reverses to $-V_o$. Assuming a linear magnetizing inductance and t_2 to be less than half of the half-period,

$$t_2 < \frac{T_h}{2} , \qquad (2.3.5\text{-}27)$$

the magnetizing inductance will be reset at $2 \cdot t_2$. Since the voltage applied across the transformer is $-V_o$ from t_2 to $2 \cdot t_2$ and again $-V_o$ from t_3 to t_5 the Volt-seconds are

$$V\text{-}s_{str} = 2 \cdot V_o \cdot t_2 = 2 \cdot \omega_o t_2 \cdot \frac{V_{in_{low}}}{\omega_o} . \qquad (2.3.5\text{-}28)$$

In PSPWM discontinuous mode, the voltage across the transformer is $-V_{c_{pk}}$ from t_2 to $t_3=T_h$ and is $-V_o$ from t_3 to t_5 the Volt-seconds are

$$V\text{-}s_{str} = V_o \cdot t_2 + V_{c_{pk}}(T_h - t_2)$$

$$= [\ \omega_o t_2 + \overline{Q} \cdot (\omega_o T_h - \omega_o t_2)\ ] \cdot \frac{V_{in_{low}}}{\omega_o} . \qquad (2.3.5\text{-}29)$$

In PWM discontinuous mode and $t_2 > T_h/2$, PWM continuous mode or PSPWM continuous mode, the voltage across the transformer is a square wave of period $2T_h$ and of amplitude V_o. For these three cases, the volt-seconds applied across the transformer are

$$V\text{-}s = \omega_o T_h\ M \cdot \frac{V_{in}}{\omega_o} = \omega_o T_h \cdot \frac{V_{in_{low}}}{\omega_o} . \qquad (2.3.5\text{-}30)$$

The current flowing in any winding of the transformer, neglecting magnetizing current, is proportional to the current flowing in the primary of the transformer. Therefore, the current stress is

$$I_{str} = I_{r_{rms}} \qquad (2.3.5\text{-}31)$$

2.3.5.7 Output Rectifier Stress

The output rectifier voltage stress depends on the full-wave rectification scheme used. Rectifying with a four-diode bridge and assuming perfect matching of the diodes, the voltage across each diode is half the output voltage

$$V_{str} \doteq \frac{1}{2} \cdot V_{in_{low}} \qquad (2.3.5\text{-}32)$$

For the center tap transformer of Figure 2-1, the maximum reverse voltage across a rectifying diode is

$$V_{str} = 2 \cdot V_{in_{low}} \qquad (2.3.5\text{-}33)$$

The average current for each diode is

$$I_{avg} = \frac{I_o}{2} = \frac{1}{2} \cdot \frac{P_o}{V_{in_{low}}} \qquad (2.3.5\text{-}34)$$

Since the average current is the same for any selection of nominal M,Q, the current stress used to compare VA_{op} for various selections of M,Q is taken to be the peak current.

$$I_{str} = I_{r_{pk}} \qquad (2.3.5\text{-}35)$$

2.3.5.8 Output Capacitor Stress

From the small-ripple assumption the maximum voltage across the output capacitor is

$$V_{str} = M \cdot V_{in} = V_{in_{low}} \qquad (2.3.5\text{-}36)$$

The capacitor rms current is found from

$$I^2_{co_{rms}} = \frac{1}{T_h} \int_{t=0}^{t=T_h} (|I_r(t)| - I_o)^2 \, \partial t$$

$$= \frac{1}{T_h} \int_{t=0}^{t=T_h} I^2_r(t) \, \partial t - 2 \frac{I_o}{T_h} \int_{t=0}^{t=T_h} |I_r(t)| \, \partial t + \frac{I^2_o}{T_h} \int_{t=0}^{t=T_h} \partial t \,. \qquad (2.3.5\text{-}37)$$

The first term is recognized to be the squared value of the resonant current rms value. Division of the integral of the second term by T_h yields the average output current, I_o. (2.3.5-37) simplifies to:

$$I^2_{co_{rms}} = I^2_{r_{rms}} - I^2_o \qquad (2.3.5\text{-}38)$$

Defining,

$$\overline{\overline{I_{r_{rms}}}} \equiv I_{r_{rms}} \cdot \frac{V_{in_{low}}}{P_o} \qquad (2.3.5\text{-}39)$$

The output capacitor stess is expressed as

$$I^2_{str} = \left[\overline{\overline{I_{r_{rms}}}}^2 - 1 \right] \cdot \left[\frac{P_o}{V_{in_{low}}} \right]^2 . \qquad (2.3.5\text{-}40)$$

CHAPTER 3: SMALL-SIGNAL ANALYSIS

3.1 CLOSED LOOP SYSTEM

In the previous chapter, the steady state-analysis of the converter is carried out. DC-to-DC converters are generally operated in closed loop to improve load and line regulation. Closed-loop systems must be designed to be stable under all operation conditions. A stability analysis is therefore performed.

The control method analyzed is voltage-mode control. In this mode the output voltage is compared to a voltage reference. The error voltage is amplified by the voltage error-amplifier. The output of the error-amp is fed to a circuit that modulates the pulse width of the converter. This system is illustrated in block form in Figure 3-1. The open loop transfer function of a voltage-mode controlled PWM converter can therefore be written as

$$\frac{v_o(s)}{v_o'(s)} = A(s)\cdot PWM(s)\cdot G(s) \quad , \qquad (3.1.0\text{-}1)$$

where,

$$A(s) \equiv \text{voltage error amplifier transfer function} \quad , \qquad (3.1.0\text{-}2)$$

$$PWM(s) \equiv \text{pulse-width modulator transfer function} \quad , \qquad (3.1.0\text{-}3)$$

$$G(s) \equiv \text{converter transfer function} \quad . \qquad (3.1.0\text{-}4)$$

The generation of transfer functions of voltage error amplifiers with operational amplifiers is a well-known subject and need not be discussed here.

The pulse-width modulator is illustrated in Figure 3-2. The output of the error-amplifier v_{amp} is compared to a constant frequency ramp. When the ramp voltage exceeds the error-amp voltage, the output pulse is terminated. The output pulse is re-initiated when the ramp is

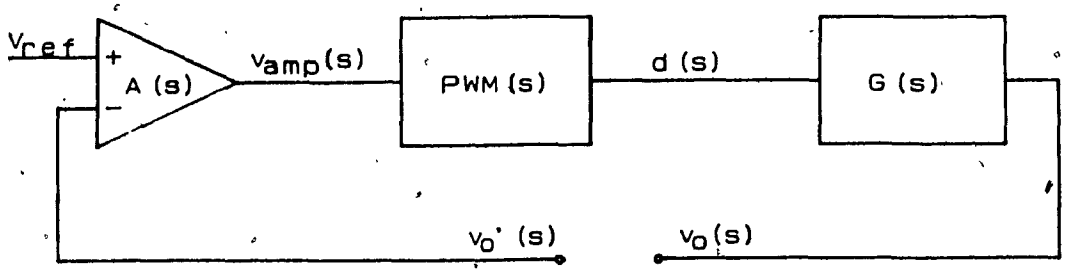

Figure 3-1: Converter Open-Loop Block Diagram

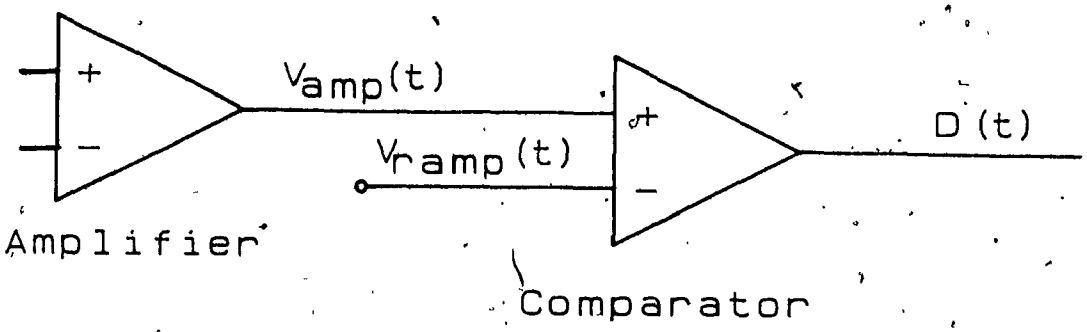

Figure 3-2: Pulse-Width Modulator

reset at the next clock pulse. Figure 3-3a) illustrates, in time, the ramp voltage, V_{ramp}, the steady-state error-amplifier voltage, V_{amp}, and a modulated error-amplifier output voltage, v_{amp}. The resulting steady-state pulse train, $D(t)$, is illustrated in Figure 3-3b). The modulated pulse train, $d(t)$ is shown in Figure 3.3c). The perturbation in pulse width,

$$\Delta d(t) = d(t) - D(t) , \qquad (3.1.0\text{-}5)$$

is illustrated in Figure 3-3d). In the small-signal limit, the sequence of pulses of Figure 3-3d) reduces to a sequence of weighted impulses. The pulse-width modulator samples the voltage error-amp output voltage.

A pulse-width modulated converter is therefore a sampled data system, and the tools of discrete time control systems can thus be used to analyze it. This fact has been recognized before in the study of switching-converters [7,14,15]. More recently, a method named *Small-Signal Frequency Response Theory for Ideal DC-to-DC Converter Systems* has been introduced [16,17]. This method is very general and it is applicable to a wide range of converters. In particular, it is applicable to the converter under study in this thesis.

Small-Signal Frequency Response Theory is therefore used to find the transfer function of the converter under study. Some of the material given in [16,17] is re-exposed as the method given therein requires some detailed explanation to be understood. The steps of the procedure are also re-arranged to be able to use the familiar block diagram approach.

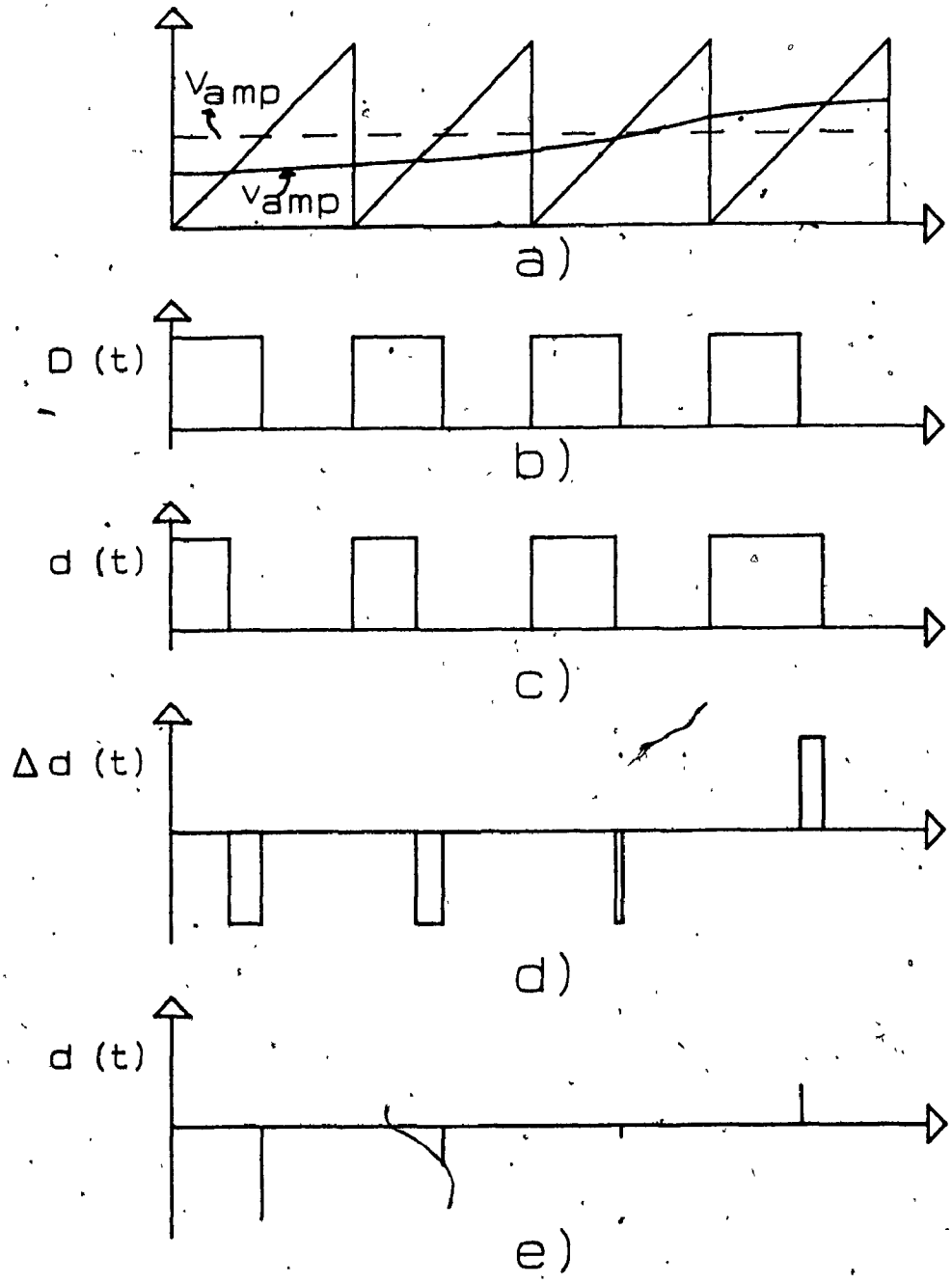

Figure 3-3: Pulse-Width Modulation
a) Comparison with ramp
b) Steady-state pulse train
c) Modulated pulse train
d) Pulse-width perturbation
e) Small-signal pulse-width perturbation

3.2 SMALL-SIGNAL FREQUENCY RESPONSE THEORY

The structure of switch-mode DC-DC converter varies in time, and consequently the DC-DC systems are non-linear. In Chapter 2, the steady state with both PWM and PSPWM was determined. *Small-Signal Frequency Response Theory*, outlines a method of linearizing DC-to-DC converters around their steady-state operating point. The mathematical formulation used is that of State Space. Since the structure of a DC-to-DC converter is variable in time, the coefficients of the state equation and output equation are a function of time. The state and output equations are of the form

$$\dot{x}(t) = A(t)\cdot x(t) + B(t)\cdot u(t) \qquad (3.2.0\text{-}1)$$

and

$$y(t) = C(t)\cdot x(t) + D(t)\cdot u(t)\ , \qquad (3.2.0\text{-}2)$$

where $x(t)$ is the state vector, $u(t)$ is the input vector, $y(t)$ is the output vector, $A(t)$ is the system matrix, $B(t)$ is the input matrix, $C(t)$ is the output matrix and $D(t)$ is the transmission matrix.

A converter must satisfy requirements listed in [17] to apply *Small-Signal Frequency Response Theory*. Summarizing these requirements, the converter must have the following properties:

1- $A(t), B(t), C(t)$, and $D(t)$ are piecewise constant functions in time.

$$(A(t), B(t), C(t), D(t)) = (A_J, B_J, C_J, D_J), \qquad (3.2.0\text{-}3)$$

for $t_J < t < t_{J+1}$

This implies that in between the switching instants, the system is described by a linear differential equation. The system differential equation has piecewise constant coefficients in

time.

2- The system is controlled by modulating the switching instants.

3- The switching time is zero.

4- In steady state, the system is periodic. That is:

a) The sequence $\{(A_j,B_j,C_j,D_j)\}$ is periodic with period N_q; i.e.;

$$(A_j,B_j,C_j,D_j) = (A_{j+N_q},B_{j+N_q},C_{j+N_q},D_{j+N_q}) \qquad (3.2.0\text{-}4)$$

b) Define $T_j = t_{j+1} - t_j$. The sequence T_j is periodic with period N_t.

$$T_j = T_{j+N_t} \qquad (3.2.0\text{-}5)$$

c) The t_j's are modulated by a given control method with a period N_m.

d) The least common multiplier of N_q, N_t, N_m is defined to be N_s, the number of switched states.

$$N_s \equiv \text{lcm}(N_q,N_t,N_m) \qquad (3.2.0\text{-}6)$$

The converter under study satisfies property 1. The steady state of the converter was determined using a differential equation with piecewise constant coefficients. The converter satisfies property 2, as it is controlled by varying the moment switches turn off. Property 3 is not a property of the physical converters but a property of the model used to represent it. It is assumed that if switching times are short enough, the model will yield significant information on the actual converter.

In Chapter 2, it is assumed that the converters operation is periodic. Solutions to the equations thus formulated are found, property 4 is therefore also satisfied. It is shown in Chapter 2 that the absolute value of the resonant current and voltage is periodic and that the value of these variables reverse sign during the period T_h. The resonant current and voltage are therefore periodic with period $2T_h$. From the analysis of Chapter 2, $N_q=6$ switched networks are therefore identified. Each half-cycle being the mirror image of the other, the T_J are periodic with $N_t=3$. The duty cycle can be controlled twice per cycle; therefore, $N_m=3$. The least common multiplier of N_q, N_t, N_m is 6, therefore, $N_s=6$; there are six switched states. The notation is established on that basis by letting

$$T_4 \equiv T_1 , \qquad (3.2.0\text{-}7)$$

$$T_5 \equiv T_2 , \qquad (3.2.0\text{-}8)$$

$$T_6 \equiv T_3 . \qquad (3.2.0\text{-}9)$$

In this thesis, *Small-Signal Frequency Response Theory* is applied by performing three steps:

1- Describe mathematically the trajectory of the state vector.

2- Subtract the trajectory of the state vector of a perturbed system from the trajectory of the state vector of a system in steady state, and describe the trajectory of the state perturbation in the small-signal limit.

3- From the time domain analysis of step 2, find the transfer function of the converter to the control input by using a block diagram approach and by using transform methods.

3.3 STATE TRAJECTORY: Third Order System

In Chapter 2, the trajectories of the resonant current and resonant voltage are found by replacing the output filter and the load by a constant voltage source. Since it is precisely the trajectory in time of the output voltage that is to be studied, this simplification must be abandoned. Nevertheless, the assumption of a much smaller output voltage ripple compared to its steady state value must be retained for the solution found in Chapter 2 to be applicable.

The set of differential equations governing the trajectory of the variables in time is now of the third order. Since this set is reformulated, the opportunity is used to include the effect of two types of parasitic resistances. First, the resistances which are in series with the resonant branch are identified. These resistances are the intrinsic resistances of the components used: switches, resonant inductor, transformer, etc. These resistances are lumped as the total resonant resistance R_{rt} in Figure 3-4. Note that the value of R_{rt} can vary from one switched state to the next. For simplicity of notation R_{rt} is assumed to be constant in the following discussion. The variation of R_{rt}, can be easily taken into account when numerically deriving the system matrices. The second type of parasitic resistance is the equivalent series resistance (esr) of the output capacitor. The esr of the output capacitor is denoted as R_c in Figure 3-4.

Note that the parasitic resistances will effectively change the steady-state trajectory of the system. For the results found in Chapter 2 to remain valid, the following must be satisfied:

$$\frac{R_{rt}}{Z_o} << 1 , \qquad (3.3.0\text{-}1)$$

$$\frac{R_c}{Z_o} << 1 . \qquad (3.3.0\text{-}1)$$

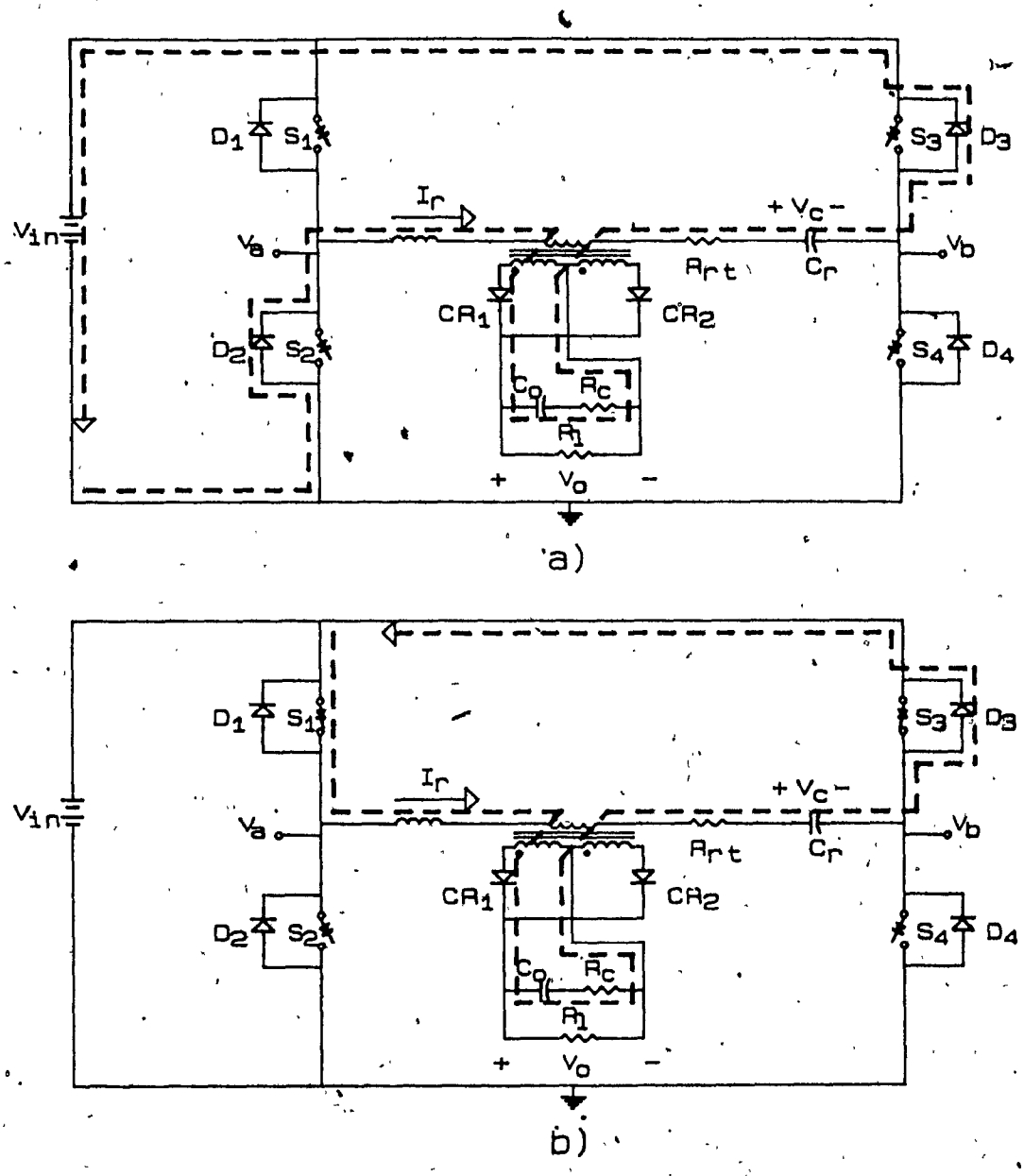

Figure 3-4: Current Path for $t_1 < t < t_2$.
a) PWM
b) PSPWM

The complete cycle of the converter can be divided in six periods. For convenience in notation, the beginning of the cycle is taken at t_1, the instant at which the pulse is terminated.

The six differential equations for both continuous and discontinuous modes are hereafter derived.

3.3.1 Continuous Mode

The current path during this first interval, $t_1 < t < t_2$, is illustrated in Figures 3-4a) and 3-4b) for PWM and PSPWM operation respectively. The resulting equivalent circuit is shown in Figure 3-5a), where β is defined by (2.2.0-9). The differential equation for this equivalent circuit is written as:

$$\begin{bmatrix} \dot{i}_r \\ \dot{v}_r \\ \dot{v}_{co} \end{bmatrix} = \begin{bmatrix} \frac{-1}{L_r}\cdot\left[\frac{R_c\cdot R_\ell}{R_c+R_\ell} + R_{rt}\right] & \frac{-1}{L_r} & \frac{-1}{L_r}\cdot\frac{R_\ell}{R_c+R_\ell} \\ \frac{1}{C_r} & 0 & 0 \\ \frac{1}{C_o}\cdot\frac{R_\ell}{R_c+R_\ell} & 0 & \frac{-1}{C_o}\cdot\frac{1}{R_c+R_\ell} \end{bmatrix} \cdot \begin{bmatrix} i_r \\ v_r \\ v_{co} \end{bmatrix}$$

$$- \begin{bmatrix} \frac{1}{L_r} \\ 0 \\ 0 \end{bmatrix} \cdot \beta\cdot V_{in} \qquad (3.3.1\text{-}1)$$

Factoring ω_o,

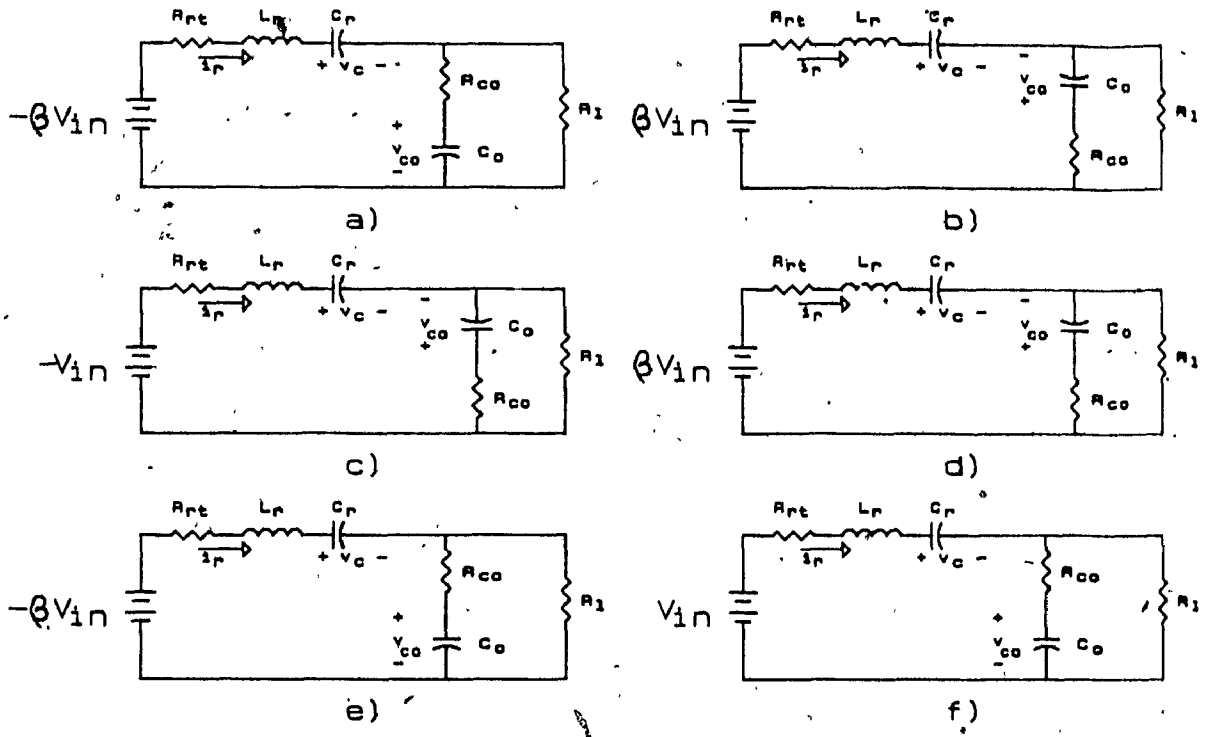

Figure 3-5: Equivalent Circuits for each Switched-State
a) $t_1 < t < t_2$
b) $t_2 < t < t_3$
c) $t_3 < t < t_4$
d) $t_4 < t < t_5$
e) $t_5 < t < t_6$
f) $t_6 < t < t_1$

$$\begin{bmatrix} \dot{i}_r \\ \dot{v}_r \\ \dot{v}_{co} \end{bmatrix} = \omega_o \begin{bmatrix} \frac{-1}{Z_o} \cdot \left[\frac{R_c \cdot R_\ell}{R_c+R_\ell} \cdot \frac{Z_o}{Z_o} + R_{rt} \right] & \frac{-1}{Z_o} & \frac{-1}{Z_o} \cdot \frac{R_\ell}{R_c+R_\ell} \cdot \frac{Z_o}{Z_o} \\ Z_o & 0 & 0 \\ \frac{1}{C_o\omega_o} \cdot \frac{Z_o}{Z_o} \cdot \frac{R_\ell}{R_c+R_\ell} \cdot \frac{Z_o}{Z_o} & 0 & \frac{1}{C_o\omega_o} \cdot \frac{1}{R_c+R_\ell} \cdot \frac{Z_o}{Z_o} \end{bmatrix} \cdot \begin{bmatrix} i_r \\ v_r \\ v_{co} \end{bmatrix}$$

$$- \omega_o \cdot \begin{bmatrix} \frac{1}{Z_o} \\ 0 \\ 0 \end{bmatrix} \cdot \beta \cdot V_{in} \qquad (3.3.1\text{-}2)$$

Defining

$$Q_{rt} \equiv \frac{Z_o}{R_{rt}} , \qquad (3.3.1\text{-}3)$$

$$Q_{co} \equiv \frac{Z_o}{R_c} , \qquad (3.3.1\text{-}4)$$

$$\bar{Z}_{co} \equiv \frac{1}{Z_o C_o \omega_o} = \frac{Z_{co}}{Z_o}, \qquad (3.3.1\text{-}5)$$

and substituting together with (2.2.0-3) into (3.3.1-2) yields

$$\begin{bmatrix} \dot{i}_r \\ \dot{v}_r \\ \dot{v}_{co} \end{bmatrix} = \omega_o \cdot \begin{bmatrix} \frac{-1}{Q+Q_{co}} + \frac{-1}{Q_{rt}} & \frac{-1}{Z_o} & \frac{-1}{Z_o} \cdot \frac{Q_{co}}{Q+Q_{co}} \\ Z_o & 0 & 0 \\ Z_o \cdot \bar{Z}_{co} \frac{Q_{co}}{Q+Q_{co}} & 0 & -\bar{Z}_{co} \cdot \frac{Q \cdot Q_{co}}{Q+Q_{co}} \end{bmatrix} \cdot \begin{bmatrix} i_r \\ v_r \\ v_{co} \end{bmatrix} - \omega_o \cdot \begin{bmatrix} \beta \cdot \frac{V_{in}}{Z_o} \\ 0 \\ 0 \end{bmatrix}$$

(3.3.1-6)

The normalized equation is obtained by multiplying the first row by Z_o/V_{in} and the second and third rows by $1/V_{in}$.

$$\begin{bmatrix} \dot{\overline{i_r}} \\ \dot{\overline{v_r}} \\ \dot{\overline{v_{co}}} \end{bmatrix} = \omega_o \cdot \begin{bmatrix} \frac{-1}{Q+Q_{co}} + \frac{-1}{Q_{rt}} & -1 & \frac{-Q_{co}}{Q+Q_{co}} \\ 1 & 0 & 0 \\ \overline{Z}_{co} \cdot \frac{Q_{co}}{Q+Q_{co}} & 0 & -\overline{Z}_{co} \cdot \frac{Q \cdot Q_{co}}{Q+Q_{co}} \end{bmatrix} \cdot \begin{bmatrix} \overline{i_r} \\ \overline{v_r} \\ \overline{v_{co}} \end{bmatrix} - \omega_o \cdot \begin{bmatrix} \beta \\ 0 \\ 0 \end{bmatrix} \qquad (3.3.1\text{-}7)$$

The output equation can be written as

$$v_o = \begin{bmatrix} \frac{R_c \cdot R_\ell}{R_c+R_\ell} & 0 & \frac{R_\ell}{R_c+R_\ell} \end{bmatrix} \cdot \begin{bmatrix} i_r \\ v_r \\ v_{co} \end{bmatrix} \qquad (3.3.1\text{-}8)$$

Normalizing the resistances to Z_o, and dividing both sides of the equations by V_{in},

$$\frac{v_o}{V_{in}} = \begin{bmatrix} \frac{Z_o}{V_{in}} \frac{1}{Q+Q_{co}} & 0 & \frac{1}{V_{in}} \frac{Q_{co}}{Q+Q_{co}} \end{bmatrix} \cdot \begin{bmatrix} i_r \\ v_r \\ v_{co} \end{bmatrix} \qquad (3.3.1\text{-}9)$$

Normalizing according to (2.2.0-6) and (2.2.0-7)

$$\overline{v_o} = \begin{bmatrix} \frac{1}{Q+Q_{co}} & 0 & \frac{Q_{co}}{Q+Q_{co}} \end{bmatrix} \cdot \begin{bmatrix} \overline{i_r} \\ \overline{v_r} \\ \overline{v_{co}} \end{bmatrix} \qquad (3.3.1\text{-}10)$$

Defining,

$$x \equiv \begin{bmatrix} \overline{i_r} \\ \overline{v_r} \\ \overline{v_{co}} \end{bmatrix} \qquad (3.3.1\text{-}11)$$

and

$$y = \overline{v_o} \ , \qquad (3.3.1\text{-}12)$$

the state and output equations can be written as follows:

$$\dot{x} = \omega_o \cdot (A_l \cdot x + B_l) \ , \qquad (3.3.1\text{-}13)$$

$$y = C_l \cdot x \ . \qquad (3.3.1\text{-}14)$$

Equivalent circuits are given in Figures 3-5a) to 3-5f) for the six switched states. The matrices for each switching interval are now given.

$t_1 < t < t_2$

$$A_1 = \begin{bmatrix} \frac{-1}{Q+Q_{co}} + \frac{-1}{Q_r t} & -1 & \frac{-Q_{co}}{Q+Q_{co}} \\ 1 & 0 & 0 \\ \frac{1}{Z_{co}} \cdot \frac{Q_{co}}{Q+Q_{co}} & 0 & -Z_{co} \cdot \frac{Q \cdot Q_{co}}{Q+Q_{co}} \end{bmatrix} \qquad (3.3.1\text{-}15)$$

$$B_1 = \begin{bmatrix} -\beta \\ 0 \\ 0 \end{bmatrix} \qquad (3.3.1\text{-}16)$$

$$C_1 = \begin{bmatrix} \frac{1}{Q+Q_{co}} & 0 & \frac{Q_{co}}{Q+Q_{co}} \end{bmatrix} \qquad (3.3.1\text{-}17)$$

$t_2 < t < t_3$

$$A_2 = \begin{bmatrix} \frac{-1}{Q+Q_{co}} + \frac{-1}{Q_{rt}} & -1 & \frac{Q_{co}}{Q+Q_{co}} \\ 1 & 0 & 0 \\ -\overline{Z_{co}} \cdot \frac{Q_{co}}{Q+Q_{co}} & 0 & -\overline{Z_{co}} \cdot \frac{Q \cdot Q_{co}}{Q+Q_{co}} \end{bmatrix} \qquad (3.3.1\text{-}18)$$

$$B_2 = \begin{bmatrix} \beta \\ 0 \\ 0 \end{bmatrix} \qquad (3.3.1\text{-}19)$$

$$C_2 = \begin{bmatrix} \frac{-1}{Q+Q_{co}} & 0 & \frac{Q_{co}}{Q+Q_{co}} \end{bmatrix} \qquad (3.3.1\text{-}20)$$

$t_3 < t < t_4$

$$A_3 = \begin{bmatrix} \frac{-1}{Q+Q_{co}} + \frac{-1}{Q_{rt}} & -1 & \frac{Q_{co}}{Q+Q_{co}} \\ 1 & 0 & 0 \\ -\overline{Z_{co}} \cdot \frac{Q_{co}}{Q+Q_{co}} & 0 & -\overline{Z_{co}} \cdot \frac{Q \cdot Q_{co}}{Q+Q_{co}} \end{bmatrix} \qquad (3.3.1\text{-}21)$$

$$B_3 = \begin{bmatrix} -1 \\ 0 \\ 0 \end{bmatrix} \qquad (3.3.1\text{-}22)$$

$$C_3 = \begin{bmatrix} \frac{-1}{Q+Q_{co}} & 0 & \frac{Q_{co}}{Q+Q_{co}} \end{bmatrix} \qquad (3.3.1\text{-}23)$$

$t_4 < t < t_5$

$$A_4 = \begin{bmatrix} \frac{-1}{Q+Q_{co}} + \frac{-1}{Q_{rt}} & -1 & \frac{Q_{co}}{Q+Q_{co}} \\ 1 & 0 & 0 \\ -\overline{Z_{co}} \cdot \frac{Q_{co}}{Q+Q_{co}} & 0 & -\overline{Z_{co}} \cdot \frac{Q \cdot Q_{co}}{Q+Q_{co}} \end{bmatrix} \qquad (3.3.1\text{-}24)$$

$$B_4 = \begin{bmatrix} \beta \\ 0 \\ 0 \end{bmatrix} \qquad (3.3.3\text{-}25)$$

$$C_4 = \begin{bmatrix} \frac{-1}{Q+Q_{co}} & 0 & \frac{Q_{co}}{Q+Q_{co}} \end{bmatrix} \qquad (3.3.3\text{-}26)$$

$t_5 < t < t_6$

$$A_5 = \begin{bmatrix} \frac{-1}{Q+Q_{co}} + \frac{-1}{Q_{rt}} & -1 & \frac{-Q_{co}}{Q+Q_{co}} \\ 1 & 0 & 0 \\ \overline{Z_{co}} \cdot \frac{Q_{co}}{Q+Q_{co}} & 0 & -\overline{Z_{co}} \cdot \frac{Q \cdot Q_{co}}{Q+Q_{co}} \end{bmatrix} \qquad (3.3.1\text{-}27)$$

$$B_5 = \begin{bmatrix} -\beta \\ 0 \\ 0 \end{bmatrix} \qquad (3.3.1\text{-}28)$$

$$C_5 = \begin{bmatrix} \frac{1}{Q+Q_{co}} & 0 & \frac{Q_{co}}{Q+Q_{co}} \end{bmatrix} \qquad (3.3.1\text{-}29)$$

$t_6 < t < t_1$

$$A_6 = \begin{bmatrix} \frac{-1}{Q+Q_{co}} + \frac{-1}{Q_r t} & -1 & \frac{-Q_{co}}{Q+Q_{co}} \\ 1 & 0 & 0 \\ \frac{}{Z_{co}} \cdot \frac{Q_{co}}{Q+Q_{co}} & 0 & -\frac{}{Z_{co}} \cdot \frac{Q \cdot Q_{co}}{Q+Q_{co}} \end{bmatrix} \qquad (3.3.1\text{-}30)$$

$$B_6 = \begin{bmatrix} 1 \\ 0 \\ 0 \end{bmatrix} \qquad (3.3.1\text{-}31)$$

$$C_6 = \begin{bmatrix} \frac{1}{Q+Q_{co}} & 0 & \frac{Q_{co}}{Q+Q_{co}} \end{bmatrix} \qquad (3.3.1\text{-}32)$$

3.3.2 Discontinuous Mode

Continuous mode equations derived for $t_1 < t < t_3$ and $t_4 < t < t_6$ are also applicable to the discontinuous case. Left are the intervals $t_3 < t < t_4$ and $t_6 < t < t_1$. The same set of equations applies for both intervals.

During the non-conducting interval, the resonant current and voltage do not vary. The resonant current is zero and the output capacitor is discharged through the load only. The equivalent circuit is given in Figure 3-6. The equations describing the circuit are found to be

$$\dot{x} = \omega_o (A_l \cdot x + B_l) , \qquad (3.3.2\text{-}1)$$

$$y = C_l \, x , \qquad (3.3.2\text{-}2)$$

where the subscript l can take the value 3 or 6 and where

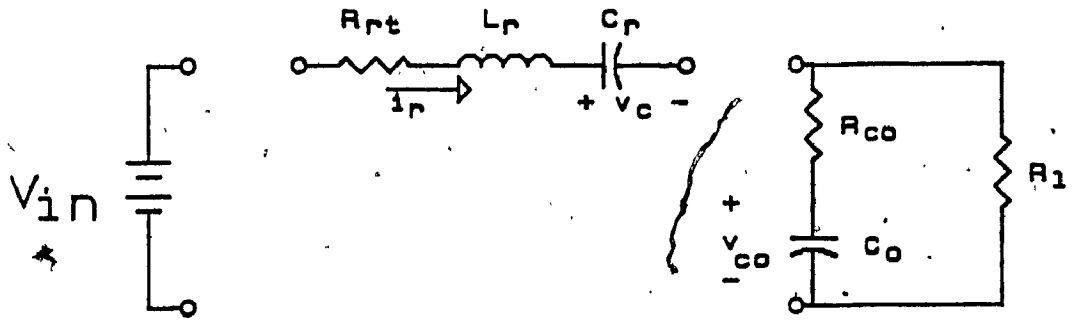

Figure 3-6: Equivalent Circuit in Discontinuous Conduction Mode for $t_2<t<t_3$ and $t_5<t<t_6$.

$$A_l = \begin{bmatrix} 0 & 0 & 0 \\ 0 & 0 & 0 \\ 0 & 0 & -\overline{Z_{co}} \cdot \frac{Q \cdot Q_{co}}{Q+Q_{co}} \end{bmatrix}, \qquad (3.3.2\text{-}3)$$

$$B_l = \begin{bmatrix} 0 \\ 0 \\ 0 \end{bmatrix}, \qquad (3.3.2\text{-}4)$$

$$C_l = \begin{bmatrix} 0 & 0 & \frac{Q_{co}}{Q+Q_{co}} \end{bmatrix}. \qquad (3.3.2\text{-}5)$$

3.4 SMALL-SIGNAL TRAJECTORY

The mathematical formulation of the state trajectory is complete. The study of the trajectory of a system which is forced to deviate from its steady-state trajectory by a signal of small amplitude added to the steady-state value of the voltage error-amplifier output is now be performed. Subtracting the perturbed trajectory from the steady state, attention is directed on the trajectory of the state perturbation.

In the following sections, continuous conduction mode is used for illustration purpose. The discontinuous mode can be seen as a special case of the continuous case. The formulation derived hereafter also applies to the discontinuous case by using the matrices of section 3.3.2.

3.4.1 Definitions

For the convenience of describing the problem, several variables are defined. Figure 3-7 illustrates the definitions using the resonant current as an example.

$$\mathbf{X}(t) \qquad (3.4.1\text{-}1)$$

is the steady-state vector of the system.

$$\mathbf{x}(t) \qquad (3.4.1\text{-}2)$$

is the state-vector of the perturbed system.

$$\Delta\mathbf{x}(t) \equiv \mathbf{x}(t) - \mathbf{X}(t) \qquad (3.4.1\text{-}3)$$

is the state perturbation of the system.

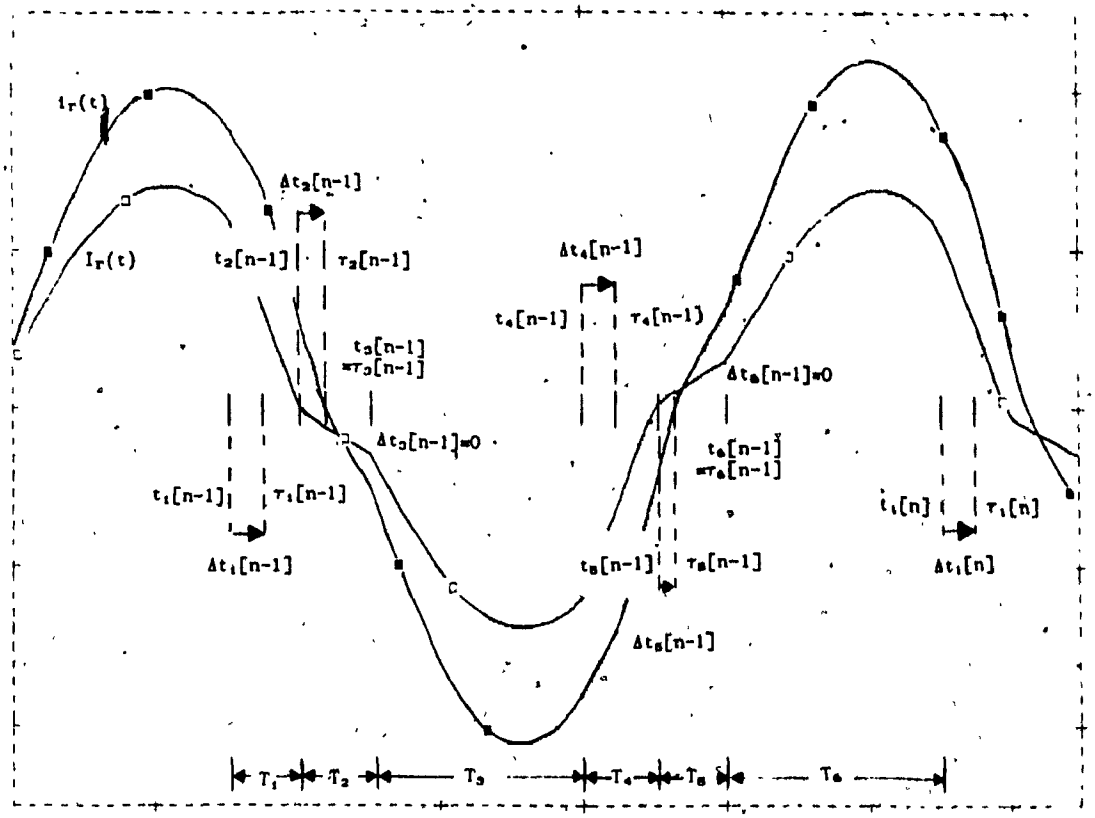

a)

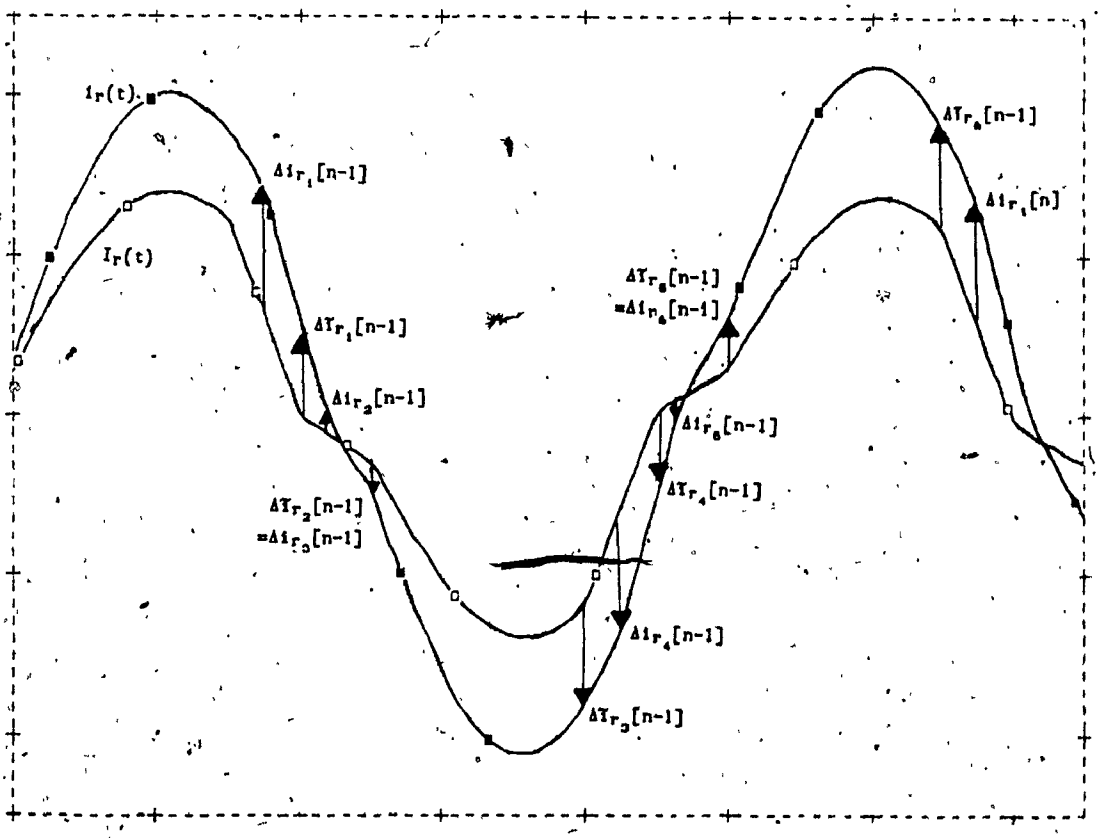

b)

Figure 3-7: Small-Signal Trajectory Variable Definitions
a) Switching instants and switched-state periods.
b) Current Perturbation

$$t_i[n] \equiv t_{i+n\cdot N_s} \qquad (3.4.1\text{-}4)$$

is the steady-state switching instant between switched state $i-1$ and switched state i at the n^{th} repetition of the cycle.

$$T_i = t_{i+1} - t_i \qquad (3.4.1\text{-}5)$$

is the steady-state period of the switched state i.

$$\tau_i[n] \equiv \tau_{i+n\cdot N_s} \qquad (3.4.1\text{-}6)$$

is the switching instant in the perturbed system between switched state $i-1$ and switched state i at the n^{th} repetition of the cycle.

$$\Delta t_i[n] \equiv \tau_i[n] - t_i[n] \qquad (3.4.1\text{-}7)$$

is the perturbation in switching instant between switched state $i-1$ and switched state i.

$$\Delta x_i[n] \equiv \Delta x_i[t_i+\max(\Delta t_i[n],0)] \qquad (3.4.1\text{-}8)$$

is the value of the perturbed state at the beginning of the switched state i, when the perturbed system or the unperturbed system makes last the transition from the switched state $i-1$ to the switched state i.

$$\Delta x_i[n] = \Delta x[t_{i+1}+\min(\Delta t_{i+1},0)] \qquad (3.4.1\text{-}9)$$

is the value of the perturbed state at the end of the switched state i, when the perturbed system or the unperturbed system makes first the transition from the switched state i to the switched state $i+1$.

3.4.2 Linearization

A linear relationship relating the state perturbation to its past history and to the control input is required. The equation relating the value of the state perturbation at the beginning of the switched state i to the state perturbation at the end of the switched state

i-1, and to the perturbation in the control variable at the instant t_i is first sought. Letting ∂x and ∂r be the small-signal limit state perturbation and input control perturbation, a relation of the form

$$\partial x_i[n] = K_i \cdot \partial \tilde{x}_{i-1} + k_i \cdot \partial r_i[n] \qquad (3.4.2\text{-}1)$$

is found for each switching instant.

There are six instants where the switched state is changed. Generally in a DC-DC converters all switching instants can be modulated. For the converter under study, the six transitions are classified into three types: time-modulated, unmodulated and naturally-modulated transitions.

To completely describe the trajectory of the state perturbation, a function relating the state perturbation at the end of the switched state i to that at the beginning of the switched state is also required, and an equation of the form

$$\partial \tilde{x}_i[n] = \Phi_i \cdot \partial x_i[n] \qquad (3.4.2\text{-}2)$$

is found for each of the six switched states.

Since the transition from one switched state to another is either governed by, or easily recognized from the resonant current, attention is focused on the resonant current. The results thus obtained in a scalar fashion are thereafter generalized to vector notation.

3.4.2.1 Time-Modulated Transitions

The instants t_1 and t_4 are modulated by the control circuit. The periods Δt_1 and Δt_4 are therefore the input control variables. The state variable perturbation $\Delta i_{r_1}[n]$ is to be related to $\Delta \tilde{r}_{r_6}[n-1]$ and to $\Delta t_1[n]$. From the geometry of Figure 3-8 the following is obtained:

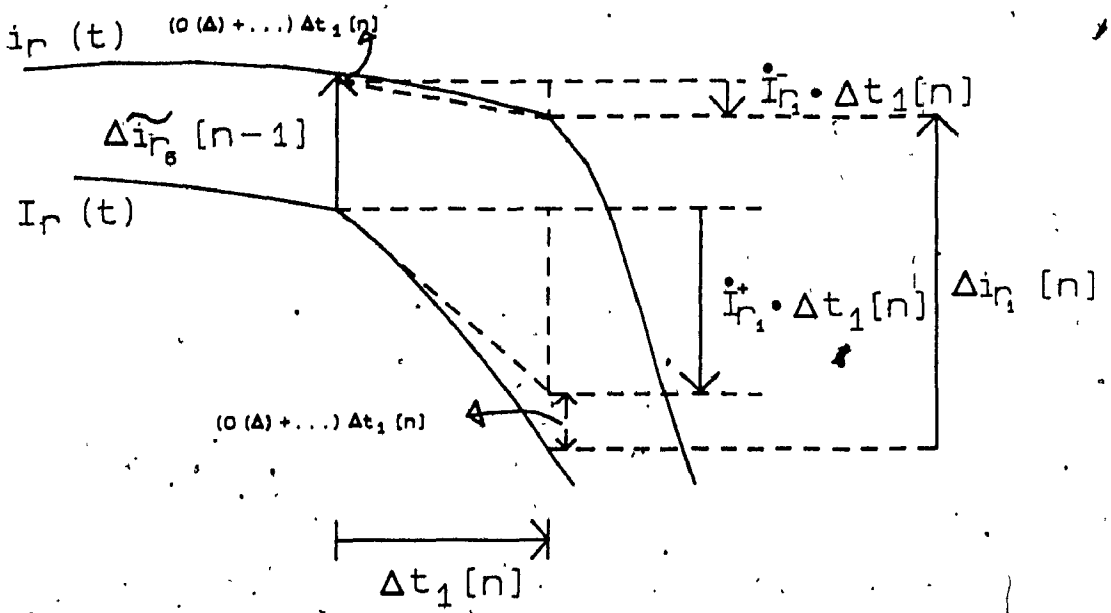

Figure 3-8: Time Modulated Transition

$$\Delta i_{r_1}[n] = \Delta \Upsilon_{r_6}[n-1] + \{ \dot{I}^-_{r_1} + O(\Delta) + \ldots \} \cdot \Delta t_1[n] - \{ \dot{I}^+_{r_1} + O(\Delta) + \ldots \} \cdot \Delta t_1[n]$$

$$= \Delta \Upsilon_{r_6}[n-1] + \{ \dot{I}^-_{r_1} - \dot{I}^+_{r_1} \} \cdot \Delta t_1[n] + O(\Delta^2) + \ldots \quad (3.4.2\text{-}3)$$

$\dot{I}^-_{r_1}$ and $\dot{I}^+_{r_1}$ are the time derivatives of the steady-state resonant current before and after the change in switched state. In the small-signal limit, high order terms are neglected and (3.4.2-3) becomes:

$$\delta i_{r_1}[n] = \delta \Upsilon_{r_6}[n-1] + \{ \dot{I}^-_{r_1} - \dot{I}^+_{r_1} \} \cdot \delta t_1[n] \quad (3.4.2\text{-}4)$$

Generalizing to vector notation yields

$$\delta x_\ell[n] = \delta \Xi_{\ell-1}[n] + (\dot{X}^-_\ell - \dot{X}^+_\ell) \cdot \delta t_\ell[n] , \quad (3.4.2\text{-}5)$$

where

$$\dot{X}^-_\ell = \omega_o \cdot (A_{\ell-1} \cdot X_\ell + B_{\ell-1}) , \quad (3.4.2\text{-}6)$$

$$\dot{X}^+_\ell = \omega_o \cdot (A_\ell \cdot X_\ell + B_\ell) . \quad (3.4.3\text{-}7)$$

and $X(t_\ell)$ is denoted as X_ℓ. Therefore,

$$K_\ell = I , \quad (3.4.2\text{-}8)$$

where I is the identity matrix and

$$k_\ell = (\dot{X}^-_\ell - \dot{X}^+_\ell) , \quad (3.4.2\text{-}9)$$

where the subscript ℓ can take the value 1 or 4.

3.4.2.2 Naturally-Modulated Transitions

When the resonant current reduces to zero at t_2 and t_5, there is a change in switched state. In continuous mode, for example, the output rectifiers switch the load such that output capacitor voltage polarity, in series with the resonant branch, reverses. Before relating $\delta x_\iota[n]$ to $\delta x_{\iota-1}[n]$ an expression for $\delta t_\iota[n]$, which is determined by the natural switching of the circuit, is first found.

The condition that must be met for the switching to occur can be expressed as

$$i_r(t) = \text{cst} \ , \qquad (3.4.2\text{-}10)$$

where cst is identically zero for the cases under study. Two cases are identified as follows: $\Delta t_\iota[n]$ is positive and $\Delta t_\iota[n]$ is negative. These two cases are illustrated in Figure 3-9. Consider the case where the $\Delta t_\iota[n]$ is positive. Around $t_\iota[n]$, $i_r(t)$ can be expressed as

$$i_r(t) = I_r(t_\iota[n]) + \Delta Y_{r_{\iota-1}}[n] + (\dot{I}_{r_\iota} + O(\Delta))\,(t - t_\iota[n]) \ . \qquad (3.4.2\text{-}11)$$

By definition, τ_ι is the moment where $i_r(t)$ satisfies (3.4.2-10). Substituting $\tau_\iota[n]$ for t into (3.4.2-11)

$$\text{cst} = I_r(t_\iota[n]) + \Delta Y_{r_{\iota-1}}[n] + (\dot{I}_{r_\iota} + O(\Delta))\,\Delta t_\iota[n] \ . \qquad (3.4.2\text{-}12)$$

In the case where Δt_ι is negative, $I_r(t)$ is expanded around τ_ι.

$$I_r(t) = i_r(\tau_\iota[n]) - \Delta Y_{r_{\iota-1}}[n] + (\dot{I}_{r_\iota} + O(\Delta))\cdot(t - \tau_\iota[n]) \qquad (3.4.2\text{-}13)$$

At t_1, $I_r(t)$ is equal to cst

$$I_r(t_\iota[n]) = i_r(\tau_\iota[n]) = \text{cst} \ . \qquad (3.4.2\text{-}14)$$

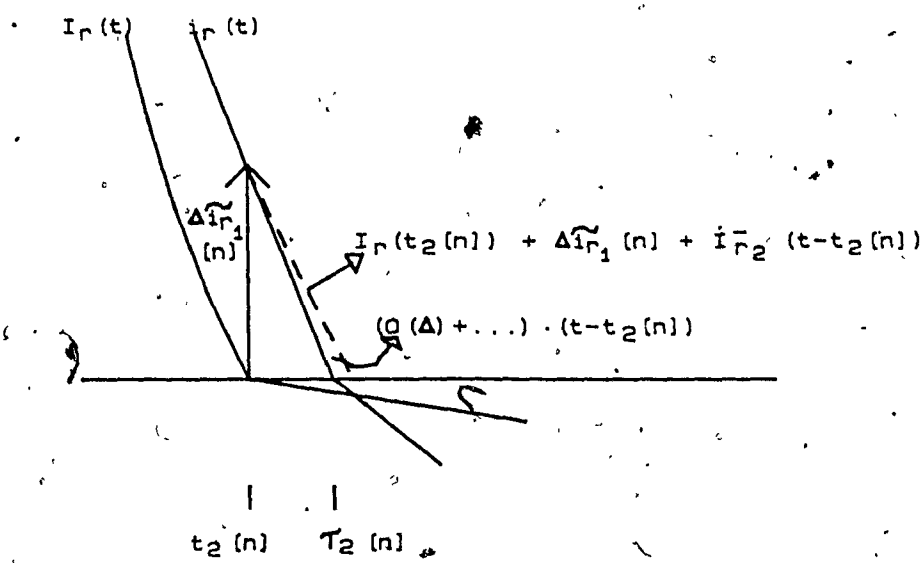

a)

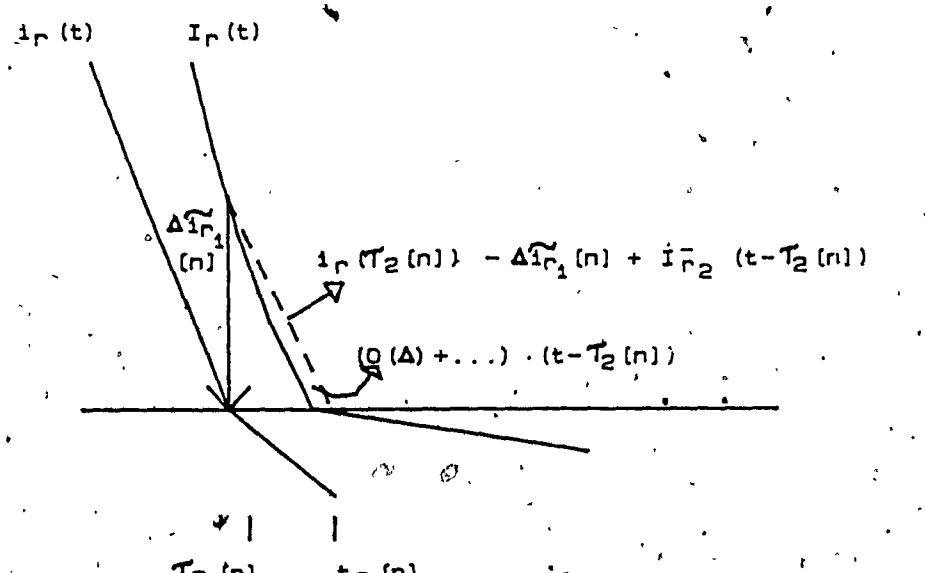

b)

Figure 3-9: Naturally Modulated Transitions
a) $\Delta t_2[n] > 0$
b) $\Delta t_2[n] < 0$

Substituting in (3.4.2-12) yields

$$cst = I_r(t_\ell[n]) + \Delta\Upsilon_{r_{\ell-1}}[n] + \left(\dot{\bar{I}}_{r_\ell} + O(\Delta) \right) \Delta t_\ell[n] \quad . \qquad (3.4.2\text{-}15)$$

This is the same expression as (3.4.2-12). Subtracting the steady-state component, $I_r(t_\ell) = cst$, and linearizing

$$\delta t_\ell[n] = - \frac{\delta\Upsilon_{r_{\ell-1}}[n]}{\dot{\bar{I}}_{r_\ell}} \quad . \qquad (3.4.2\text{-}16)$$

This equation can be obtained directly from Figure 3-9. Nevertheless, the formulation of (3.4.2-12) and (3.4.2-15) is useful for the generalization to vector notation. Defining the instant of a natural modulation transition as the time where the weighted sum of the state variable is equal to a predefined constant, and generalizing (3.4.2-10) to vector notation yields

$$f_\ell^t \cdot x(\tau_\ell[n]) = cst_\ell \quad . \qquad (3.4.2\text{-}17)$$

f_ℓ is the weight vector and cst_ℓ is the predefined constant. Generalizing (3.4.2-15) to vector notation, taking into account (3.4.2-17), gives

$$f_\ell^t \cdot \left[X(t_\ell[n]) + \Delta\mathfrak{X}_{\ell-1}[n] + \left(\dot{\bar{X}}_\ell + O(\Delta) \right) \cdot \Delta t_\ell[n] \right] = cst_\ell \quad . \qquad (3.4.2\text{-}18)$$

Subtracting the steady-state component, $f_\ell^t \cdot X(t_\ell[n]) = cst_\ell$, and linearizing, the expression for δt_ℓ is

$$\delta t_\ell[n] = - \left[f_\ell^t \cdot \dot{\bar{X}}_\ell \right]^{-1} \cdot f_\ell^t \cdot \delta\mathfrak{X}_{\ell-1}[n] \quad . \qquad (3.4.2\text{-}19)$$

$\delta x_\ell[n]$ can now be related to $\delta\mathfrak{X}_{\ell-1}[n]$. Substituting (3.4.2-19) into

(3.4.2-5) gives the relationship sought.

$$\delta x_\ell[n] = [\ I - (\ \dot{X}_\ell^- - \dot{X}_\ell^+\ )\cdot[\ f_\ell^t\cdot\dot{X}_\ell^-\ ]^{-1}\cdot f_\ell^t\ ]\cdot\delta\bar{x}_{\ell-1}[n] \qquad (3.4.2\text{-}20)$$

Therefore,

$$K_\ell = I - (\ \dot{X}_\ell^- - \dot{X}_\ell^+\ )\cdot[\ f_\ell^t\cdot\dot{X}_\ell^-\ ]^{-1}\cdot f_\ell^t\ , \qquad (3.4.2\text{-}21)$$

and

$$k_\ell = 0\ . \qquad (3.4.2\text{-}22)$$

The subscript ℓ can assume the values 2 or 5. Note that, since the instant of switching is determined by the resonant current,

$$f_\ell^t = [\ 1\ \ 0\ \ 0\ ]\ . \qquad (3.4.2\text{-}23)$$

3.4.2.3 Unmodulated Transitions

The transitions at t_3 and t_6 are initiated by a clock. The transition is unmodulated, consequently

$$\Delta t_\ell[n] = 0 \qquad (3.4.2\text{-}24)$$

and

$$\Delta i_{r_\ell}[n] = \Delta\bar{r}_{r_{\ell-1}}[n]\ . \qquad (3.4.2\text{-}25)$$

This can be seen from Figure 3-7b). Generalizing to vector notation is trivial and

$$\Delta x_\ell[n] = \Delta\bar{x}_{\ell-1}[n]\ . \qquad (3.4.2\text{-}26)$$

Consequently

$$K_\ell = I \qquad (3.4.2\text{-}27)$$

and

$$k_\ell = 0. \qquad (3.4.2\text{-}28)$$

The subscript i can assume the values 3 or 6.

3.4.2.4 Switched-states

The relation between the state perturbation at the beginning of a switched state and the state perturbation at the end of the switched state is easily found. Consider the differential equation that governs the behavior of the system for $\{ \max(t_i[n],\tau_i[n]) < t < \min(t_{i+1}[n],\tau_{i+1}[n]) \}$:

$$\begin{aligned} \Delta\dot{x}(t) &= \dot{x}(t) - \dot{X}(t) \\ &= \omega_o A_i \cdot (x(t) - X(t)) . \end{aligned} \qquad (3.4.2\text{-}29)$$

The solution to this equation is

$$\Delta x(t) = \exp(\omega_o A_i (t - \max(t_i[n],\tau_i[n])) \cdot \Delta x_i[n] . \qquad (3.4.2\text{-}30)$$

The state perturbation at any time during a switched state is therefore described. In particular the state perturbation at the end of a switched state is

$$\begin{aligned} \Delta\tilde{x}_i[n] = &\exp(\omega_o A_i (\min(t_{i+1}[n],\tau_{i+1}[n]) - \max(t_i[n],\tau_i[n])) \cdot \Delta x_i[n]) \\ &\exp(\omega_o A_i (T_i + \min(0,\Delta t_{i+1}[n]) - \max(0,\Delta t_{i-1}[n])) \cdot \Delta x_i[n] \\ &\exp(\omega_o A_i \cdot T_i) \cdot (I + O(\Delta t_i[n]) + O(\Delta t_{i+1}[n]) + \ldots) \cdot \Delta x_i[n] \end{aligned} \qquad (3.4.2\text{-}31)$$

In the small-signal limit, neglecting higher order terms,

$$\delta\tilde{x}_i[n] = \exp(\omega_o A_i \cdot T_i) \cdot \delta x_i[n] . \qquad (3.4.2\text{-}32)$$

Therefore,

$$\Phi_i = \exp(A_i \cdot \omega_o T_i) \qquad (3.4.2\text{-}33)$$

for all values the subscript i can assume.

3.5 STATE PERTURBATION TRANSFER FUNCTION

The operation of the pulse-width modulator has been described in section 3.1 as that of a sampler. The sample of $\delta v_{amp}(t)$, $\delta d(t)$, is fed to the converter. $\delta d(t)$ is a discrete variable, therefore, it is convenient to use discrete system formulation to determine the response of the converter to the sampled input and consider the converter as a sampled-data system. Using the material developed in the preceding section, the state perturbation at a sampling instant can be related to the the state perturbation at the preceding sampling instant. The pulse response of the sampled-data representation of the converter is denoted by $S(t)$ on Figure 3-10.

The output of the sampled-data system is $\delta x^*(t)$, a discrete variable. Since the error voltage amplifier is assumed to be realized using an linear amplifier which continuously senses the output voltage, the variables of interest are the continuous variables. The system between the sampling moments is governed by a piecewise linear differential equation. Therefore, the state perturbation between the sampling instants is uniquely determined by the state perturbation at the sampling instants. The continuous state perturbation and the output vector can be reconstructed using the differential equation, and the output equation. The impulse response of the reconstruction process is denoted by $R(t)$, for the reconstruction of the state perturbation, and by $R_y(t)$ for the reconstruction of the output vector perturbation.

To find the transfer function of the system, the Laplace transform of each block is taken to yield the block diagram of Figure 3-10b).

$$\frac{\delta y(s)}{\delta v_{amp}(s)} = \frac{\delta y(s)}{\delta x^*(s)} \frac{\delta x^*(s)}{\delta d(s)} \cdot \frac{\delta d(s)}{\delta v_{amp}(s)}$$

$$= R_y(s) \cdot S(s) \cdot PWM(s) \qquad (3.5.0\text{-}1)$$

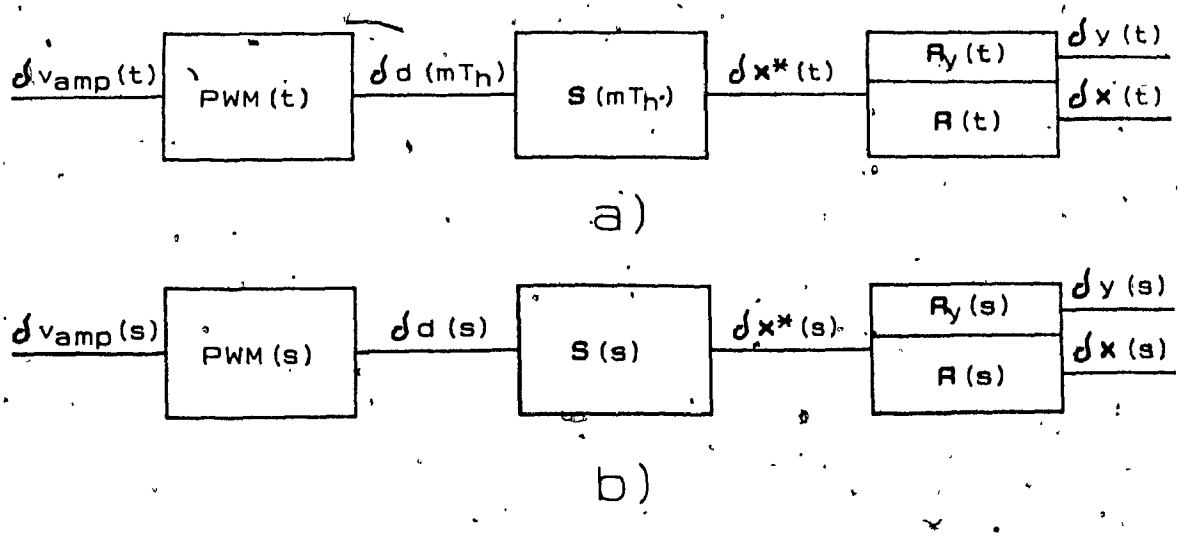

Figure 3-10: Small-Signal Analysis Block Diagram
a) Time domain
b) Frequency domain

3.5.1 Pulse Width Modulator

The operation of the pulse-width modulator is described in section 3.1. Essentially the output of the error-amplifier is compared to the ramp and the pulse is terminated when the ramp reaches the level of the error amplifier voltage. In practice, the comparator drives a cascade of buffers which ultimately drive the switch. All stages of this cascade, including the comparator and the switches, have an inherent propagation delay. Assuming that the t_i's are offset from the origin by an amount $t_i[0]$, and and assuming that the sampling period is T_s, then the output of the pulse-width modulator is a sequence of impulses defined by

$$\delta d(mT_s+t_i[0]) = K_{pwm}\cdot\delta v^*_{amp}(mT_s+t_i[0]-T_{d_{pwm}}) \ , \qquad (3.5.1\text{-}1)$$

where K_{pwm} is a constant determined by the amplitude of the ramp and $T_{d_{pwm}}$ is the delay introduced by the pulse-width modulator and the cascaded driving stages. Taking the Laplace transform of both sides yields

$$\delta d(s) = K_{pwm}\cdot e^{-sT_{d_{pwm}}}\ \mathcal{L}(\delta v^*_{amp}(mT_s+t_i[0])) \ . \qquad (3.5.1\text{-}2)$$

In order to find the ratio of $\delta d(s)$ to $\delta v_{amp}(s)$ the ratio of $\mathcal{L}(\delta v^*_{amp}(mT_h+t_i[0]))$ to $\delta v_{amp}(s)$ must first be found. This ratio is not well defined for an arbitrary signal. In practice transfer functions are measured by injecting a sinusoidal signal and by measuring the response at this frequency using a narrow band instrument. It is shown in Appendix A, section A.3, that for the special case where $\delta v_{amp}(t)=e^{j\omega t}$

$$\frac{\mathcal{L}(\delta v^*_{amp}(mT_s+t_i[0])}{\delta v_{amp}(s)} = \frac{1}{T_s} \ . \qquad (3.5.1\text{-}3)$$

The sampling period is T_h, consequently

$$PWM(s) = \frac{1}{T_h} K_{pwm} e^{-st_{dpwm}} \quad (3.5.1\text{-}4)$$

In the next section, the operation of the pulse-width modulator is modeled as that of two samplers with outputs

$$\delta_e(2nT_h+T_1[0]) = K_{pwm} \cdot \delta^*_{vamp}(2nT_h+T_1[0]-T_{d_{pwm}}) \quad (3.5.1\text{-}4)$$

and

$$\begin{aligned}\delta_o((2n+1)T_h+T_1[0]) &= K_{pwm} \cdot \delta^*_{vamp}((2n+1)T_h+T_1[0]-T_{d_{pwm}}) \\ &= K_{pwm} \cdot \delta^*_{vamp}(2nT_h+T_4[0]-T_{d_{pwm}}) \quad (3.5.1\text{-}5)\end{aligned}$$

The sampling period of the equivalent modulators is $2T_h$ and the transfer functions are found to be

$$PWM_e(s) = \frac{1}{2T_h} K_{pwm} \cdot e^{-st_{dpwm}} \quad (3.5.1\text{-}6)$$

and

$$PWM_o(s) = \frac{1}{2T_h} K_{pwm} \cdot e^{-st_{dpwm}} \quad (3.5.1\text{-}7)$$

3.5.2 Converter Sampled-Data System Representation

The duty cycle is modulated twice per cycle. A difference equation that relates the sample of the state perturbation to the previous samples of state perturbation and duty cycle perturbation is sought. Defining,

$$\delta x(m) \equiv \delta x(m \cdot T_h+t_i[0]) \quad (3.5.2\text{-}1a)$$

and

$$\delta d(m) \equiv \delta d(m \cdot T_h+t_i[0]) \quad (3.5.2\text{-}1b)$$

and noting that

$$\delta d(\dot{m}) = \frac{\partial t(m \cdot T_h + t_i[0])}{T_h} \quad (3.5.2\text{-}2)$$

(3.4.2-1) and (3.4.2-2) are repeatedly applied to relate $\delta x(2n)$ to $\delta x(2n-1)$ and to $\delta d(2n)$.

$$\begin{aligned}
\delta x(2n) = {} & \delta x_1[n] \\
& K_1 \cdot \delta x_6[n-1] + T_h k_1 \cdot \delta d(2n) \\
& K_1\Phi_6 \cdot \delta x_6[n-1] + T_h k_1 \cdot \delta d(2n) \\
& K_1\Phi_6K_6 \cdot \delta x_5[n-1] + T_h k_1 \cdot \delta d(2n) \\
& K_1\Phi_6K_6\Phi_5 \cdot \delta x_5[n-1] + T_h k_1 \cdot \delta d(2n) \\
& K_1\Phi_6K_6\Phi_5K_5 \cdot \delta x_4[n-1] + T_h k_1 \cdot \delta d(2n) \\
& K_1\Phi_6K_6\Phi_5K_5\Phi_4 \cdot \delta x_4[n-1] + T_h k_1 \cdot \delta d(2n) \\
& K_1\Phi_6K_6\Phi_5K_5\Phi_4 \cdot \delta x(2n-1) + T_h k_1 \cdot \delta d(2n)
\end{aligned} \quad (3.5.2\text{-}3)$$

Simplifying the notation,

$$\delta x(2n) = \Phi_{sh} \cdot \delta x(2n-1) + T_h k_1 \delta d(2n) , \quad (3.5.2\text{-}4)$$

where

$$\Phi_{sh} = K_1\Phi_6K_6\Phi_5K_5\Phi_4 . \quad (3.5.2\text{-}5)$$

Similarly it can be shown that

$$\delta x(2n-1) = \Phi_{fh} \cdot \delta x(2n-2) + T_h k_4 \cdot \delta d(2n-1) , \quad (3.5.2\text{-}6)$$

where

$$\Phi_{fh} = K_4\Phi_3K_3\Phi_2K_2\Phi_1 . \quad (3.5.2\text{-}7)$$

Combining (3.5.2-4) with (3.5.2-6)

$$\delta x(2n) = \Phi_{sh}\Phi_{fh} \cdot \delta x(2n-2) + \Phi_{sh} \cdot T_h k_4 \delta d(2n-1) + T_h k_1 \delta d(2n) . \quad (3.5.2\text{-}8)$$

Proceeding in an identical fashion, the system's difference equation, $\partial S(m)$, can be completely defined by the following pair of difference equations

$$\partial S(\delta x(m), \delta d(m)) \equiv$$

$$\left| \begin{array}{l} \delta x(2n) = \Phi_{sh}\Phi_{fh} \cdot \delta x(2n-2) + \Phi_{sh} \cdot T_h k_4 \cdot \delta d(2n-1) + T_h k_1 \cdot \delta d(2n) \\ \delta x(2n+1) = \Phi_{fh}\Phi_{sh} \cdot \delta x(2n-1) + \Phi_{fh} \cdot T_h k_1 \cdot \delta d(2n) + T_h k_4 \cdot \delta d(2n+1) \end{array} \right. \qquad (3.5.2\text{-}9)$$

It is shown in Appendix A, section A.2, that the system described by this difference equation is linear. It is specifically shown that the system response can be obtained by summing up the response obtained by modulating the t_1's ($\delta d(2n)$) to the response obtained by modulating the t_4's ($\delta d(2n+1)$). Breaking the system into two linearly independent equations facilitates taking the Laplace transform of the reconstruction equation which is derived in the next section. The block diagram of Figure 3-10 is therefore modified as in Figure 3-11 where the subscript "e" refers to the system for which the $\delta d(m)$ are modulated for even m's and the subscript "o" refers to the system for which the $\delta d(m)$ are modulated for odd m's.

The difference equation that defines the system from sample to sample when only the t_1's are modulated is found, from (3.5.2-9), to be

$$\delta x_e(2n) = \Phi_{sh}\Phi_{fh} \cdot \delta x(2n-2) + T_h k_1 \delta d(2n) \; . \qquad (3.5.2\text{-}10)$$

For modulating the t_4's only, the difference equation is

$$\delta x_o(2n+1) = \Phi_{fh}\Phi_{sh} \cdot \delta x(2n-1) + T_h k_4 \delta d(2n+1) \; . \qquad (3,5.2\text{-}11)$$

The pulse response of these two systems can easily be found to be

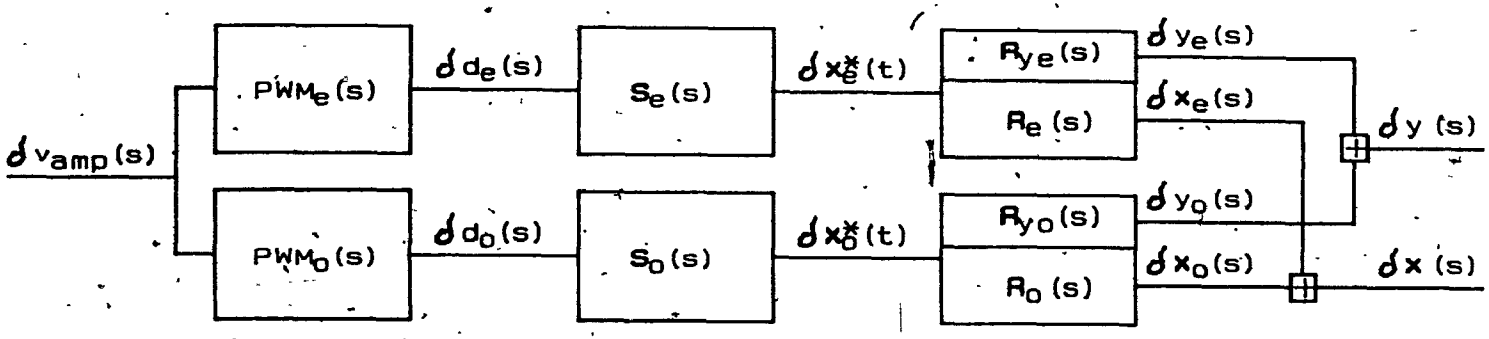

Figure 3-11: Block Diagram for Linear Superposition of the Effects of Modulating δd(m) for Even an Odd Values of m Separately.

$$\delta x_e(2n) = (\Phi_{sh}\Phi_{fh})^n \cdot T_h k_1 \cdot \delta d(0) \quad (3.5.2\text{-}12)$$

$$\delta x_o(2n+1) = (\Phi_{fh}\Phi_{sh})^n \cdot T_h k_4 \cdot \delta d(1) \quad (3.5.2\text{-}13)$$

The transfer function is the Laplace transform of the pulse response. Rather than taking the Laplace transform of (3.5.2-12) and (3.5.2-13), it is more convenient to first obtain the discrete transfer function and then apply the Laplace transform. Applying the $\mathcal{Z}$ transform to the difference equation yields

$$\delta x_e(z) = [\, I - z^{-2} \cdot \Phi_{sh}\Phi_{fh}]^{-1} \cdot T_h k_1 \delta d_e(z) \quad (3.5.2\text{-}14)$$

and

$$\delta x_o(z) = [\, I - z^{-2} \cdot \Phi_{sh}\Phi_{fh}]^{-1} \cdot T_h k_4 \delta d_o(z) \quad (3.5.2\text{-}15)$$

It is shown in Appendix A, section A.4, that the Laplace transform of a function $v^*(t)$, in a sample data system where the sampling train of impulses is offset from the origin by t_{ofs} is:

$$v^*(s) = e^{-st_{ofs}} \cdot v^*(z) \Big|_{z = e^{sT_s}} \quad (3.5.2\text{-}16)$$

For both systems, the sampling time is $2 \cdot T_h$. For the system modulated when m is even, the offset is $t_1[0]$ and for the m odd system the offset is $t_4[0]$. Applying (3.5.2-16) to (3.2.5-14) and (3.5.2-15) yields

$$\begin{aligned} \delta x_e^*(s) &= e^{-st_1[0]} [\, I - e^{-2sT_h} \cdot \Phi_{sh}\Phi_{fh}]^{-1} \cdot T_h k_1 \delta d_e(z) \Big|_{z = e^{2sT_h}} \\ &= [\, I - e^{-2sT_h} \cdot \Phi_{sh}\Phi_{fh}]^{-1} \cdot T_h k_1 \left[e^{-st_1[0]} \, \delta d_e(z) \right] \Big|_{z = e^{2sT_h}} \\ &= [\, I - e^{-2sT_h} \cdot \Phi_{sh}\Phi_{fh}]^{-1} \cdot T_h k_1 \delta d_e(s) \end{aligned} \quad (3.5.2\text{-}17)$$

and

$$\delta x_o^M(s) \triangleq e^{-st_4[0]} \left[I - e^{-2sT_h} \cdot \Phi_{fh}\Phi_{sh} \right]^{-1} \cdot T_h k_4 \delta d_o(z) \Big|_{z = e^{2sT_h}}$$

$$= \left[I - e^{-2sT_h} \cdot \Phi_{fh}\Phi_{sh} \right]^{-1} \cdot T_h k_4 \left[e^{-st_4[0]} \, \delta d_o(z) \right] \Big|_{z = e^{2sT_h}}$$

$$= \left[I - e^{-2sT_h} \cdot \Phi_{fh}\Phi_{sh} \right]^{-1} \cdot T_h k_4 \delta d_o(s) \quad . \qquad (3.5.2\text{-}18)$$

Consequently,

$$S_e(s) = T_h \cdot \left[I - e^{-2sT_h} \cdot \Phi_{sh}\Phi_{fh} \right]^{-1} \cdot k_1 \quad . \qquad (3.5.2\text{-}19)$$

and

$$S_o(s) = T_h \cdot \left[I - e^{-2sT_h} \cdot \Phi_{fh}\Phi_{sh} \right]^{-1} \cdot k_4 \quad . \qquad (3.5.2\text{-}20)$$

3.5.3 State Perturbation Reconstruction

It is seen from section 3.4.2.4 that for

$$\max(t_j, \tau_j) < t < \min(t_{j+1}, \tau_{j+1}) \quad , \qquad (3.5.3\text{-}1)$$

where

$$j = n \cdot N_s + i \quad , \qquad (3.5.3\text{-}2)$$

the state perturbation is expressed by

$$\Delta x(t) = \exp(\omega_o A_i (t - \max(t_j, \tau_j))) \cdot \Delta x_j \quad . \qquad (3.4.2\text{-}30)$$

Recognizing that in the small-signal limit τ_j tends to t_j, the state perturbation is approximated by

$$\partial x(t) = \exp(\omega_o A_i (t - t_j)) \cdot \partial x_j \quad , \qquad (3.5.3\text{-}3)$$

for

$$t_j < t \leq t_{j+1} \quad . \qquad (3.5.3\text{-}4)$$

It has been shown in [17] that the error introduced by (3.5.3-3)

vanishes in the small-signal limit. Using the following special notation, the state perturbation is expressed for a complete cycle of the system with even arguments

$$\delta x_e(t) = e^{\omega_0 A_\ell (t-t_\ell)} \cdot K_\ell \Phi_{\ell-1} \cdots K_2 \Phi_1 \cdot \delta x_e(2n) \quad , \qquad (3.5.3\text{-}5)$$

where

$$K_1 \Phi_0 \cdots K_2 \Phi_1 = I \qquad (3.5.3\text{-}6)$$

and where the proper index ℓ must be used in the expression for

$$t_{\ell+n\cdot N_s} < t \leq t_{\ell+1+n\cdot N_s} \quad . \qquad (3.5.3\text{-}7)$$

(3.5.3-5) describes $\delta x_e(t)$ for

$$2nT_h + t_1[0] < t < 2(n+1)T_h + t_1[0] \quad . \qquad (3.5.3\text{-}8)$$

Defining

$$t_\ell \equiv \sum_{k=0}^{\ell-1} T_k \quad , \qquad (3.5.3\text{-}9)$$

where

$$T_0 \equiv 0 \quad , \qquad (3.5.3\text{-}10)$$

the impulse response of the reconstruction block is[1]

---

[1]The expression for $R_e(t)$ is verified to be correct by performing a convolution integral:

$$\delta x_e(t) = \int_{-\infty}^{\infty} R_e(t-\lambda)\ \delta x_e^*(\lambda)\ \partial\lambda$$

From the property of convoluting with an impulse [26],

$$R_e(t) = \begin{cases} e^{\omega_o A_\ell (t-t_\ell)} \cdot K_\ell \Phi_{\ell-1} \cdots K_5 \Phi_4 & \text{for } 0 < t < 2T_h \\ 0 & \text{for } t < 0 \text{ or } t > 2T_h \end{cases} \qquad (3.5.3\text{-}11)$$

The transfer function of the reconstruction block is found by taking the Laplace transform of the impulse response.

$$R_e(s) = \int_{-\infty}^{\infty} R_e(t)\, e^{-st}\, \partial t$$

$$= \sum_{\ell=1}^{6} \int_{t_\ell}^{t_{\ell+1}} e^{\omega_o A_\ell (t-t_\ell)} \cdot K_\ell \Phi_{\ell-1} \cdots K_2 \Phi_1\, e^{-st}\, \partial t$$

$$= \sum_{\ell=1}^{6} R_{e_\ell}(s) \qquad (3.5.3\text{-}12)$$

Integrating by parts over each interval,

$$R_{e_\ell}(s) = -\frac{e^{-st}}{s} \cdot e^{\omega_o A_\ell (t-t_\ell)} \cdot K_\ell \Phi_{\ell-1} \cdots K_2 \Phi_1 \Big|_{t=t_\ell}^{t=t_{\ell+1}}$$

$$+ \frac{\omega_o A_\ell}{s} \int_{t_\ell}^{t_{\ell+1}} e^{\omega_o A_\ell (t-t_\ell)} \cdot K_\ell \Phi_{\ell-1} \cdots K_2 \Phi_1\, e^{-st}\, \partial t$$

$$\delta x_e(t) = \sum_{n=-\infty}^{\infty} R_e(t-2nT_h-t_1[0]) \cdot \delta x_e(2nT_h+t_1[0]).$$

Therefore, for $2nT_h+t_1[0] < t < 2(n+1)T_h+t_1[0]$,

$$\delta x_e(t) = e^{\omega_o A_\ell (t-t_\ell)} \cdot K_\ell \Phi_{\ell-1} \cdots K_2 \Phi_1\, \delta x_e(2n)$$

$$R_{e_\ell}(s) = \frac{1}{\omega_o} e^{-st_\ell} \left[\frac{s}{\omega_o} \cdot I - A_\ell \right]^{-1} \left(I - e^{-sT_\ell} e^{A_\ell \omega_o T_\ell} \right) \cdot K_\ell \Phi_{\ell-1} \cdots K_2 \Phi_1 \ . \tag{3.5.3-13}$$

Similarly the impulse response for the system with odd arguments is

$$R_o(t) = \begin{cases} e^{\omega_o A_\ell (t - t_\ell)} \cdot K_\ell \Phi_{\ell-1} \cdots K_5 \Phi_4 & \text{for } 0 < t < 2T_h \\ 0 & \text{for } t < 0 \text{ or } t > 2T_h \end{cases} \tag{3.5.3-14}$$

where

$$K_4 \Phi_3 \cdots K_5 \Phi_4 = I \ . \tag{3.5.3-15}$$

The ℓ sequence

$$\ell \in \{ \ldots 4, 5, 6, 7, 8, 9 \ldots \} \tag{3.5.3-16}$$

corresponds one to one to the t sequence[3]

$$t \in \{ \ldots 4, 5, 6, 1, 2, 3 \ldots \} \tag{3.5.3-17}$$

and

$$t_\ell = \sum_{k=3}^{\ell-1} T_{k-3} \ , \tag{3.5.3-18}$$

where T_0 is identically zero.

The integration by parts over each switched states yields

$$R_{o_\ell}(s) = \frac{1}{\omega_o} e^{-st_\ell} \left[\frac{s}{\omega_o} \cdot I - A_\ell \right]^{-1} \left(I - e^{-sT_\ell} e^{A_\ell \omega_o T_\ell} \right) \cdot K_\ell \Phi_{\ell-1} \cdots K_5 \Phi_4 \ . \tag{3.5.3-19}$$

---

[3] e.g. $T_7 = T_1$

Consequently,

$$R_o(s) = \sum_{\ell=4}^{9} R_{o_\ell}(s) \quad . \qquad (3.5.3\text{-}20)$$

3.5.4 Reconstruction of the Output Variable Perturbation

The transfer function of the state perturbation to the perturbation in control signal is found. However, in the assumed mode of control, the variable of interest, the output voltage, is not a state variable. The state vector $x(t)$ is continuous in time, however, the sequence of matrices C_ℓ is not. This can be easily seen by comparing the expressions for C_1 and C_2, (3.3.1-17) and (3.3.1-20) respectively. This discontinuity has two implications. First, the discontinuity in the sequence of output matrices introduces a discontinuity in the output variable at the switching instants. Secondly, since $C(t)$ is constant only between switching instants, the output variable $\delta y(t)$ can be expressed in between the switching instants as a piecewise linear combination of $\delta x(t)$, but $\delta y(s)$ cannot be expressed as a linear combination of $\delta x(s)$.

It has been shown in [17] that the discontinuity in output matrix introduces a train of pulses of width δt_ℓ and of magnitude

$$(C_{\ell-1}-C_\ell)\cdot X(t_\ell) \quad . \qquad (3.5.4\text{-}1)$$

For the converter under study, it is seen from the development of section 3.3 that $C(t)$ is discontinuous at t_2 and t_6 only. Considering the transition at t_2, substituting (3.3.1-17) and (3.3.1-20) yields

$$(C_1-C_2)\cdot X(t_2)$$

$$= \left[\begin{bmatrix} \frac{1}{Q+Q_{co}} & 0 & \frac{Q_{co}}{Q+Q_{co}} \end{bmatrix} - \begin{bmatrix} \frac{-1}{Q+Q_{co}} & 0 & \frac{Q_{co}}{Q+Q_{co}} \end{bmatrix} \right] \cdot \begin{bmatrix} \overline{I_r}(t_2) \\ \overline{V_r}(t_2) \\ \overleftarrow{V_{co}}(t_2) \end{bmatrix}$$

$$= \frac{2}{Q+Q_{co}} \overline{I_r}(t_2) \; . \qquad (3.5.4\text{-}1)$$

Since $I_r(t_2)$ is zero, the amplitude of the pulse is zero. The same conclusion also applies at t_5. For the converter of interest $\delta y(t)$ is continuous and the discontinuity in output matrix does not introduce a series of train of impulses at the output.

Since $\delta y(s)$ cannot be expressed as a linear combination of $\delta x(s)$, the perturbation of the output variable is first expressed as a piecewise linear combination of $\delta x(t)$. For the system where the t_i's only are modulated, the following reconstruction equation is found from (3.3.1-14) and (3.5.3-5) to be

$$\delta y_e(t) = C_l \cdot \left[e^{\omega_o A_l (t-t_J)} \cdot K_l \Phi_{l-1} \cdots K_2 \Phi_1 \cdot \delta x_e(2n) \right] . \qquad (3.5.4\text{-}2)$$

Proceeding as in section 3.5.3, the transfer functions of the output variable reconstructing blocks are found to be:

$$R_{ye}(s) = \sum_{l=1}^{6} R_{ye_l}(s) \qquad (3.5.4\text{-}3)$$

and

$$R_{yo}(s) = \sum_{l=4}^{9} R_{yo_l}(s) \; . \qquad (3.5.4\text{-}4)$$

where,

$$R_{ye_\ell}(s) = \frac{C_\ell}{\omega_o} e^{-st_\ell} \left[\frac{s}{\omega_o} I - A_\ell \right]^{-1} \left(I - e^{-sT_\ell} e^{A_\ell \omega_o T_\ell} \right) \cdot K_\ell \Phi_{\ell-1} \cdots K_2 \Phi_1 \qquad (3.5.4\text{-}5)$$

$$R_{yo_\ell}(s) = \frac{C_\ell}{\omega_o} e^{-st_\ell} \left[\frac{s}{\omega_o} I - A_\ell \right]^{-1} \left(I - e^{-sT_\ell} e^{A_\ell \omega_o T_\ell} \right) \cdot K_\ell \Phi_{\ell-1} \cdots K_6 \Phi_4 \qquad (3.5.4\text{-}6)$$

3.5.5 Complete Transfer Function

The complete transfer function is found, by linear superposition, to be.

$$\frac{\delta y(s)}{\delta v_{amp}(s)} = R_{ye}(s) \cdot S_e(s) \cdot PWM_e(s) + R_{yo}(s) \cdot S_o(s) \cdot PWM_o(s) \; . \qquad (3.5.5\text{-}1)$$

where $R_{ye}(s)$, $S_e(s)$, $PWM_e(s)$, $R_{yo}(s)$, $S_o(s)$ and $PWM_o(s)$ are expressed by (3.5.4-5), (3.5.2-19), (3.5.1-6), (3.5.4-6), (3.5.2-20) and (3.5.1-7) respectively. The term $1/T_h$ of (3.5.1-6) and (3.5.1-7) cancels the factor T_h of (3.5.2-19) and (3.5.2-20). From (3.4.2-6), (3.4.2-7) and (3.4.2-9), it is noted that ω_o can be factored out of k_1 and k_4. ω_o can therefore be factored out from (3.2.5-19) and (3.2.5-20) and be canceled with the term $1/\omega_o$ of (3.5.4-5) and (3.5.4-6). Factoring $K_{pwm} e^{-st_{d_{pwm}}}$, (3.5.5-1) can be rewritten as

$$\frac{\delta y(s)}{\delta v_{amp}(s)} = K_{pwm} e^{-st_{d_{pwm}}} \overline{G(s)} \; , \qquad (3.5.5\text{-}2)$$

where the dimensionless quantity $\overline{G(s)}$ is referred to as the normalized converter transfer function.

3.6 EQUIVALENT MODEL

The mathematical formulation of the *Small-Signal Frequency Response Theory* yields the frequency response of the converter that would otherwise be unknown. However, this method suffers from two major drawbacks. First, it is very computationally intensive, and obtaining the frequency response is time consuming. Secondly, the method is very abstract and its use does not refer to concepts for which a trained design engineer has an intuitive understanding. To overcome these difficulties an equivalent model is developed in this section.

Numerous plots of $\overline{G(s)}$ have been done for various operating points and values of $\overline{Z_{co}}$. Four examples, for which R_{rt} and R_c are assumed to be negligible, are shown in Figures 3-12 to 3-15.

By comparing the plots for the various operating points, it becomes apparent that, in continuous mode, the transfer function is similar to that of a second order filter. The resonant frequency is noted to be independent of $\overline{M}$ or $\overline{Q}$. It is solely dependant of $\overline{Z_{co}}$. The damping on the other hand increases with the load. The converter behaves as if an equivalent inductor L_e was resonating with the output capacitor C_o, the damping being a function of the load resistance. Figure 3-16 illustrates the equivalent circuit where the amplifier with gain K_{dc} models the DC gain of the converter.

Letting

$$L_e = \frac{L_r}{k_c^2}, \qquad (3.6.0\text{-}1)$$

the natural frequency of the second-order pole is

$$\omega_{po} = \left[\frac{1}{\frac{L_r}{k_c^2} \cdot C_o} \right]^{1/2}, \qquad (3.6.0\text{-}2)$$

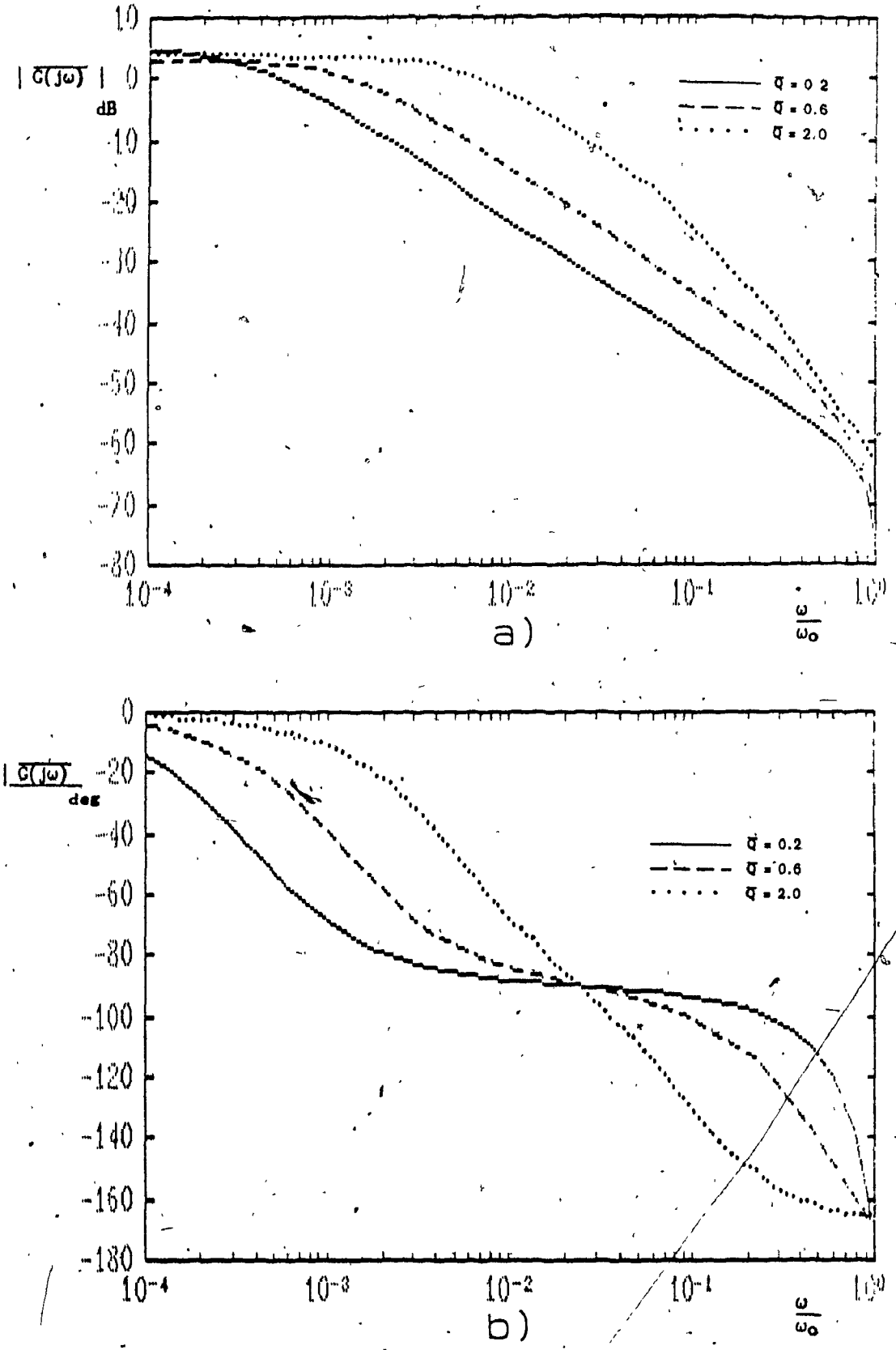

Figure 3-12: PWM Frequency Response for M=0.6 and $\overline{Z_{co}}$= 0.001
a) Magnitude
b) Phase

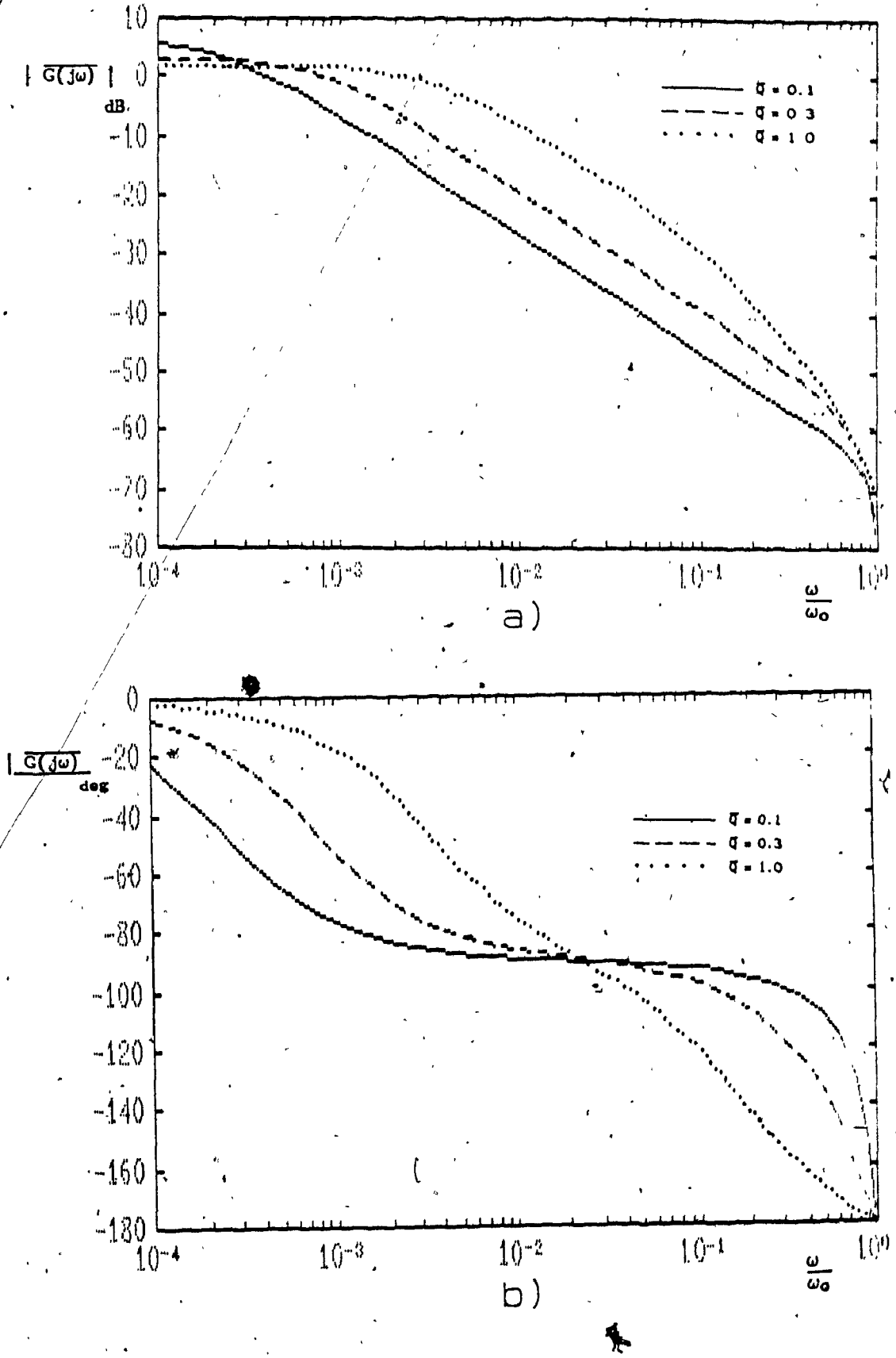

Figure 3-13: PSPWM Frequency Response for M=0.6 and $\overline{Z_{co}}$= 0.001
a) Magnitude
b) Phase

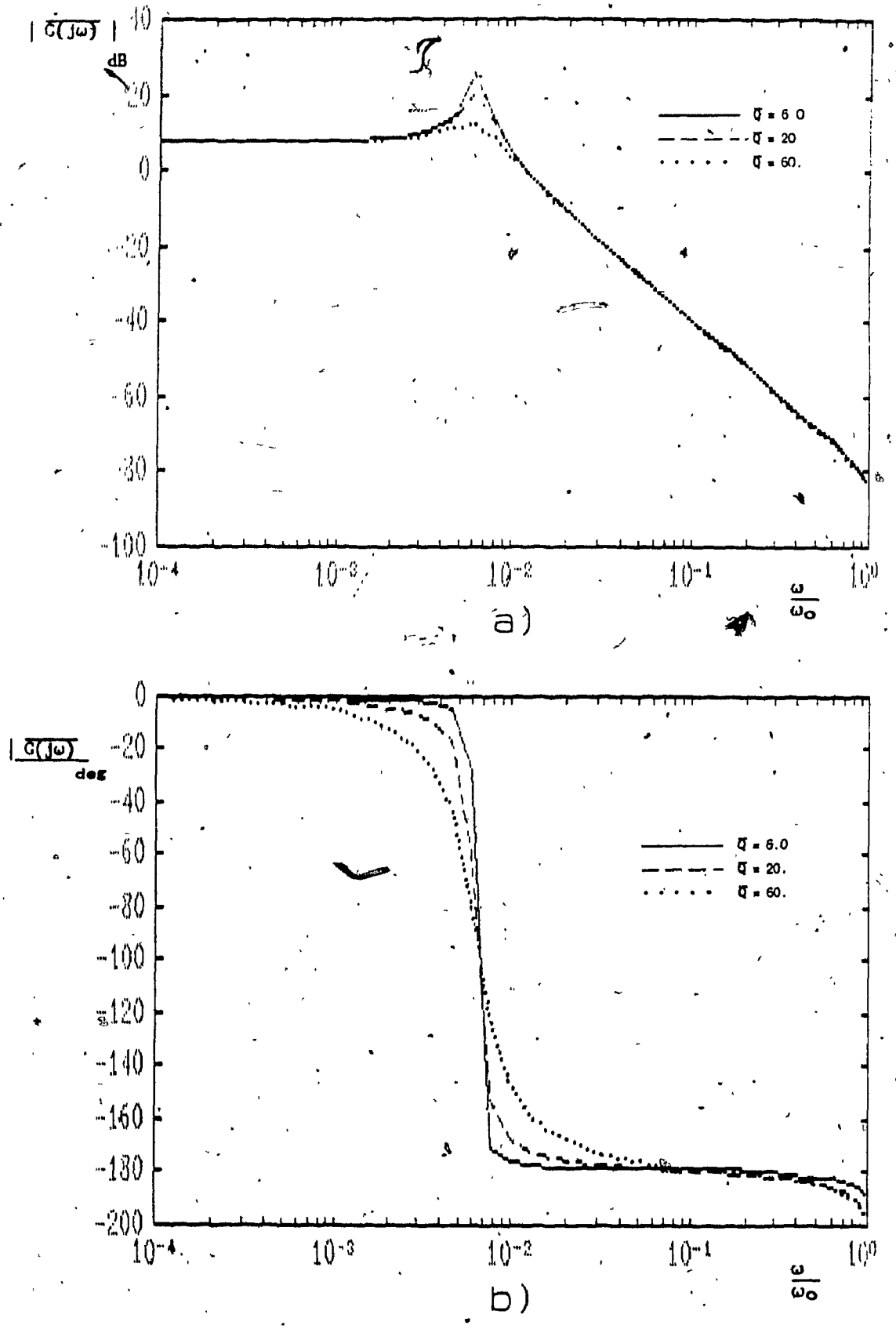

Figure 3-14: PWM Frequency Response for M=0.3 and $\overline{Z_{co}}$= 0.0001
a) Magnitude
b) Phase

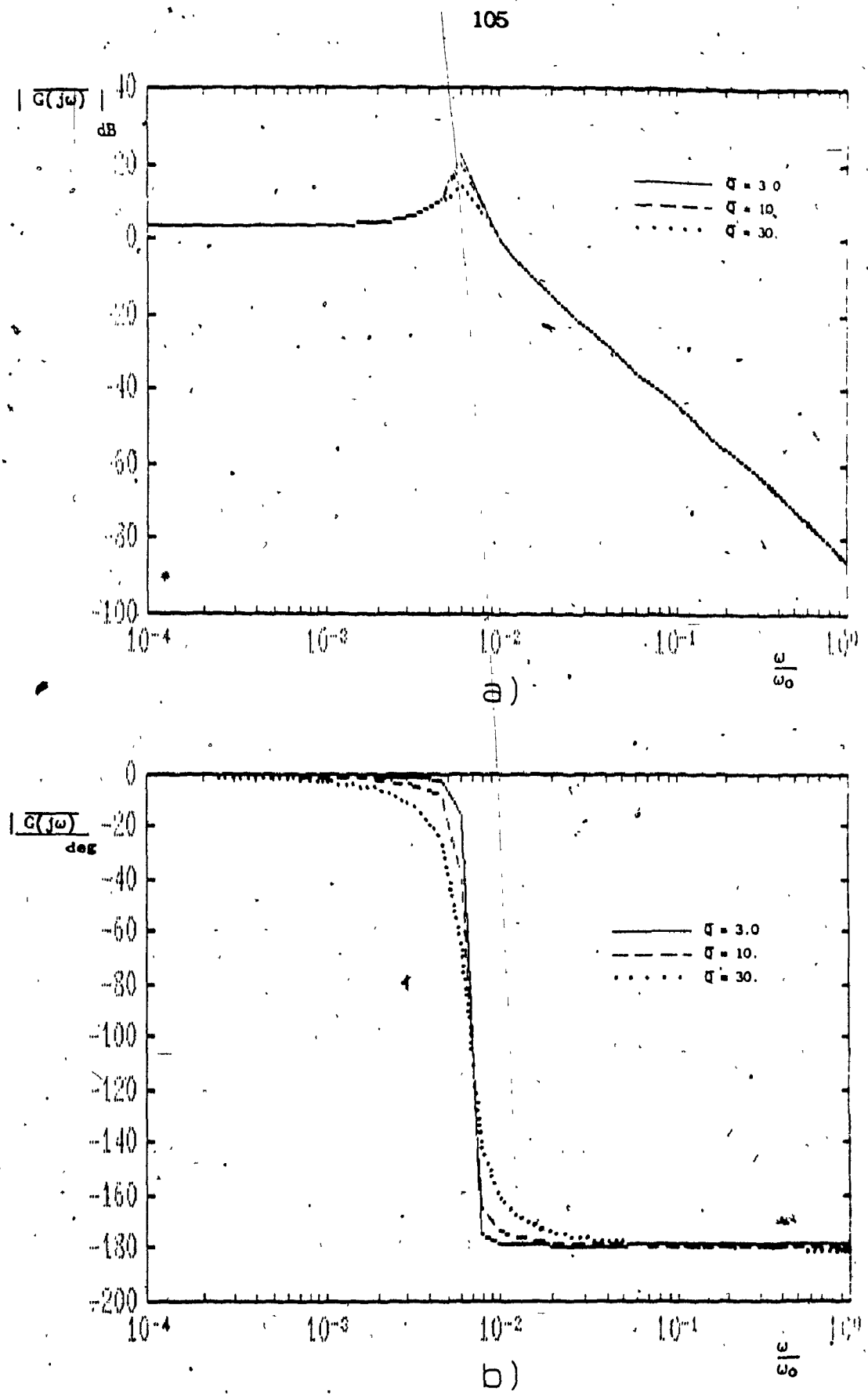

Figure 3-15: PSPWM Frequency Response for M=0.3 and $\overline{Z_{co}}$= 0.0001
a) Magnitude
b) Phase

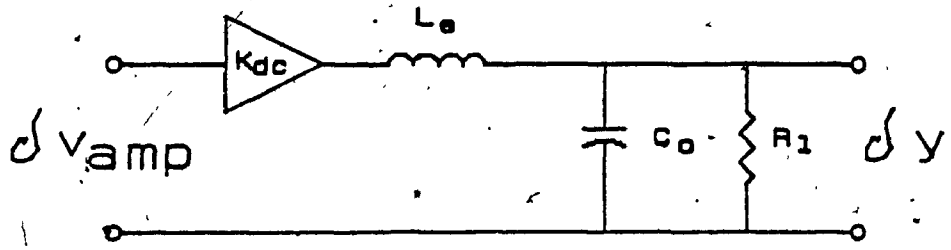

Figure 3-16: Equivalent Model for Continuous Conduction

$$\frac{\omega_{po}}{\omega_o} = k_c \cdot \left[\frac{1}{L_r\omega_o \cdot C_o\omega_o} \right]^{1/2}$$

$$= k_c \cdot \left[\frac{Z_{co}}{Z_o} \right]^{1/2} = k_c \cdot \overline{Z_{co}}^{1/2} . \qquad (3.6.0\text{-}3)$$

Studying the plots, the numerical value for k_c has been found to approach

$$k_c \doteq \frac{2\pi}{10} . \qquad (3.6.0\text{-}4)$$

The normalized transfer function in continuous mode is found, from the equivalent circuit of Figure 3-16, to be

$$\overline{G(s)} = \frac{K_{dc}}{L_eC_os^2 + \frac{L_e}{R_\ell} s + 1} = \frac{K_{dc}}{L_eC_o\, s^2 + \frac{L_eC_o}{R_\ell C_o} s + 1}$$

$$= \frac{\beta K_{dc}}{1 - \left[\frac{\omega/\omega_o}{\omega_{po}/\omega_o} \right]^2 + j \frac{2}{\pi} \overline{Q}\, \overline{Z_{co}} \left[\frac{\omega_o}{\omega_{po}} \right]^2 \cdot \frac{\omega}{\omega_o}} . \qquad (3.6.0\text{-}5)$$

In discontinuous mode, the converter also exhibits a second order behavior, however the poles are distinct and real. The first pole of the system is heavily dependant on the load. The frequency of the first pole is lower at low load. This behavior is similar to that of a capacitor filter in parallel with a resistor fed by a current source. Examining the plots, it is seen that the frequency of the pole is not strictly linear with load and that it is also dependant on M. The first pole frequency is therefore found to be

$$\frac{\omega_{p1}}{\omega_o} = k'_d(M,\overline{Q}) \cdot \frac{1}{R_\ell C_o\omega_o} = k_d(M,\overline{Q}) \cdot \overline{Q} \cdot \overline{Z_{co}} . \qquad (3.6.0\text{-}6)$$

$k_d(M,\overline{Q})$ is plotted in Figure 3-17. Since the system is of the second

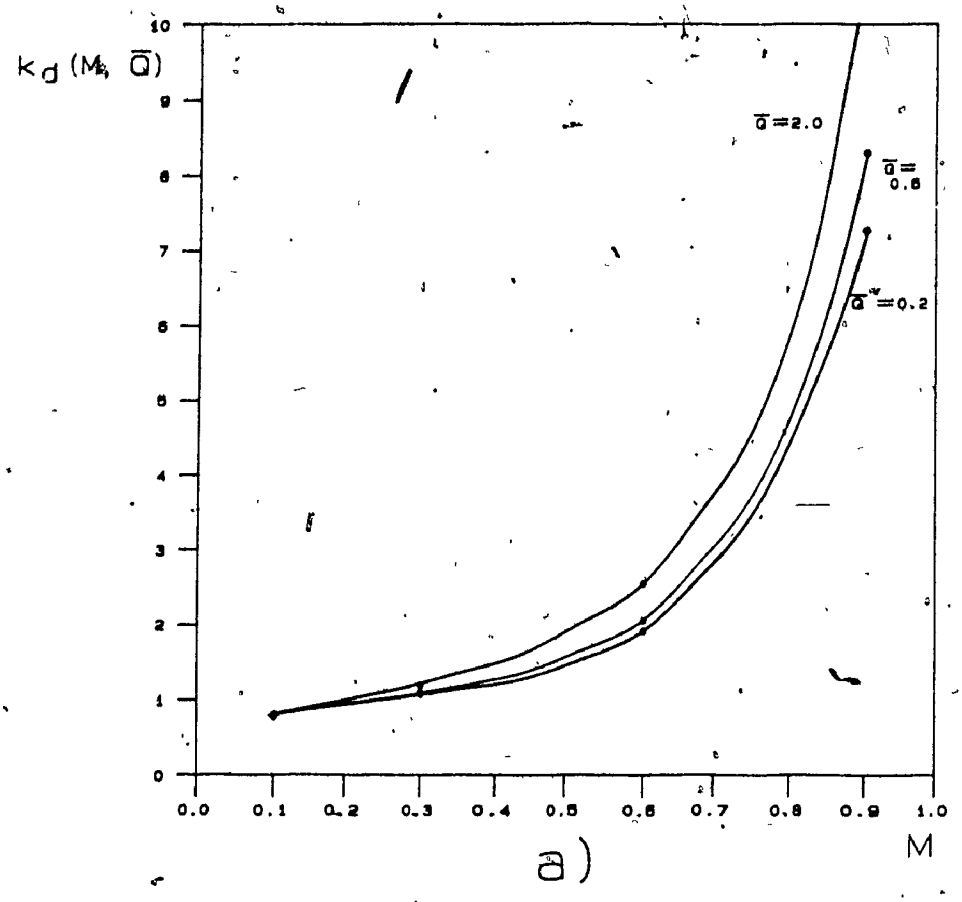

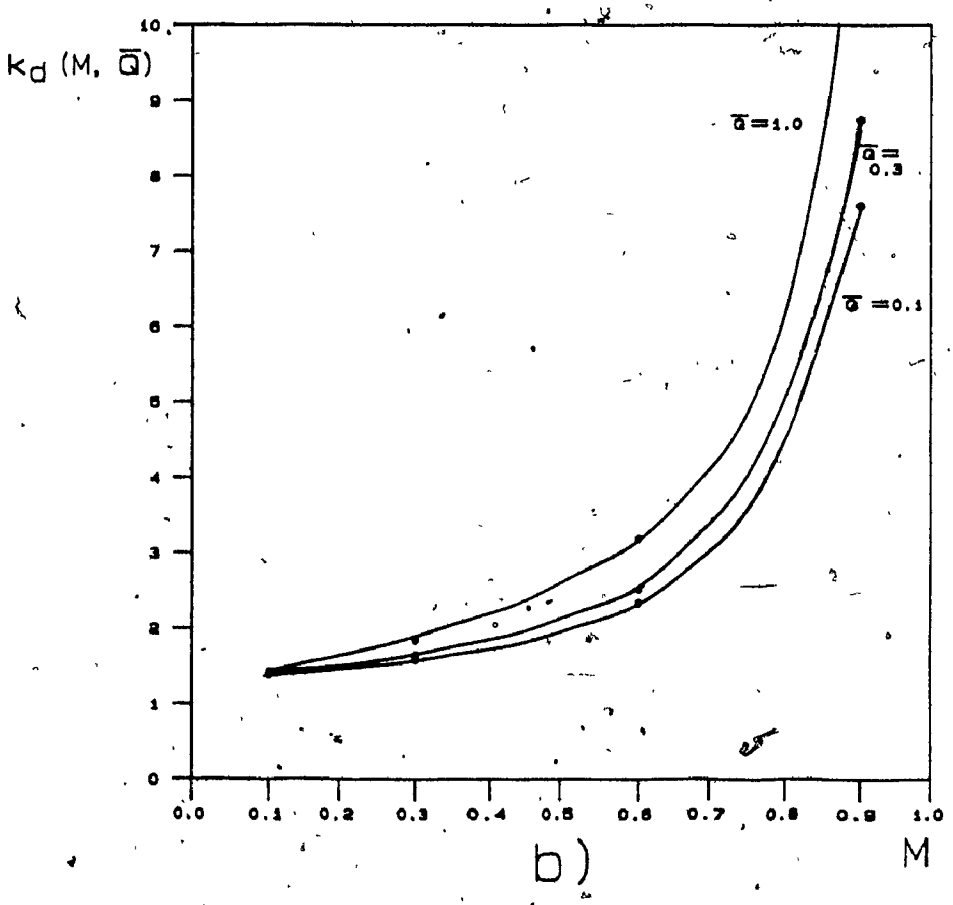

Figure 3-17: Pole Scaling Factor for Discontinuous Mode
a) PWM
b) PSPWM

order, its transfer function can be expressed as

$$G(s) = \frac{K_{dc}}{\left[1 + \frac{j\omega}{\omega_{p1}}\right] \cdot \left[1 + \frac{j\omega}{\omega_{p2}}\right]}$$

$$= \frac{K_{dc}}{1 - \frac{\omega^2}{\omega_{p1}\omega_{p2}} + j\omega\left[\frac{1}{\omega_{p1}} + \frac{1}{\omega_{p2}}\right]} \qquad (3.6.0\text{-}7)$$

It is noted from Figure 3-12 and 3-13 that, at ω_o, the phase lag is -90^o for all values of $\overline{Q}$. This is the case for all values of $\overline{Z_{co}}$. From (3.6.0-7), ω_{p2} is therefore found to be[4]

$$\omega_{p2} = \frac{\omega_{po}^2}{\omega_{p1}} \qquad (3.6.0\text{-}8)$$

The DC gain is obtained by numerically performing the differentiation

$$K_{dc} = \frac{\partial M}{\partial D} \qquad (3.6.0\text{-}9)$$

The DC gain for PWM and PSPWM is shown in Figure 3-18. Note that for M greater than 0.9 the gain falls sharply, so control of the converter in this region is not very effective.

The predictions of the simplified model versus the results obtained with the formal method are shown in Figures 3-19 and 3-20. The agreement is very good up to $0.5\omega_o$. This has been verified to be the case for many operating points. The simplified model can therefore be used to design the loop compensation as, in general, the loop crossover frequency is designed to be below $0.5\omega_o$.

---

[4]For large values of $M \cdot \overline{Z_{co}}$, (eg. $M \cdot Z_{co} > 0.05$), ω_{p1} and ω_{p2} become complex conjuguates. (3.6.0-8) still holds and the transfer function exhibits a resonance at ω_{po}. If the use of Figure 3-17 yields ω_{p1} greater than ω_{po}, the transfer function is better modeled by using (3.6.0-6) and replacing $\overline{Q}$ by $1/\overline{Q}$ in the denominator of this expression. K_{dc} is evaluated using the correct value for $\overline{Q}$.

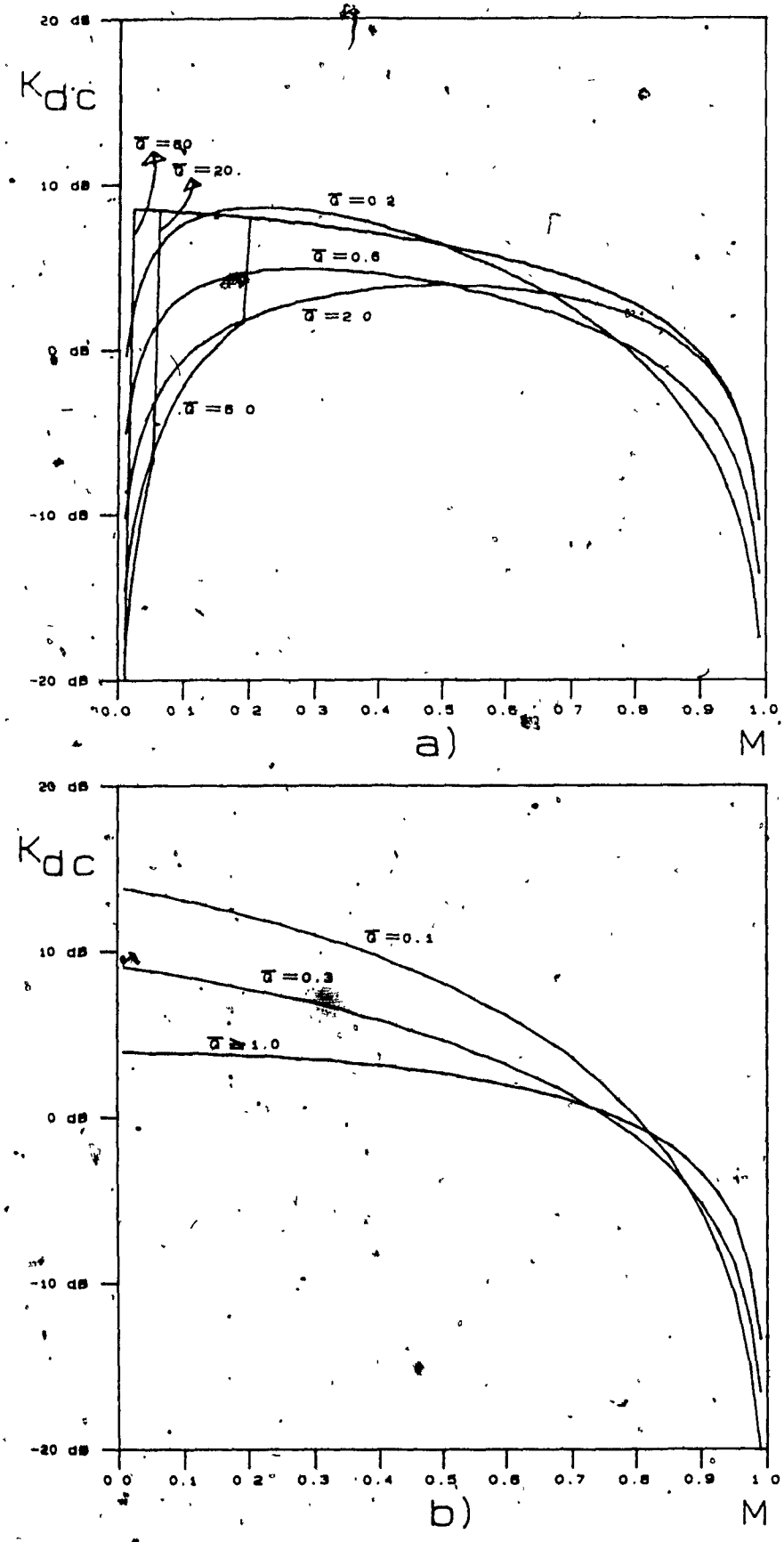

Figure 3-18: Normalized DC Gain of the Converter

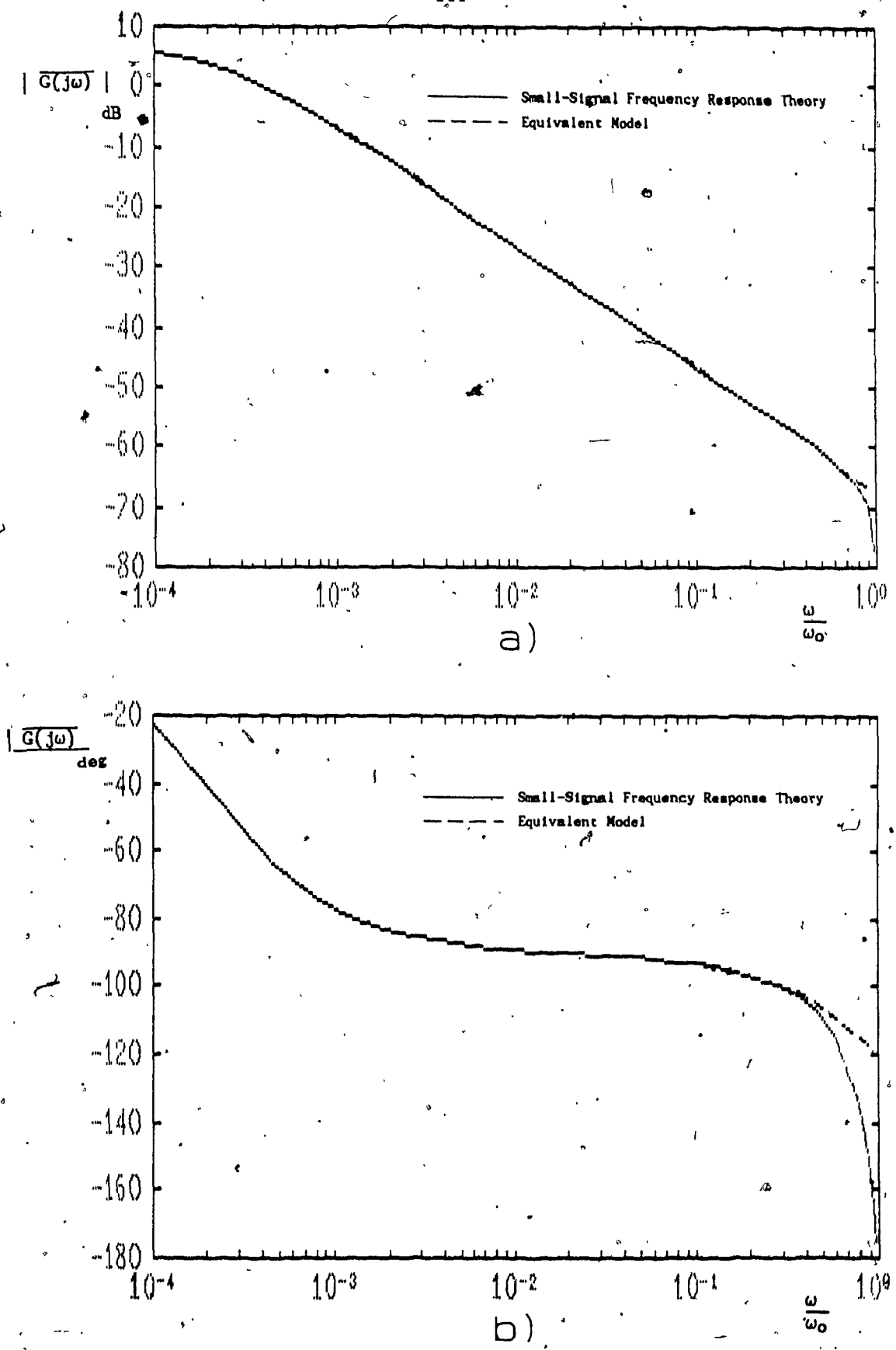

Figure 3-19: Equivalent Model versus Small-Signal Frequency Response Theory for PSPWM, M=0.6, $\overline{Q}$=0.1 and $\overline{Z_{co}}$=0.001.
a) Magnitude
b) Phase

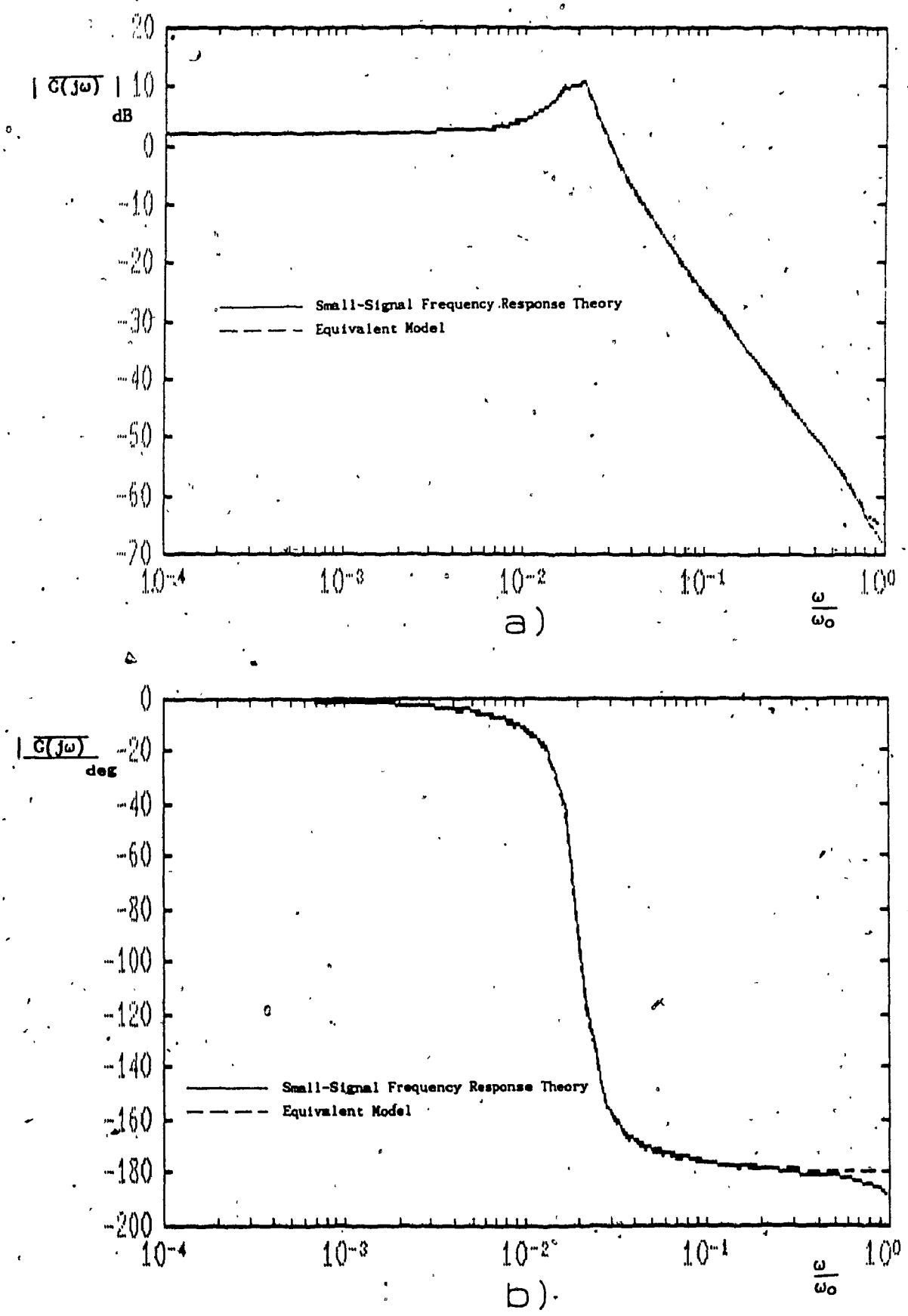

Figure 3-20: Equivalent Model versus Small-Signal Frequency Response Theory for PSPWM, M=0.6, $\overline{Q}$=10. and $\overline{Z_{co}}$=0.001.
a) Magnitude
b) Phase

If the esr (R_c) of the output capacitor is non-negligible, then the simplified model can be adjusted by multiplying the numerator of (3.6.0-5) and (3.6.0-7) by

$$1 + j\omega \cdot R_c C_o = 1 + j \frac{\omega}{\omega_o} \frac{Q_{co}}{Z_{co}} \qquad (3.6.0\text{-}10)$$

which is adds a zero to these functions.

CHAPTER 4: EVALUATION, SELECTION, VERIFICATION

In this chapter, PWM and PSPWM in continuous or discontinuous conduction mode are compared using material derived in the preceding chapters. A selection of switching strategy and conduction mode is made based on the comparative evaluation. A design example and experimental verification are carried out.

4.1 STEADY-STATE STRESS

Component stresses are compared for various operating points. Since the use of a transformer is assumed, the voltage transfer ratio M can be arbitrarily selected. Once an operating M and turns ratio are selected the value of the characteristic impedance can be arbitrarily selected. Referring the impedance of the load to the primary side, selecting a value for Z_o is synonymous to selecting Q. The stress levels are therefore plotted for various values of $\bar{Q}$. The operational VA of critical components are shown in Figures 4-1 to 4-7, both for PWM and PSPWM operation.

In constant output voltage applications the graphs can easily be used to evaluate the variation of the stress with variation in input voltage. A decreasing M is synonymous of an increasing output voltage. The graphs cover the range $V_{in_{low}} = V_o$ (M=1) to $V_{in} = 40V_o$ (M=.025). The graphs can also be used in variable output voltage applications. For that case, it has to be kept in mind that actual power, for a given $\bar{Q}$, is proportional to V_o^2. Since the curves yield VA/P_o, the stresses must be scaled by the square of the relative output voltage. For example, if it is desired to compare the stress at $V_{in}=1.5*V_{in_{low}}$ and $V_o=V_{in_{low}}/2$, that is M = .333, and to the stress at $V_{in}=V_o=V_{in_{low}}$, that is M=1, then the reading at M=.333 must be divided by 4 to obtain the relative stresses.

Figures 4-1 to 4-7 are now individually analyzed.

4.1.1 Input Bus VA

Figure 4-1 shows the input VA stress. As the voltage is the bus voltage, this figure conveys information on the input current stress. Since operation in PWM returns energy to the bus, it is expected that this mode of operation will generate more stress than PSPWM operation. Figures 4-1a) and 4-1b) allow to quantitatively evaluate this difference.

4.1.2 Switch VA

For simplicity, the VA of the switches and of the anti-parallel diodes are lumped. VA_{sw} of Figure 4-2 is the product of the rms current flowing into S_t and D_t,

$$I_{sw_{rms}} = \frac{I_{r_{rms}}}{2^{1/2}} \qquad (4.1.2\text{-}1)$$

multiplied by the standoff voltage. Since the standoff voltage is simply expressed in term of the input voltage, Figure 4-2 yields information on the rms current flowing in the switches and the resonant tank components. It is seen that for high $\bar{Q}$ there is no difference in rms current stress between the two switching strategies. This contradicts the intuitive notion that, since operation in PSPWM does not return energy to the bus, the current stress in the switches and resonant elements must be lower with PSPWM operation than for PWM operation. This contradiction is explained as follows. For $\bar{Q}$ approaching infinity, the current in the resonant tank becomes perfectly sinusoidal. Since the resonant current is full-wave rectified into the load, the amplitude of the resonant current is dependant only on the output voltage and current. This amplitude is

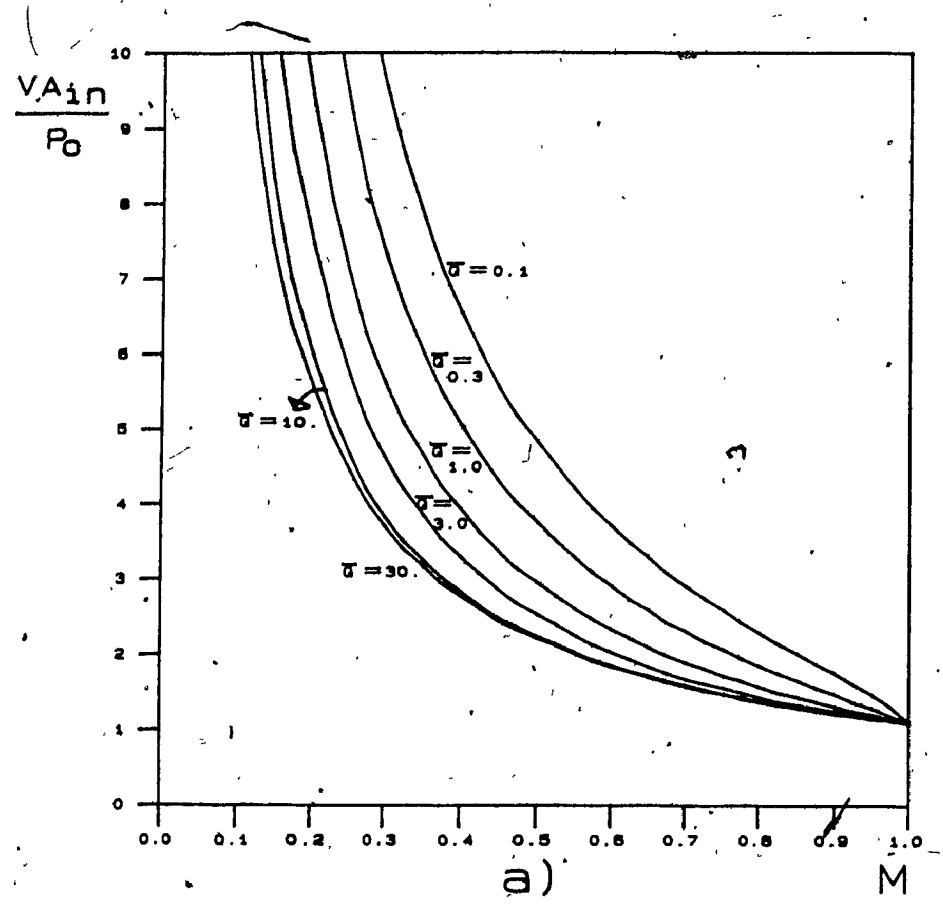

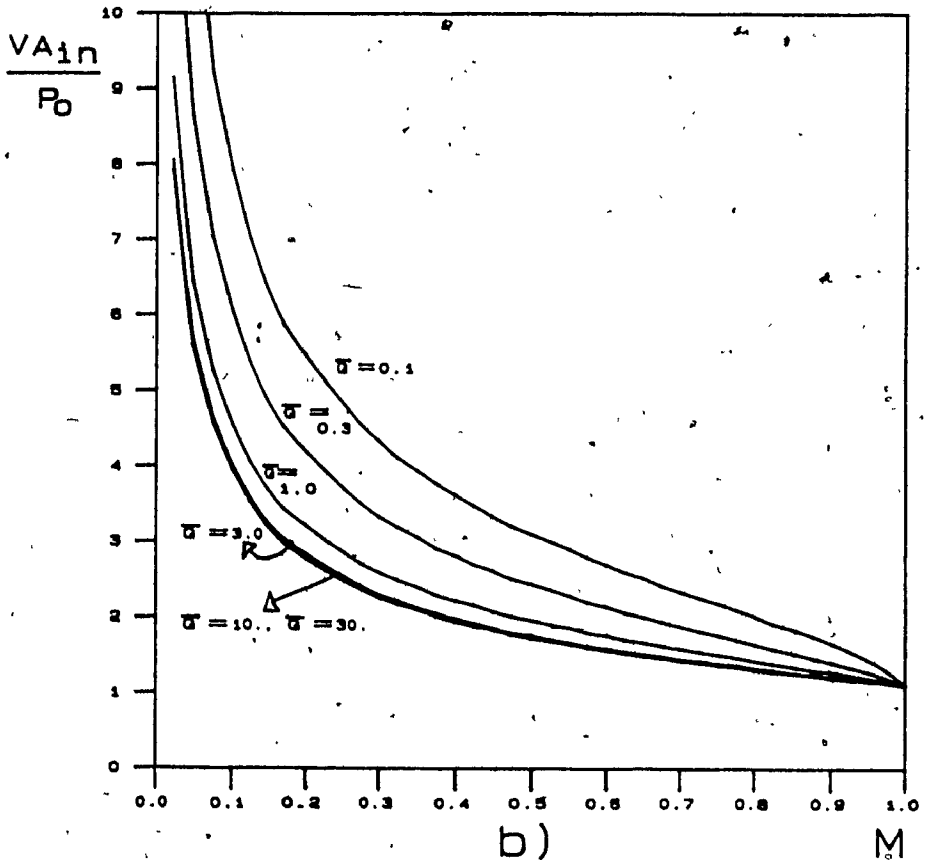

Figure 4-1: Input Bus VA_{op}
a) PWM
b) PSPWM

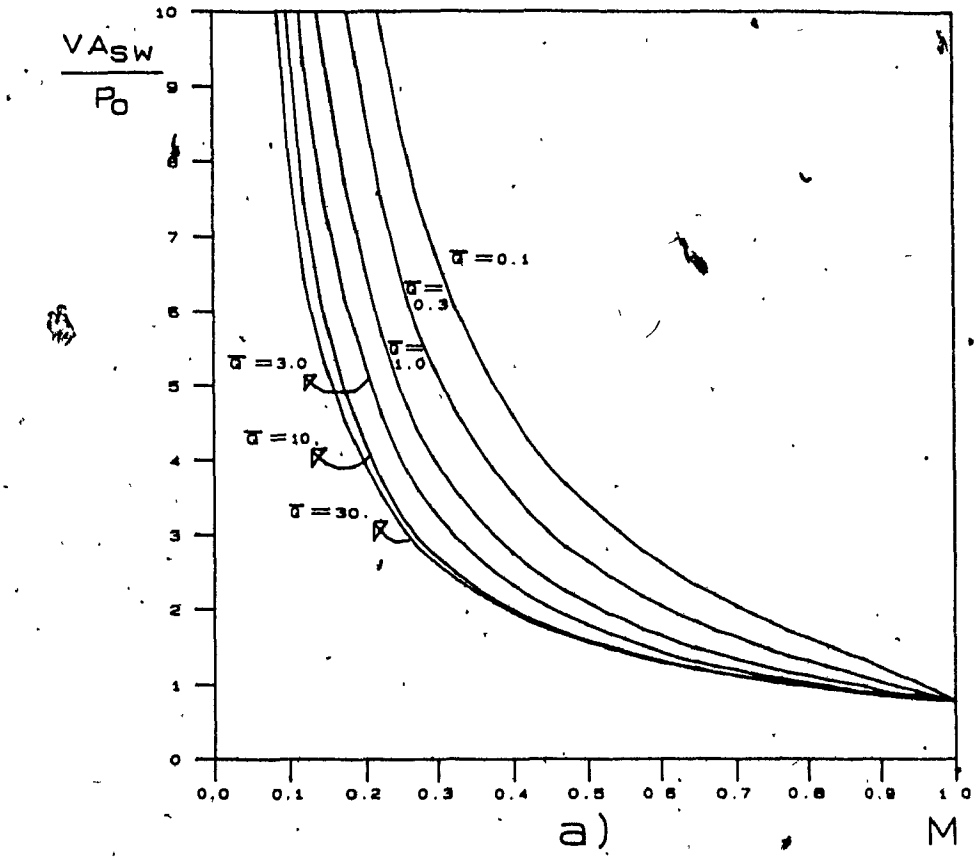

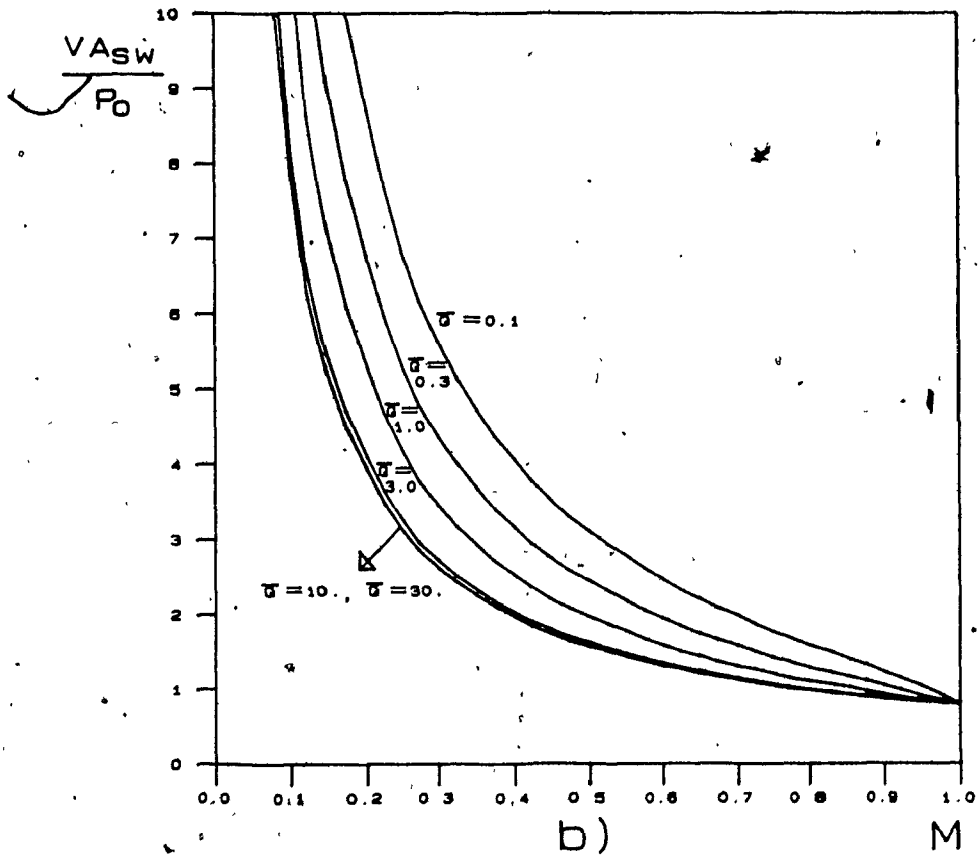

Figure 4-2: Switch VA_{op}
a) PWM
b) PSPWM

not dependant on the mechanism used to generate it.

For smaller loads, PSPWM operation will generate smaller current stress. One case of interest is the operation at the boundary between continuous and discontinuous conduction. For PSPWM this boundary is $\bar{Q}=1$. Since the maximum value for M is 1, it is seen from (2.2.3-4) that in PWM discontinuous conduction is guaranteed for for all duty cycles for $\bar{Q} < 2$. $\bar{Q} = 2$ is the boundary between the two modes for maximum duty cycle when M=1. Interpolating for $\bar{Q}=2$ on Figure 4-2b) and comparing with $\bar{Q}=1$ on Figure 4-2a), it is seen that the current stress is almost identical for both control strategies except for very low M where the stress is less in PSPWM.

4.1.3 Resonant Tank VA

It is seen, from Figures 4-3 and 4-4, that the resonant component stresses are identical at M=1 and become larger for operation in PWM as M tends to zero. The difference is even more pronounced for the resonant inductor as its volt-second stress is, from (2.3.5-22), a function of the peak current. Since peak current and rms current are related, the dependence of the inductor stress is related to the current stress by a second order dependence. The difference between PWM and PSPWM stress is therefore more pronounced for low values of M where the resonant current rms and peak values are larger for PWM operation.

4.1.4 Transformer VA

Transformer VA's are similar for the two switching strategies. Detailed comparison between the two sets of curve families does not yield significant information. Note that, in Figure 4-5b), the changes in slope are coincident to the operation points where the core resets just before the start on the next half-cycle.

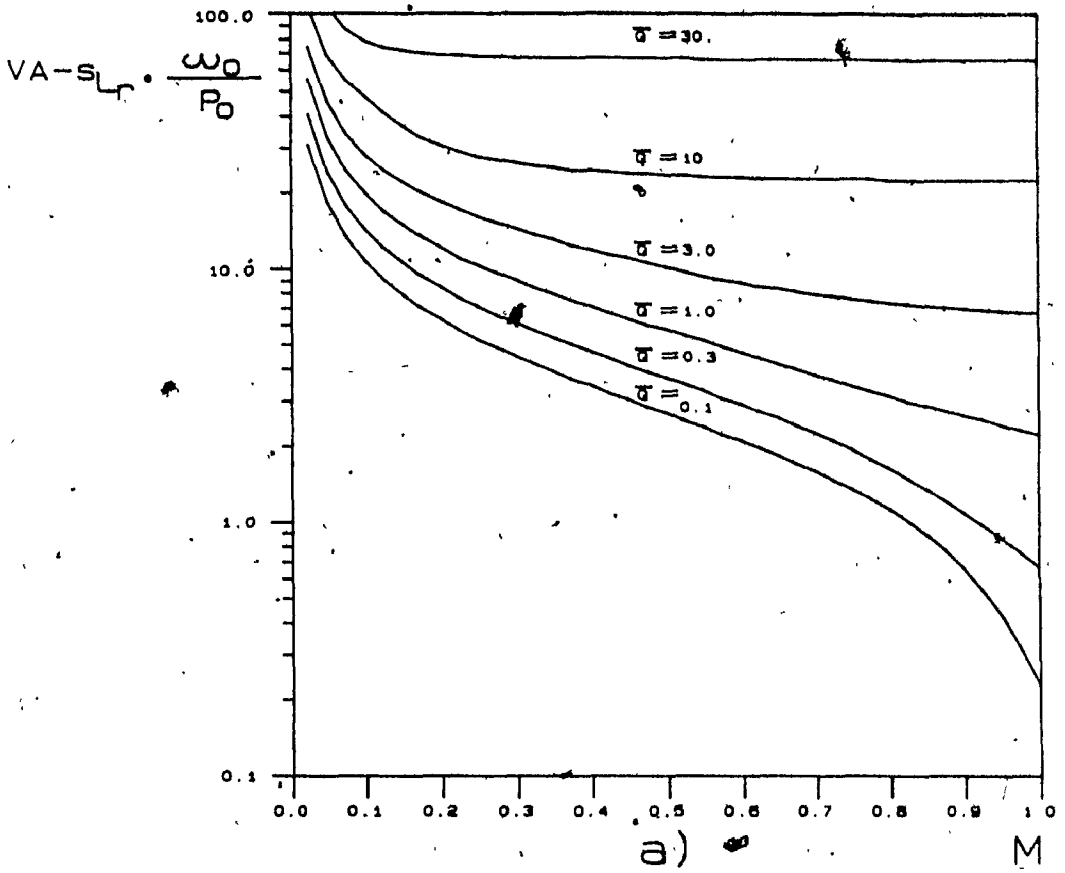

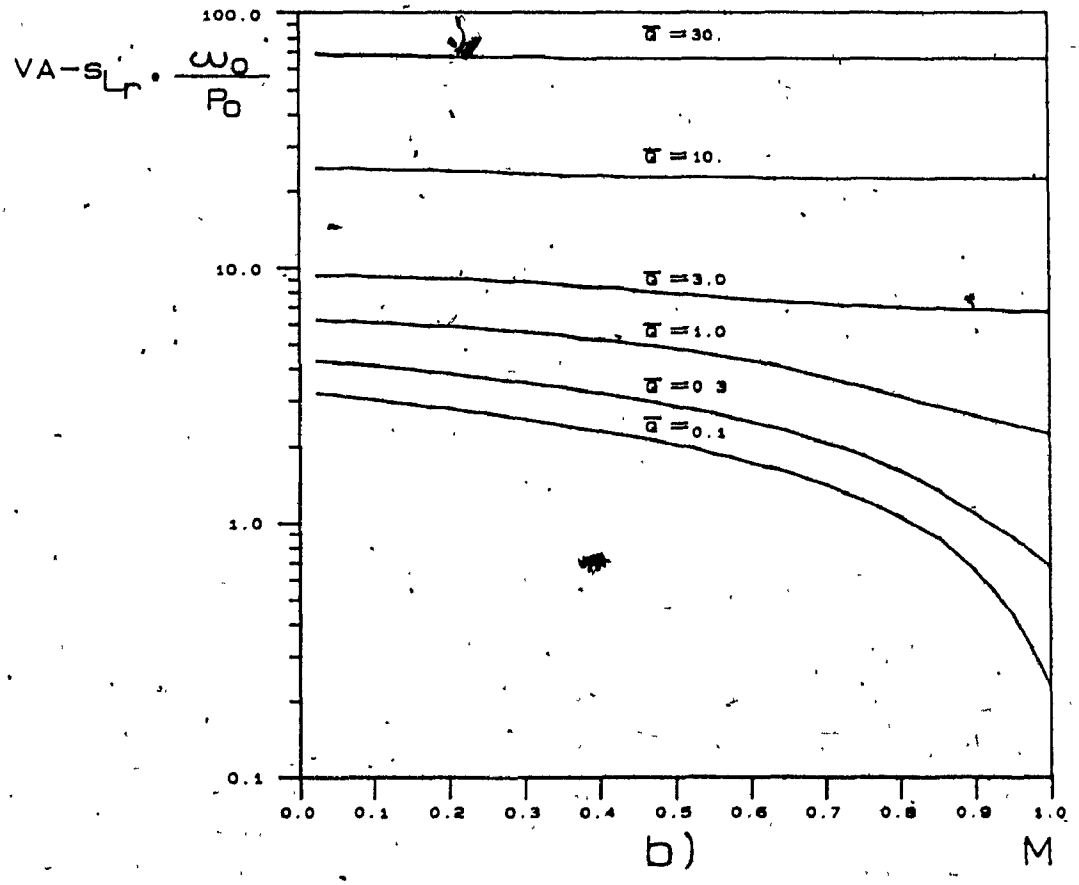

Figure 4-3: Resonant Inductor VA-s_{op}
a) PWM
b) PSPWM

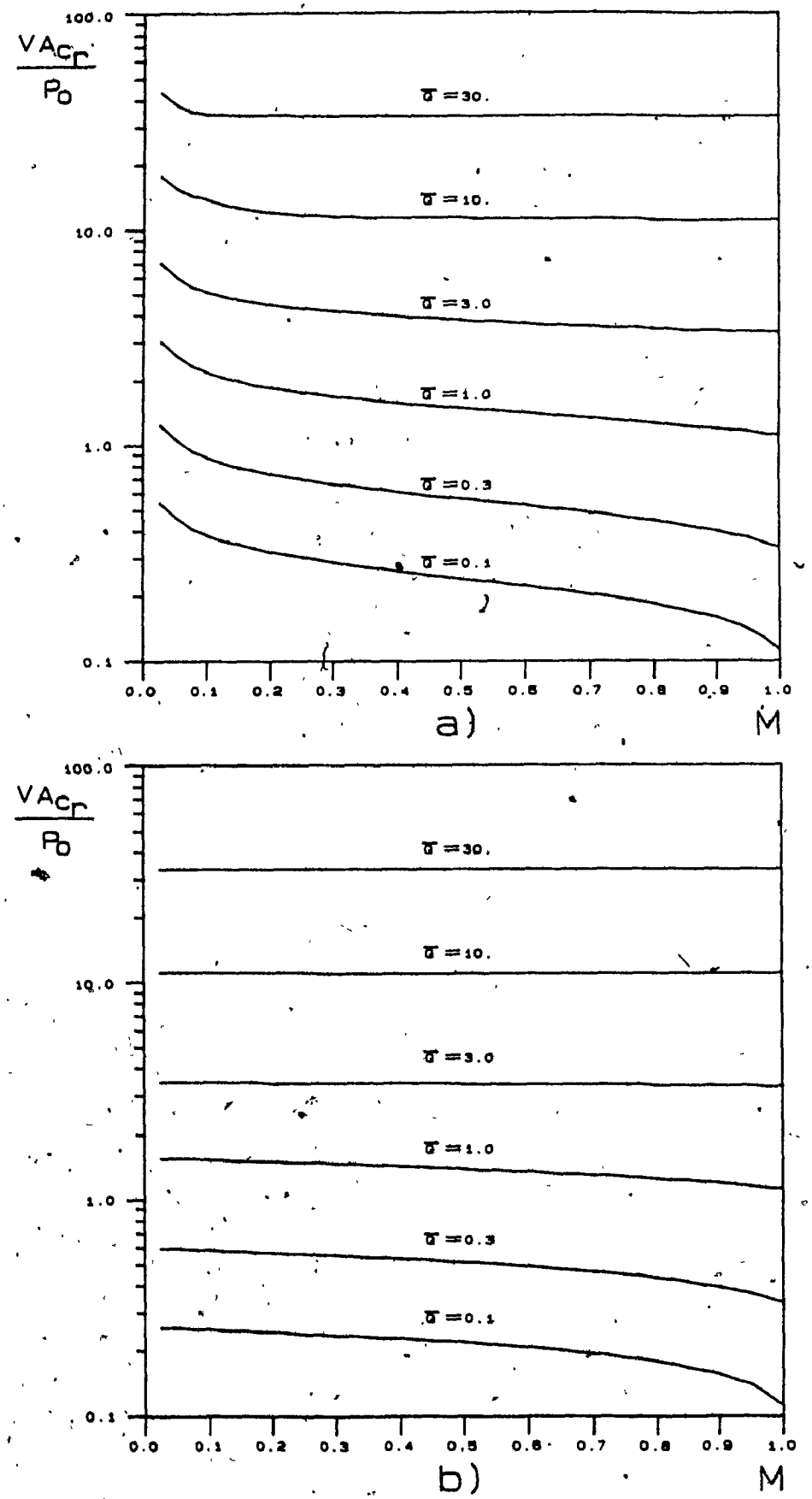

Figure 4-4: Resonant Capacitor VA_{op}
a) PWM
b) PSPWM

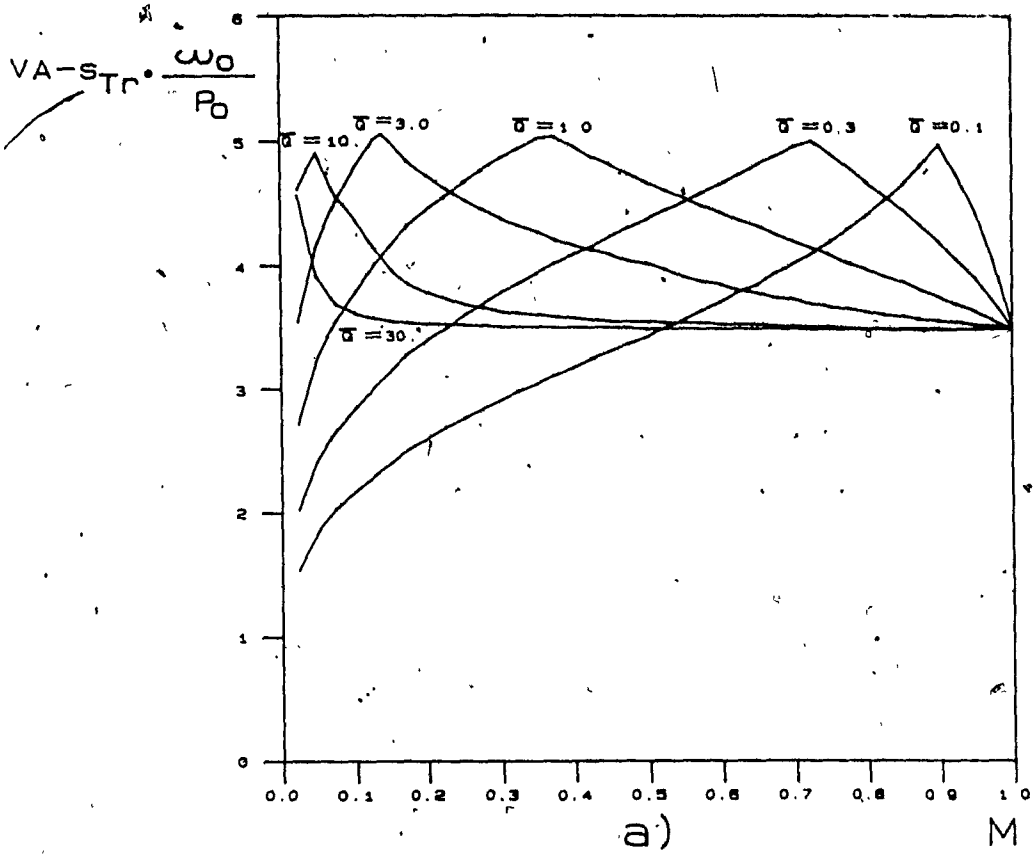

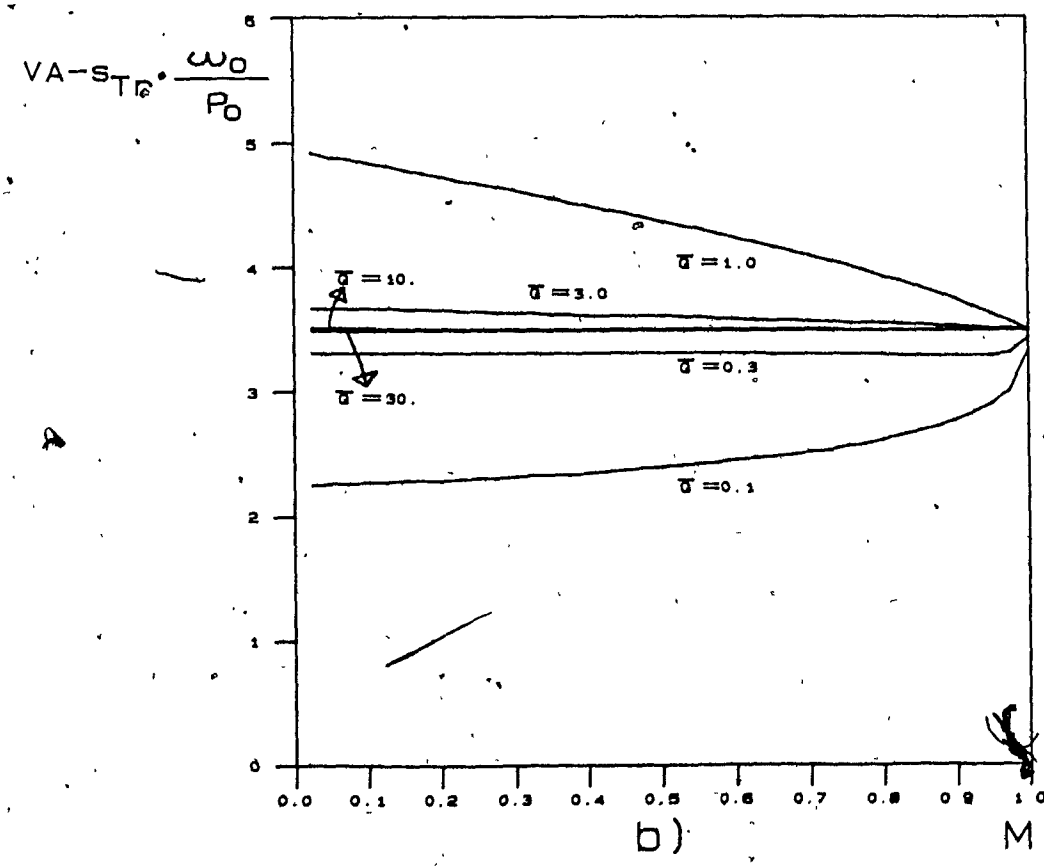

Figure 4-5: Transformer VA-s_{op}
a) PWM
b) PSPWM

4.1.5 Output Components VA

From (2.3.5-32), (2.3.5-33), (2.3.5-35) and (2.3.3-10), the VA of the output rectifiers becomes

$$VA_{CR_{op}} = cst \cdot \frac{I_{pk}}{I_o} \cdot \frac{V_{in_{low}}}{V_o} = cst \cdot \frac{I_{pk}}{I_o} . \qquad (4.1.5\text{-}1)$$

Figures 4-6 is plotted for a constant multiplier equal to 1.

From (2.3.5-36), (2.3.5-38) and (2.3.3-10), the VA of the output capacitor becomes

$$VA_{Co_{op}} = \frac{I_{co_{rms}}}{I_o} \frac{V_{in_{low}}}{V_o} = \frac{I_{co_{rms}}}{I_o} . \qquad (4.1.5\text{-}2)$$

The output capacitor stress is plotted in Figure 4-7.

As for the resonant tank stress, it is seen that the component stresses are identical at M=1 and become larger for operation in PWM as M tends to zero. The asymptotic behavior of the current stress curves as M tends toward zero for PWM operation compared to the moderate increase for PWM operation can be understood as follows. Consider an operation point where $M << 1$. For ease of illustration it is also considered that $Q << 1$. The slope of the current waveform in PWM is therefore defined by V_{in}/L_r. The resonant current is illustrated in Figure 4-8a). If the input voltage is doubled, and the output voltage is kept constant, the area under the current waveform must remain constant. As seen in dashed lines this implies that the peak current doubles. In PSPWM, energy is not returned to the bus during the off-time and the slope of the current is defined by V_o/L_r. For the same 2 to 1 input voltage variation, and the same area under

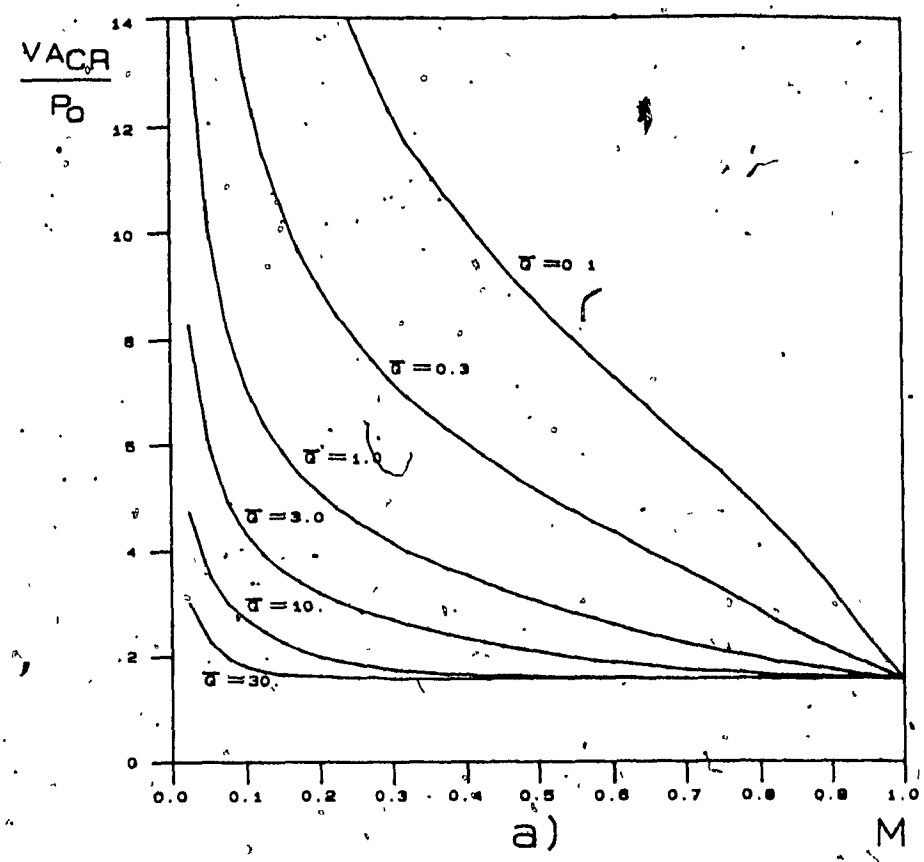

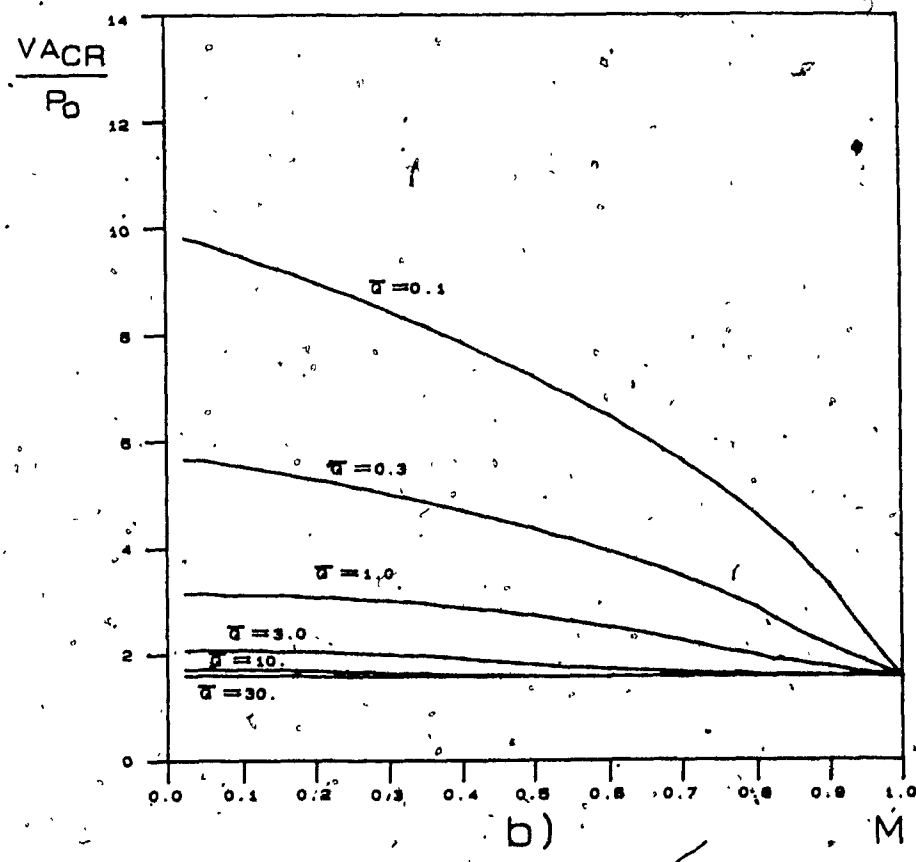

Figure 4-6: Output Rectifier VA_{op}
a) PWM
b) PSPWM

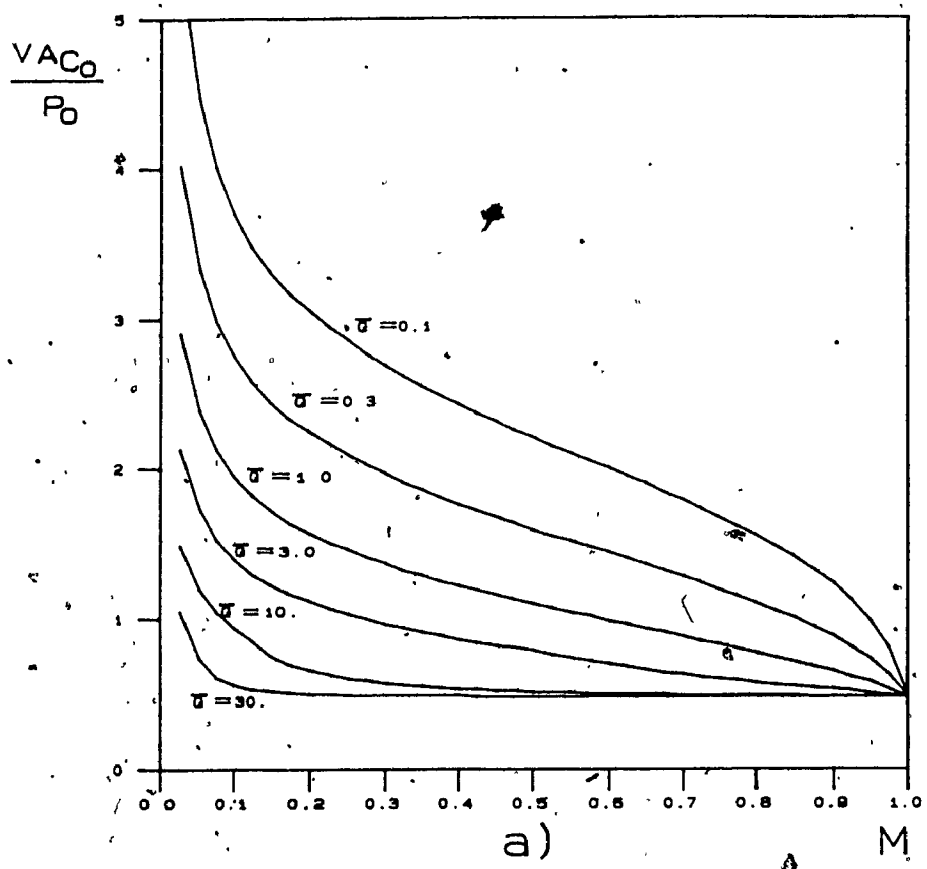

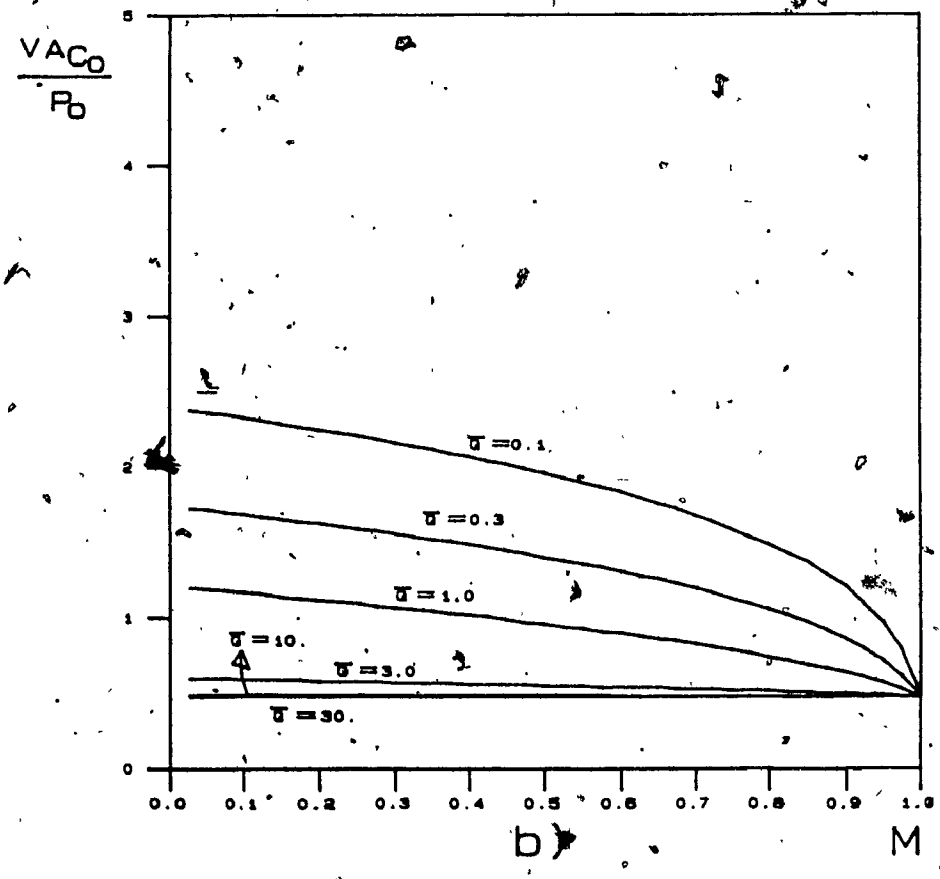

Figure 4-7: Output Capacitor VA_{op} -
a) PWM
b) PSPWM

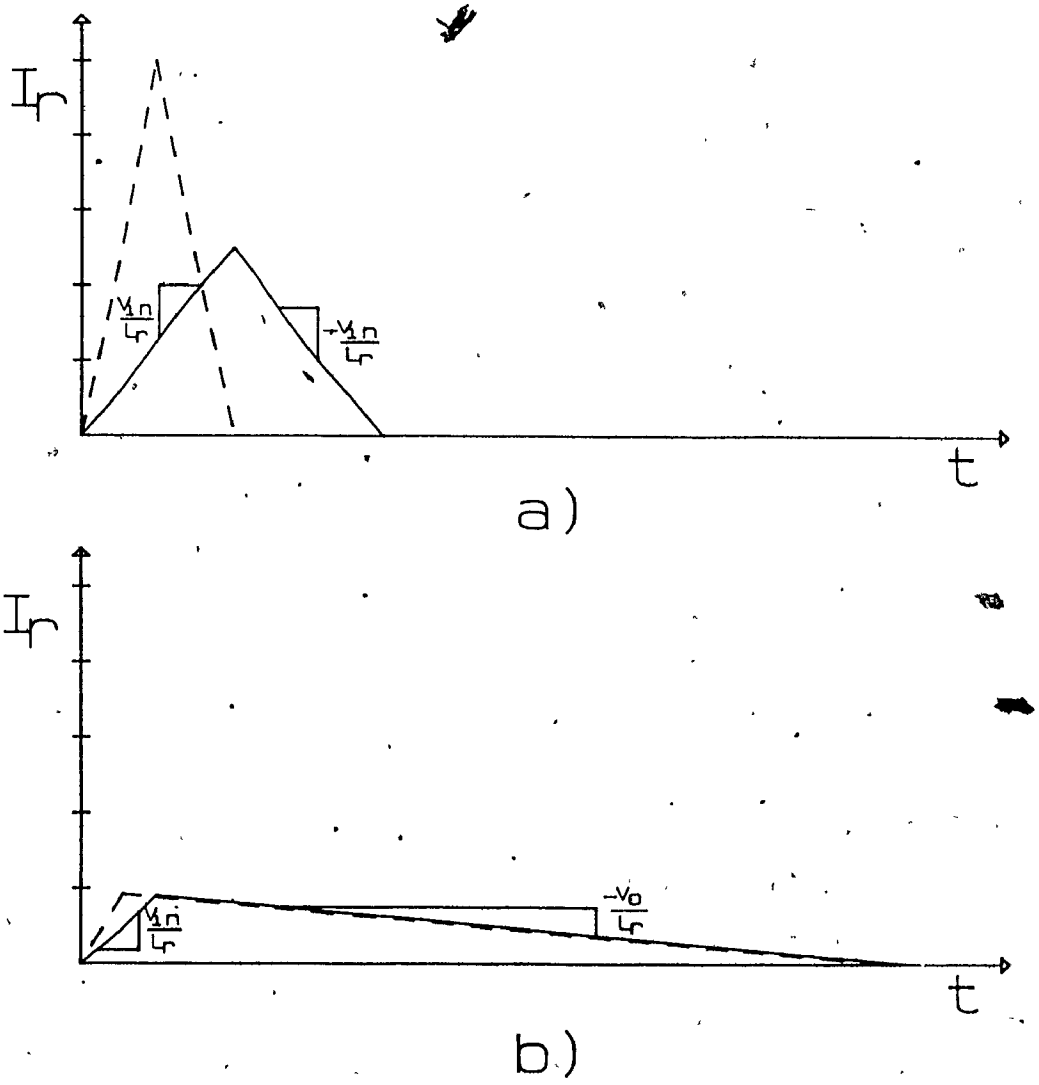

Figure 4-8: Resonant Current for Low Values of M
a) PWM
b) PSPWM
(The dashed-line waveforms are for twofold increase in input voltage.)

the current waveform, it is seen from Figure 4-8b) that the peak current remains almost unchanged. If the assumption that $\bar{Q}$ is small is relaxed, continuous conduction is approached. As $\bar{Q}$ approaches infinity the resonant current waveform approaches a perfect sinusoid and the ratios of peak and rms current to output current are constant as seen on the curves for PSPWM. In PWM, continuous conduction is not achieved for the values of $\bar{Q}$ illustrated and the stress curves are asymptotic as M tends to zero.

4.2 SWITCHING STRESS

4.2.1 PWM, Discontinuous Mode

As can be seen from Figure 2-2a), turn-on switching losses in this mode are low. The switches are closed on zero current. Turn-off losses are similar to "square-wave" PWM converters as an appreciable current has to be commutated. Capacitive snubbing would reduce the turn-off losses. However, at turn-on, the snubber capacitor would be charged either to $(1+M\bar{Q}-M))\cdot V_{in}$, (2.1.1-9), if $t_2 \geq T_h/2$ or otherwise would be charged $(1+M\bar{Q})\cdot V_{in}$. (See section 2.3.5.7, on transformer reset). The snubber capacitor thus charged, would have to be discharged trough the switch at turn-on generating a power loss. Capacitive snubbing is therefore not advantageous.

4.2.2 PWM, Continuous Mode

As seen from Figure 2-2b), switching characteristics in continuous mode are not attractive. Large currents have to be commutated both at turn-on and turn-off. In applications where the input voltage is preregulated, these losses could acceptable. With a preregulated voltage, only a small modulation of the duty cycle is required. The turns ratio of the transformer can therefore be designed in order that the nominal duty cycle is close to unity. (At unity duty cycle the

current is in phase with the voltage and the switching occurs at the zero crossing of the current.)

4.2.3 PSPWM, Discontinuous Mode

Figure 2-4a) shows that switching characteristics are different from one pair of switches to the other. S_1 and S_2 turn on at zero current and a voltage equal to V_{th}'. These switches also turn off on zero current. (Zero voltage turn off is also achieved as the delay necessary to avoid cross conduction, insures that S_1 is off before S_2 turns on.) The switching characteristic of this pair of switch is therefore that of zero current switching converters [18]. S_3 and S_4 present zero current, zero voltage turn-on, as their anti-parallel diode conducts first. The only switching losses in this scheme occur when S_3 or S_4 turn off. Since the switches turn on at zero voltage, capacitive snubbing, as illustrated later in Figure 4-11, is possible and near zero turn-off voltage can be achieved. These switching characteristics are that of zero voltage switching converters [10].

4.2.4 PSPWM, Continuous Mode

In continuous mode, it is seen from Figure 2-4b) that S_1 and S_2 no longer turn on at zero current but commutate the diode of the opposite switch. Zero current, zero voltage turn-off is guaranteed as current flows in the anti-parallel diode at turn-off. S_3 and S_4 retain their zero voltage switching characteristics. It is seen that S_1 and S_2 are only stressed upon turn-on. Inductive snubbing is therefore possible. However inductive snubbing is always accompanied with voltage spikes and is not retained for study in this thesis.

4.3 FREQUENCY RESPONSE

For operation in discontinuous mode, the frequency response characteristic is slightly better for PWM operation. Because energy is immediately returned to the bus when the pulse is terminated, there is not as much phase shift when the perturbation signal approaches the resonant frequency.

For operation in continuous mode, the frequency response characteristic is slightly better for PSPWM. The DC gain characteristic is flatter over the range of M as seen by comparing Figure 3-18a) to Figure 3-18b). The boundary between continuous and discontinuous conduction mode is also more readily determined. For a given load, the conduction mode will remain the same over the full range of input voltages thus avoiding the sudden change in gains of Figure 3-18a). For a given M, the frequency range for which the phase lag is less than 180° is generally wider in PSPWM.

Generally, discontinuous conduction mode will allow for a wider loop bandwidth as the phase shift is usually less than 180°, while in continuous mode the phase shift is already nearing 180° at ω_{po}.

4.4 SWITCHING STRATEGY AND CONDUCTION MODE SELECTION

As mentioned in the Introduction, one of the main reasons for using resonant converters is to minimize or eliminate switching stress and losses. Of the four combinations of PWM or PSPWM and continuous or discontinuous conduction, it is seen from section 4.2 that the only possibility to eliminate switching losses is to use PSPWM in discontinuous mode. This implies the use of PSPWM over PWM and the choice of discontinuous conduction over continuous conduction. These two choices are discussed separately.

As can be seen from Figures 4-1 to 4-7, the stresses are generally

similar if a converter is to be operated with M relatively high. For converters which must operate over a wide range of input voltages, PSPWM operation presents lower stresses. This is true for most devices in the circuit, and it is particularly evident in Figure 4-1 which shows the stress imposed of the input bus. In general, the selection of PSPWM over PWM is therefore advantageous.

Operation in discontinuous mode rather than continuous mode is not as easily justifiable. As seen from Figures 4-1, 4-2, 4-6 and 4-7, operating in continuous mode rather than discontinuous mode lowers the current stress of the devices. Since losses are proportional to the square of the rms current, minimizing this variable is particularly critical. Considering Figures 4-2 and 4-7 versus 4-3 and 4-4, it becomes evident that operating with a nominal $\bar{Q}$ above 3 does not yield a significant reduction in rms current stress while VA rating of the resonant components, L_r and C_r, increase dramatically with $\bar{Q}$. An optimal selection for $\bar{Q}$ would appear to be a value of 3, which implies continuous conduction. This selection would be adequate at low frequency where switching losses become insignificant compared with "on" losses. At higher frequencies, nevertheless, minimization of switching losses becomes more important and operation in discontinuous mode becomes more attractive. Selection of $\bar{Q}$ as close as possible of the mode boundary, $\bar{Q} = .1$, minimizes the increase in rms current. Selection of discontinous conduction also offers the possibility of achieving a greater bandwidth as mentioned in section 4.3.

For these reasons PSPWM, and in particular PSPWM in discontinuous mode is retained for further study.

4.5 DESIGN EXAMPLE

The design of a PSPWM Series Resonant Converter in discontinuous conduction is illustrated by an example. Consider a 48V converter that has to be operated off-line, from both 200V and 100V nominal line. In Europe the nominal line to line voltage, is $240V_{rms}$. At the converter input, the voltage can be supplied continuously 10% above its nominal. This represents a maximum instantaneous voltage of 375Vdc. In North America 110V is used. The power supply must meet regulation even during line sag. For that reasons power supplies are designed to regulate at 66% of the line voltage. Using a voltage "doubler" yields an average voltage which is approximately 1.8 times the peak voltage; this is 185V. Allowing for ripple on the input filter capacitor, the minimum input voltage is taken to be 166V. The following specifications are therefore assumed.

$$166V_{dc} \leq V_{in} \leq 375V_{dc} \qquad (4.5\text{-}1)$$

$$V_{o_{sec}} = 48V_{dc} \qquad (4.5\text{-}2)$$

$$1.5A \leq I_{o_{sec}} \leq 15A \qquad (4.5\text{-}3)$$

Since one pair of MOSFET's exhibit zero current switching and the other zero voltage switching, switching losses are low. High-frequency operation is therefore possible. Nevertheless, there are losses associated with the turn-on of S_1 and S_2. These switches do not theoretically experience switching stress as, in discontinuous mode, the turn-on current and turn-off current is zero. In practice, though, these switches discharge their parasitic capacitance at turn-on. This discharge causes losses within the switches. This is a well-known drawback of zero current switching converters [10]. As mentioned in the Introduction, these losses become more important as the frequency is increased. A frequency of 200Khz is selected as a compromise.

Considering diode technology, the rectifier can be built using a center-tap transformer and only two diodes. The steady-state reverse voltage on the diodes will be roughly 100V.

As seen from Figures 4-1 to 4-7, it is desirable to select M as close as possible to 1 to minimize the stresses. It is noted in section 3.6 that, above M=0.9, the gain drops dramatically, and consequently control is poor. M=0.9 is therefore selected for operation at the minimum specified input voltage. Lumping 1V of rectifier drop into the output voltage, the transformer turns ratio is found to be

$$N = \frac{0.9 * 166V_{dc}}{49V_{dc}} \approx 3. \qquad (4.5\text{-}4)$$

The load impedance reflected to the primary of the converter is therefore

$$R_\ell = N^2 \cdot \frac{V_o}{I_o} = 9 \cdot \frac{49}{15} \approx 29\Omega \ . \qquad (4.5\text{-}5)$$

The characteristic impedance is selected such that Q be as close as possible to 1 (Q=.64). To leave some margin Q is selected to be 0.6. The characteristic impedance and the value of the resonant components are found to be

$$Z_o = Q * R_\ell \approx 17.5\Omega \ , \qquad (4.5\text{-}6)$$

$$L_r = \frac{Z_o}{\omega_o} = \frac{17.5}{2\pi \cdot 200 \cdot 10^3} = 14\mu H \ , \qquad (4.5\text{-}7)$$

$$C_r = \frac{1}{Z_o \omega_o} = \frac{1}{17.5 \cdot 2\pi \cdot 200 \cdot 10^3} = 45.5nF \ . \qquad (4.5\text{-}8)$$

For the small-ripple assumption to be valid, the output capacitor impedance must be much smaller than Z_o. The capacitor must also be able to carry the ripple current. The capacitor used in the realization of the converter, reported in the next section, has a

value of 160μF. This is

$$\overline{Z_{co}} = \frac{Z_{co}}{Z_o} = N^2 \frac{1}{\omega_o C_o \cdot Z_o} = 9 \cdot \frac{1}{2\pi \cdot 200 \cdot 10^3 \cdot 160 \cdot 10^{-6} \cdot 17.5} = 0.0025 \quad . \quad (4.5\text{-}9)$$

The actual design or selection of the components must account for actual stresses. Current and voltage stresses must be plotted over the range of M and $\overline{Q}$. These plots, not shown here, are summarized. All current stresses and the resonant inductor volt-second stress are maximum at maximum input voltage (M minimum) and maximum load ($\overline{Q}$ maximum). The switches voltage stress is maximum at maximum input voltage. The resonant capacitor voltage stress is independent of input voltage, and is maximum at maximum load. The output rectifier and output capacitor voltage stresses are independent of input voltage and load. The transformer volt-seconds is maximum at minimum input voltage. Maximum diode current has not been calculated in Chapter 2, However it can be verified that at M=.4 (V_{in}=375V) it is equal $I_{r_{pk}}$. The maximum stress values have been recorded and are now listed. A discussion on component selection is beyond the scope of this thesis. In particular, optimization of transformers and inductors can become very involved [19,20].

In chapter 2, stresses are normalized to $V_{in_{low}}$, which for the example under study is

$$V_{in_{low}} = 0.9 \cdot 166V_{dc} = 150V_{dc} \quad . \quad (4.5\text{-}10)$$

Since operation at low input voltage is usually an abnormal condition, it is more customary to normalize to the maximum input voltage as is done in [21,22]. Voltage and current stresses are therefore renormalized to V_m=375V_{dc}. The normalized stress figures apply to any converter that is to be operated over a 2.5 to 1 theoretical input voltage range with Q=0.6 at full load and M=1 at $V_{in_{low}}$. The numerical values are specific to this design. The stress are now listed. The product of I_{str} by V_{str} as defined in section 2.3.2 will yield VA_{rat}, (2.3.1-2).

The stresses are now listed for all devices.

- S_1 or S_2

$$I_{rms} = 2.6 \cdot \frac{P_o}{V_m} = 5.0A \qquad (4.5\text{-}11)$$

$$V_{pk} = V_m = 375V \qquad (4.5\text{-}12)$$

- D_1 or D_2

$$I_{avg} = 0 \qquad (4.5\text{-}13)$$

$$I_{pk} = 0 \qquad (4.5\text{-}14)$$

$$V_{pk} = V_m = 375V \qquad (4.5\text{-}15)$$

- S_3 or S_4

$$I_{rms} = 1.6 \cdot \frac{P_o}{V_m} = 3.1A \qquad (4.5\text{-}16)$$

$$V_{pk} = V_m = 375V \qquad (4.5\text{-}17)$$

- D_3 or D_4

$$I_{avg} = 0.8 \cdot \frac{P_o}{V_m} = 1.5A \qquad (4.5\text{-}18)$$

$$I_{pk} = 7.6 \cdot \frac{P_o}{V_m} = 14.6A \qquad (4.5\text{-}19)$$

$$V_{pk} = V_m = 375V \qquad (4.5\text{-}20)$$

- L_r

$$I_{rms} = 3.7 \cdot \frac{P_o}{V_m} = 7.1A \qquad (4.5\text{-}21)$$

$$\text{Volt-seconds} = 1.4 \cdot \frac{V_m}{\omega_o} = 420V\text{-}\mu s \qquad (4.5\text{-}22)$$

- C_r

$$I_{rms} = 3.7 \cdot \frac{P_o}{V_m} = 7.1A \qquad (4.5\text{-}23)$$

$$I_{pk} = 7.6 \cdot \frac{P_o}{V_m} = 14.6A \qquad (4.5\text{-}24)$$

$$V_{pk} = 0.4 \cdot V_m = 150V \qquad (4.5\text{-}25)$$

- Transformer

$$I_{rms} = 3.7 \cdot \frac{P_o}{V_m} = 7.1A \qquad (4.5\text{-}26)$$

$$\text{Volt-seconds} = 1.3 \frac{V_m}{\omega_o} = 390V\text{-}\mu s \qquad (4.5\text{-}27)$$

-CR_1 or CR_2

$$I_{avg} = \frac{I_o}{2} = 7.5A \qquad (4.5\text{-}28)$$

$$I_{pk} = 2.9 \cdot I_o = 43.5A \qquad (4.5\text{-}29)$$

$$V_{pk} = 2 \cdot V_o = 96V \qquad (4.5\text{-}30)$$

- C_o

$$I_{rms} = 1.0 \cdot I_o = 15A \qquad (4.5\text{-}31)$$

$$V_{pk} = V_o = 48V \qquad (4.5\text{-}32)$$

To design the loop compensation, it is required to know the range of M over which the converter operates. At the minimum input voltage specified M has been fixed at 0.9. At maximum input voltage M is therefore

$$M_{min} = 0.9 \frac{166V_{dc}}{375V_{dc}} = 0.4 \; . \qquad (4.5\text{-}33)$$

The actual gain of transfer function of the converter output voltage to the amplifier output is:

$$\frac{\delta v_o(s)}{\delta v_{amp}(s)} = \frac{\delta y(s)}{\delta v_{amp}(s)} \cdot \frac{V_{in}}{N} = K_{pwm} \cdot e^{-st_{dpwm}} \cdot \overline{G(s)} \cdot \frac{V_{in}}{N} \qquad (4.5\text{-}34)$$

Nyquist's theorem implies that the output voltage loop cannot be controlled at frequencies above half the sampling frequency. In practice though the limit is generally around one fifth of the sampling frequency. Since the output voltage is sampled twice per cycle, this is 0.4 of the resonant frequency. At this frequency and over the range of $\overline{Q}$ and M, the gain and the phase lag of $\overline{G(s)}$ are maximum at full load ($\overline{Q} \approx 1$) and M=0.4. Since the the input voltage is also maximum at M=0.4, maximum gain and and maximum phase lag of the transfer function of (4.5-34) will occur at this operating point. For $\overline{Q} = 1$, M=.4, $\overline{Z_{co}}$=0.0025,

$$| G(j \cdot 0.4\omega_o) | = -41dB , \qquad (4.5\text{-}35)$$

$$\underline{| G(j \cdot 0.4\omega_o)} = -160^o \qquad (4.5\text{-}36).$$

Assuming,

$$K_{pwm} = \frac{1}{2.5V} , \qquad (4.5\text{-}37)$$

$$T_{dpwm} \approx 0 , \qquad (4.5\text{-}38)$$

and substituting in (4.5-34),

$$\left| \frac{\partial v_o(j \cdot 0.4\omega_o)}{\partial v_{amp}(j \cdot 0.4\omega_o)} \right| = -41dB + 20 \cdot \log \left[\frac{375V_{dc}}{3} \cdot \frac{1}{2.5V_{dc}} \right]$$

$$= -41dB + 34dB = -7dB \qquad (4.5\text{-}39)$$

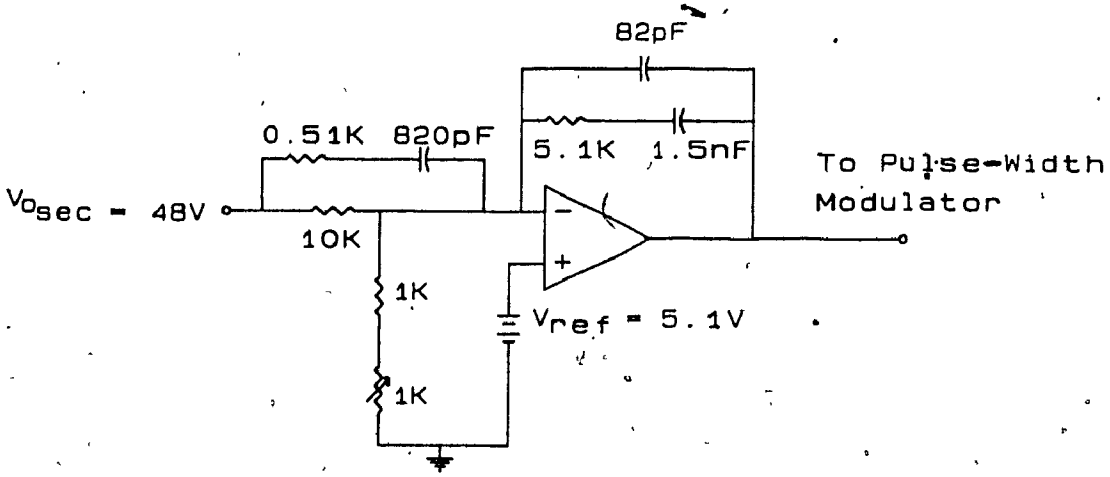

Figure 4-9: Voltage-Error Amplifier

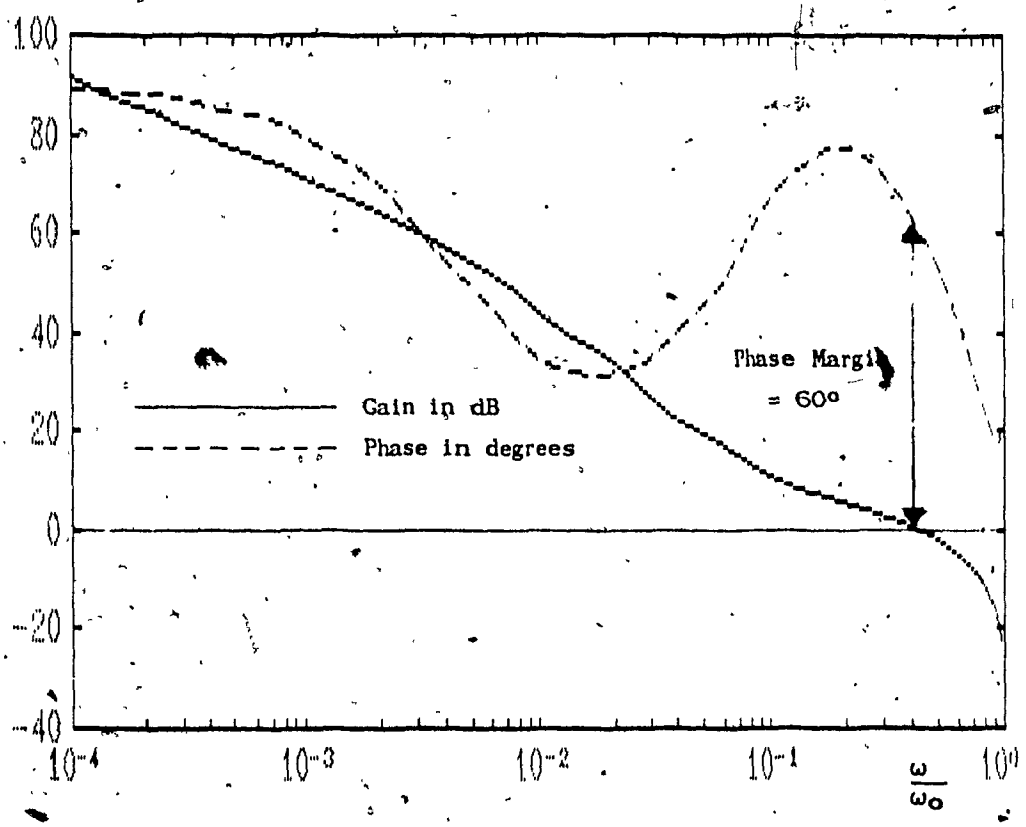

Figure 4-10: Open Loop Frequency Response at 375V_{dc} Input Voltage and Full Load Current

$$\left| \frac{\partial v_o(j \cdot 0.4\omega_o)}{\partial v_{amp}(j \cdot 0.4\omega_o)} \right| = -160^o \qquad (4.5\text{-}40)$$

The voltage error-amplifier of Figure 4-9 has been synthesized using conventional techniques [23]. At ω/ω_o=0.4, it has a gain of 7dB and gives a phase boost of 40°. The resulting open loop transfer function, including the amplifier gain, is shown in Figure 4-10, for V_{in} = 375V_{dc}. At lower input voltages the gain is lower and the converter phase lag is smaller. Consequently, the gain and phase margins are wider.

4.6 EXPERIMENTAL VERIFICATION

An experimental converter, has been built to validate the analysis. The simplified schematic of the converter is shown in Figure 4-11.

Figure 4-12 shows the load branch voltage (V_{aL} on Figure 2.1-3) and resonant current for two operating points.

Figure 4-13 shows the voltage transfer ratio for Q=0.6 ($\bar{Q}$=.94) and Q = 0.1 ($\bar{Q}$=0.157) for a constant input voltage of 160V_{dc}. The actual voltage transfer ratio particularly departs from the calculated value at high load and duty cycle above 50%. This is mainly due to the drops across the MOSFET's, which are more significant at higher currents. This factor is not taken into account in the theoretical development.

Next, the stress formulas are verified by checking predicted efficiency versus measured efficiency. To perform the calculations, the characteristics of the components were obtained by measurements on an impedance bridge or from data sheets. The calculated losses at the worst operating point; maximum load and maximum input voltage are calculated from the stress figures given in the preceding section.

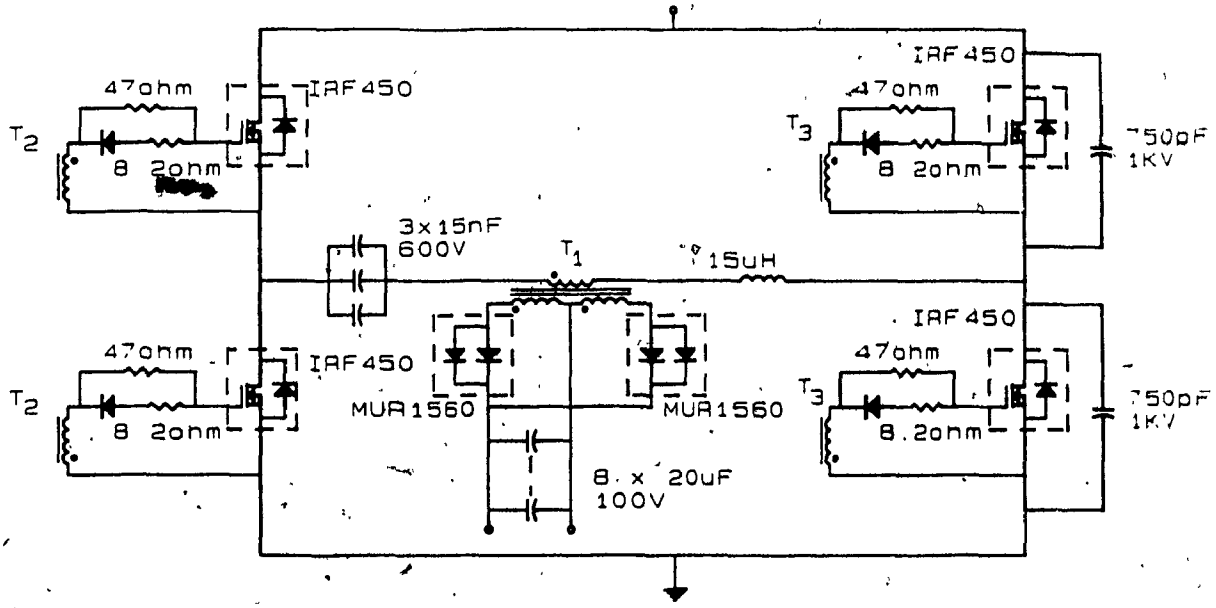

T_2 and T_3 primary resistance. 3.5ohm

Maximum gate voltage: ±12V

Figure 4-11: Experimental Converter Simplified Schematic

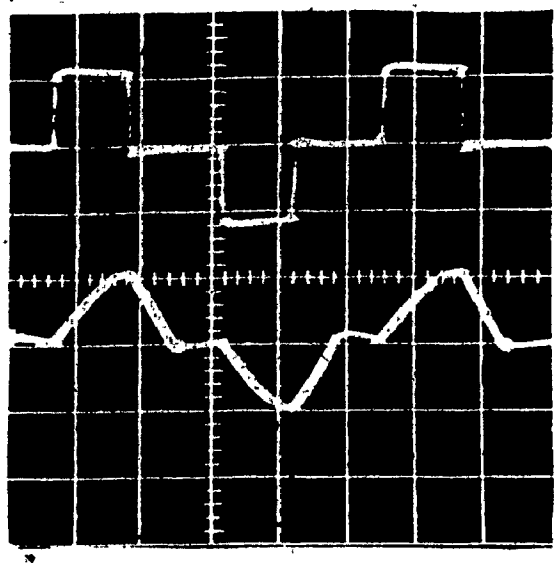

a)

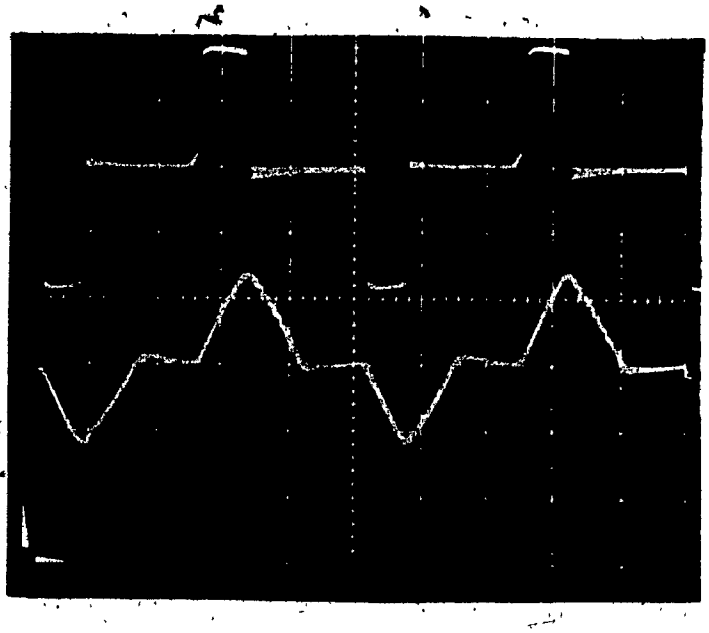

b)

Figure 4-12: Experimental Waveform
a) V_{in}=240V_{dc}, I_o=14A
b) V_{in}=375V_{dc}, I_o=14A
top trace : V_{ab}, 200V/cm
bottom trace: I_r, 10A/cm

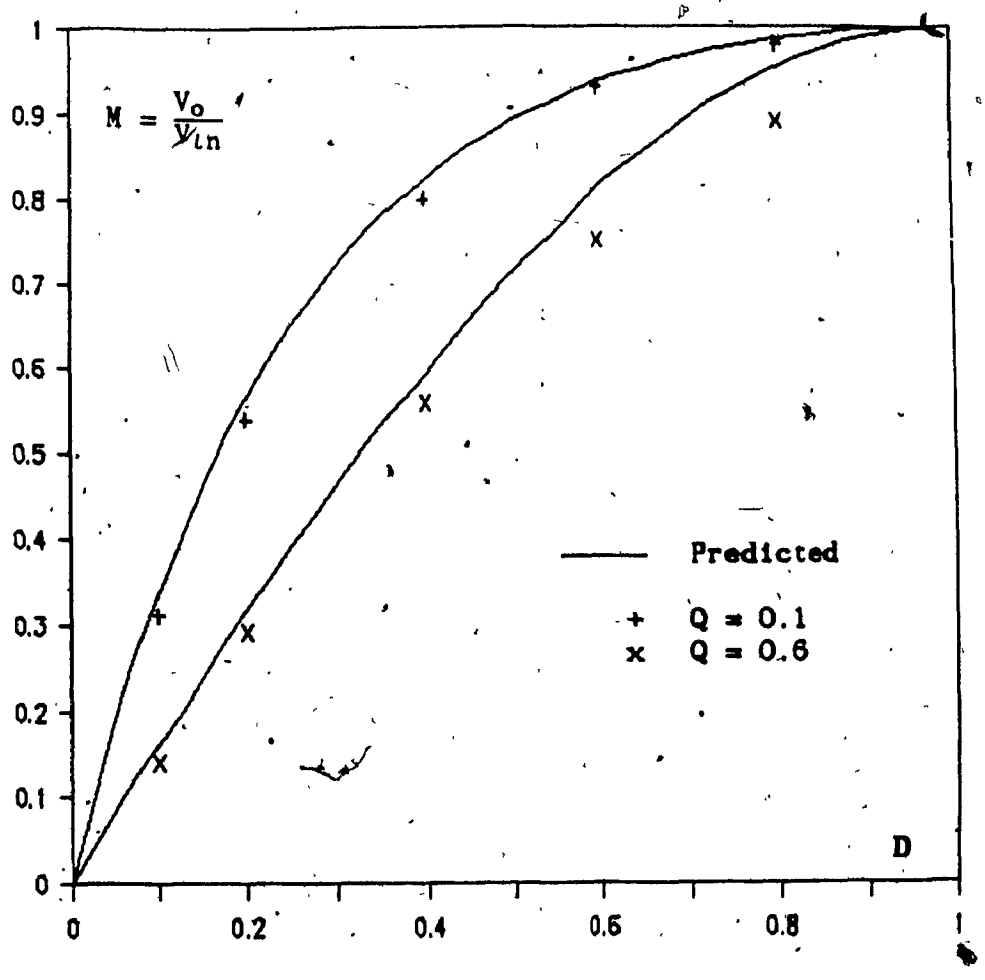

Figure 4-13: Experimental Voltage Tranfer Ratio in Discontinuous Conduction Mode.

- S_1 or S_2

"On" resistance at 80°C junction temperature is 0.6Ω.

$$P_{\ell oss} = 0.6\Omega \cdot [\ 5.0A\ ]^2 = 15W. \qquad (4.6\text{-}1)$$

- D_1 or D_2

$$P_{\ell oss} = 0 \qquad (4.6\text{-}2)$$

- S_3 or S_4

"On" resistance at 80°C junction temperature is 0.6Ω.

$$P_{\ell oss} = 0.6\Omega \cdot [\ 3.1A\ ]^2 = 5.8W \qquad (4.6\text{-}3)$$

- D_3 or D_4

Forward voltage drop is approximately 1V.

$$P_{\ell oss} = 1.5A \cdot 1V = 1.5W \qquad (4.6\text{-}4)$$

L_r

The winding resistance measured at 200Khz and compensated for temperature rise is 0.11Ω. The copper losses are therefore:

$$P_{\ell oss} = 0.11\Omega \cdot [\ 7.1A\ ]^2 = 5.6W. \qquad (4.6\text{-}5)$$

From (4.5-22) there 420V-μs applied to generate the peak-to-peak flux.

swing. For the core selected and the number of turns used this represents 0.4W of core losses.

$$P_{core} = 0.4W \qquad (4.6\text{-}6)$$

- C_r

The equivalent series resistance of the resonant capacitor is 12mΩ at 200Khz.

$$P_{\ell loss} = 0.012\Omega \cdot [\ 7.1A\ ]^2 = 0.6W \qquad (4.6\text{-}7)$$

- Transformer

The equivalent AC resistance seen from the primary of the transformer when the secondary is shorted is 0.11. The AC copper losses are therefore

$$P_{ac} = 0.11\Omega \cdot [\ 7.1A\ ]^2 = 5.6W\ . \qquad (4.6\text{-}8)$$

In addition, each half of the secondary winding carries a direct current of 7.5A. The DC resistance of each half of the secondary winding is 8mΩ. The DC copper losses are therefore

$$P_{dc} = 2 \cdot 0.008\Omega \cdot [\ 7.1A\ ]^2 = 0.9W\ . \qquad (4.6\text{-}9)$$

Although maximum flux swing does not occur for maximum input voltage the figure of 390V-μs is used to estimate the core losses. For the core selected and the number of turns used, this represents 0.8W of core losses.

$$P_{core} = 0.8W \qquad (4.6\text{-}10)$$

- CR_1 or CR_2

The forward voltage drop is approximately 0.9V.

$$P_{loss} = 7.5A \cdot 0.9V = 6.8W \qquad (4.6\text{-}11)$$

- C_o

The series resistance of the bank of capacitors used is 1.25mΩ.

$$P_{loss} = 0.00125\Omega \cdot [\ 15.0A\ ]^2 = 0.3W \qquad (4.6\text{-}12)$$

Adding the losses together yields 72W. The calculated efficiency is therefore:

$$\eta = \frac{720W}{720 + 72W} = 0.91 \qquad (4.6\text{-}13)$$

The actual efficiency was measured at 90%.

Although the correlation between predicted and measured efficiency is very good, the losses due to parasitic capacitance discharge are now evaluated. At turn-on of S_1, its parasitic capacitance must be discharged from V_{in} to zero while the capacitance of S_2 is charged from zero to V_{in}. The switches in this circuit being realized with MOSFET's, using the body diodes as the anti-parallel diodes, this capacitance is composed of the non-linear drain-source capacitance (C_{ds}) and drain-gate capacitance (C_{dg}). At this turn-on transition, the charge required to raise the voltage across C_{ds} of S_2, from zero to V_{in}, $Q_{ds}(V_{in})$, is drawn from the bus. The energy drawn from the bus, which is equal to the energy stored in C_{ds} of S_2 is

$$W_{ds} = Q_{ds}(V_{in}) \cdot V_{in} \qquad (4.6\text{-}14)$$

S_1 discharges its drain-source capacitance within its own body. This capacitor is discharged from V_{in} to zero and an amount of energy equal

to W_{ds} is therefore dissipated.

The energy dissipation related to C_{gd} is more difficult to evaluate as there are interactions with the gate drive circuit. Provided that V_{in} is much larger than the gate drive voltage, this energy can be approximated by

$$W_{dg} = Q_{dg}(V_{in}) \cdot V_{in} \qquad (4.6\text{-}15)$$

Recognizing that $Q_{ds}(V_{in}) + Q_{dg}(V_{in})$ is $Q_{oss}(V_{in})$, and since there are two turn-on transitions per cycle, the power dissipation is

$$P_{swon} = 2 \cdot Q_{oss}(V_{in}) \cdot V_{in} \cdot \frac{\omega_o}{2\pi} . \qquad (4.6\text{-}16)$$

$Q_{oss}(375V_{dc})$ for the IRF450 is 75nC, the additional power dissipation at 200Khz is therefore 11W. Recalculating the efficiency with this additional loss yields 90%. This coincidence of the measured efficiency is fortuitous, as a different evaluation of the "on" resistance of the mosfet could easily raise or lower the calculated efficiency by 1%.

Frequency response predictions are also verified. A sinusoidal signal of small amplitude is superimposed to the DC signal at the input of the pulse-width modulator. The exciting signal is automatically swept across a preset range of frequencies. The component of the output voltage ripple at the exciting frequency is extracted using Fourier transform methods. This operation is carried out using a special purpose Frequency Analyzer [24]. Since the upper frequency of the Frequency Analyzer is 100Khz, and since it has also been experienced in the past that measurements performed above 50Khz are not very reliable, the resonant frequency of the converter is lowered to 25Khz. The value of the resonant inductor is changed to 900μH. The transformers are also changed to operate at this frequency. Figures 4-14 and 4-15 show the results for M=0.3 and various values of Q. Some of the data points are scaled and put onto the corresponding

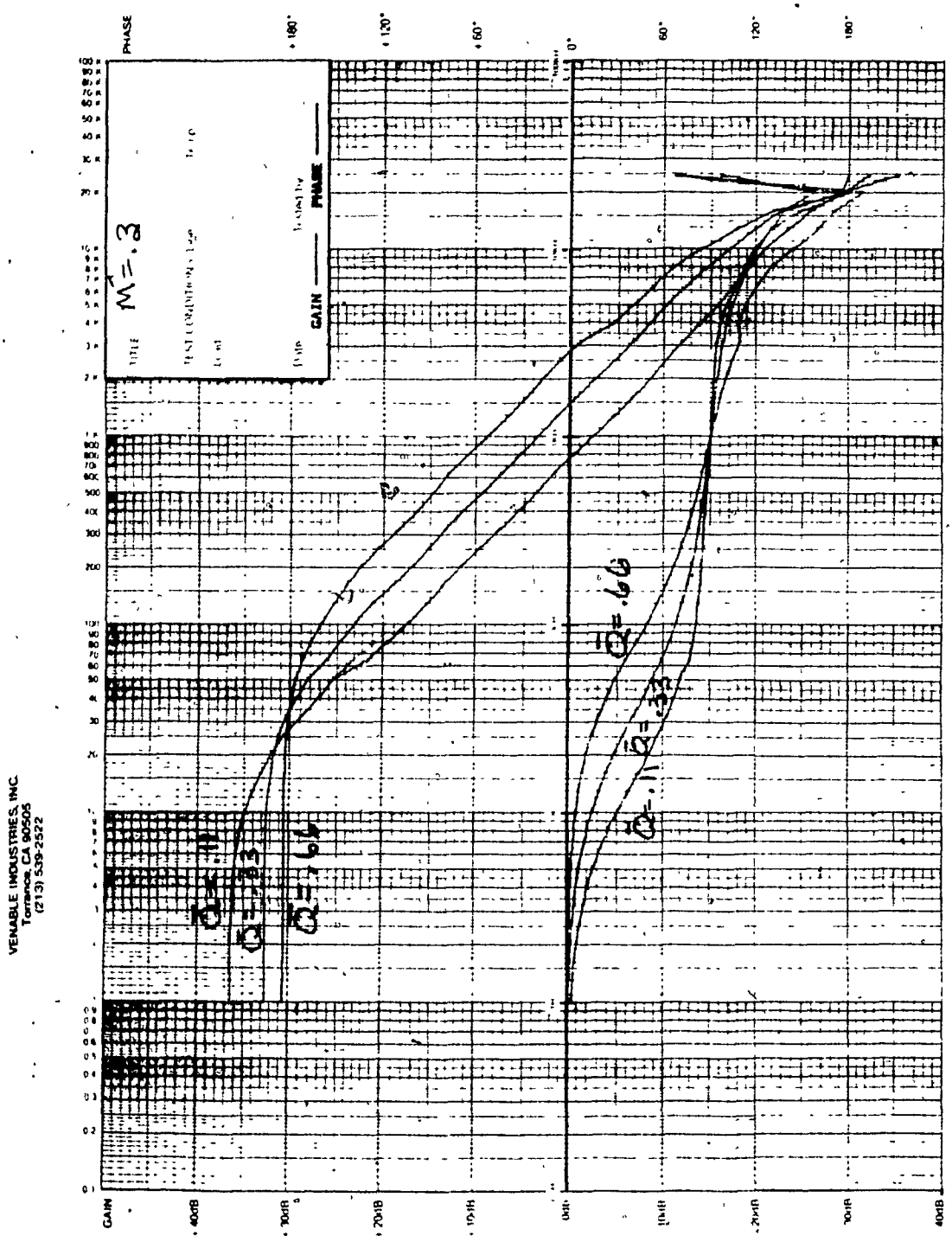

Figure 4-14: Experimental Frequency Response for $\bar{Q}$=0.11, $\bar{Q}$=0.33 and $\bar{Q}$=0.66

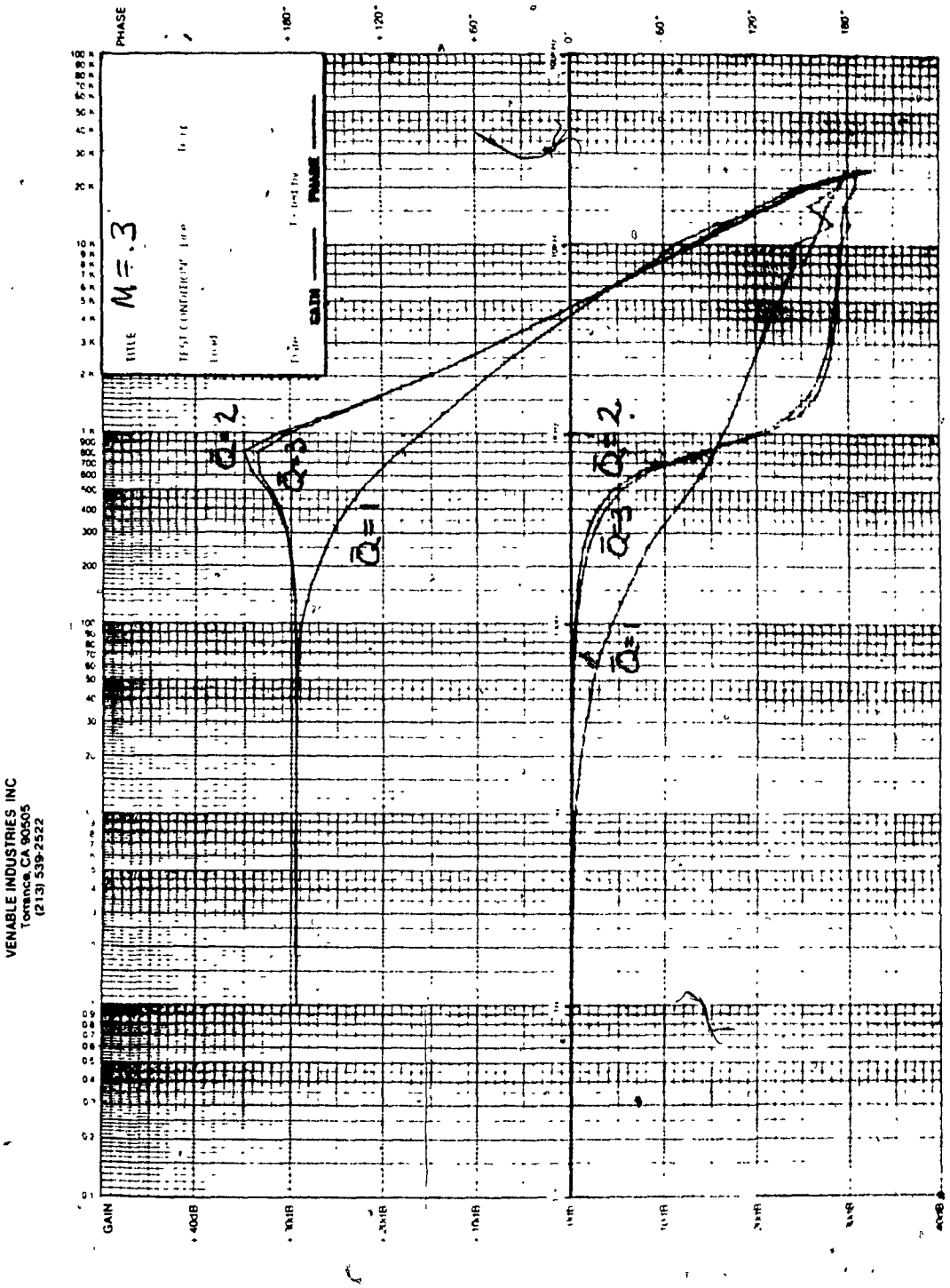

Figure 4-15: Experimental Frequency Response for $\bar{Q}$=1.0, $\bar{Q}$=2.0 and $\bar{Q}$=3.

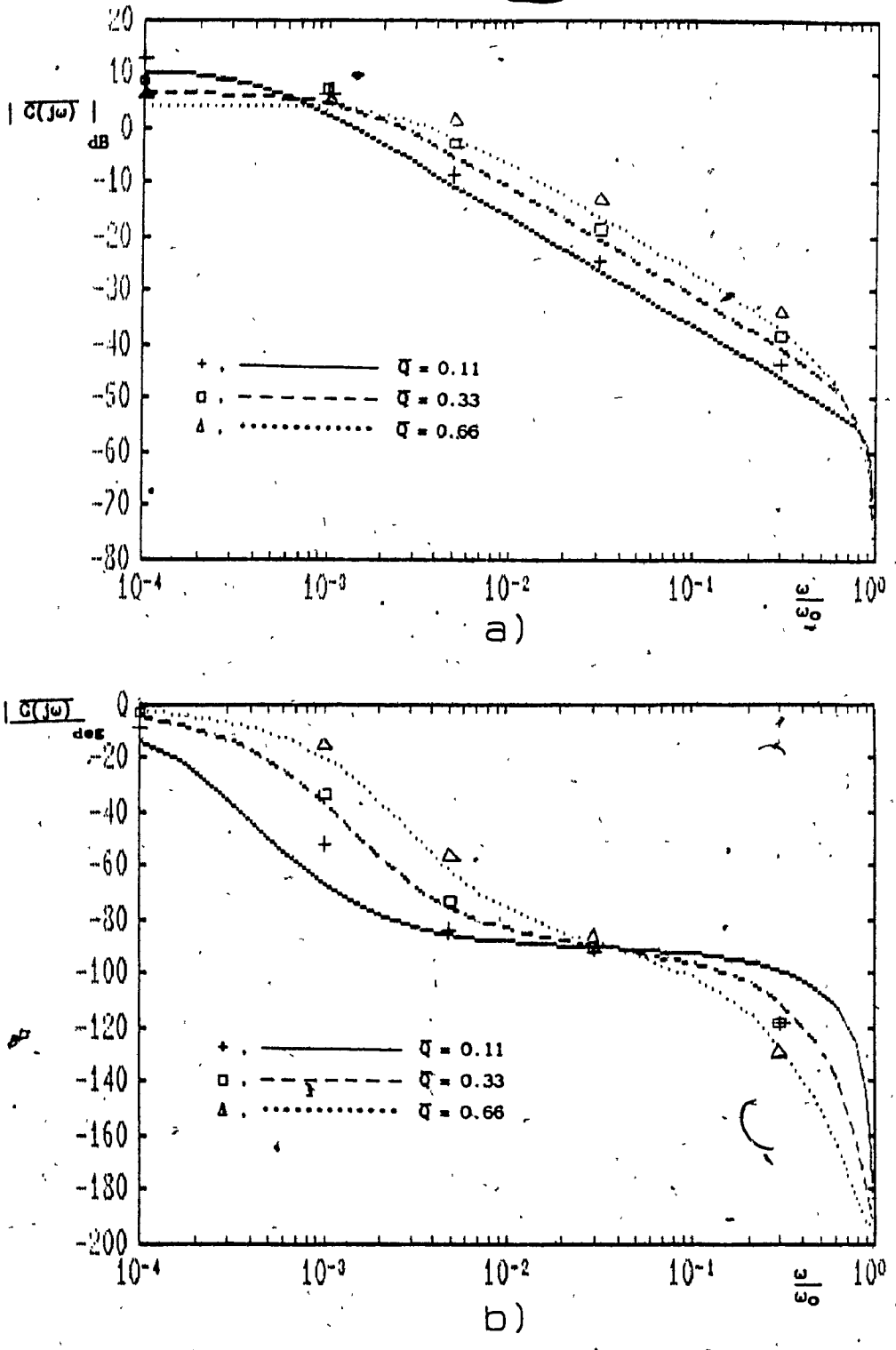

Figure 4-16: Predicted vs Measured Converter Frequency Response for $\overline{Q}$ = 0.11, 0.33, 0.66 and M=0.3.
a) Magnitude
b) Phase

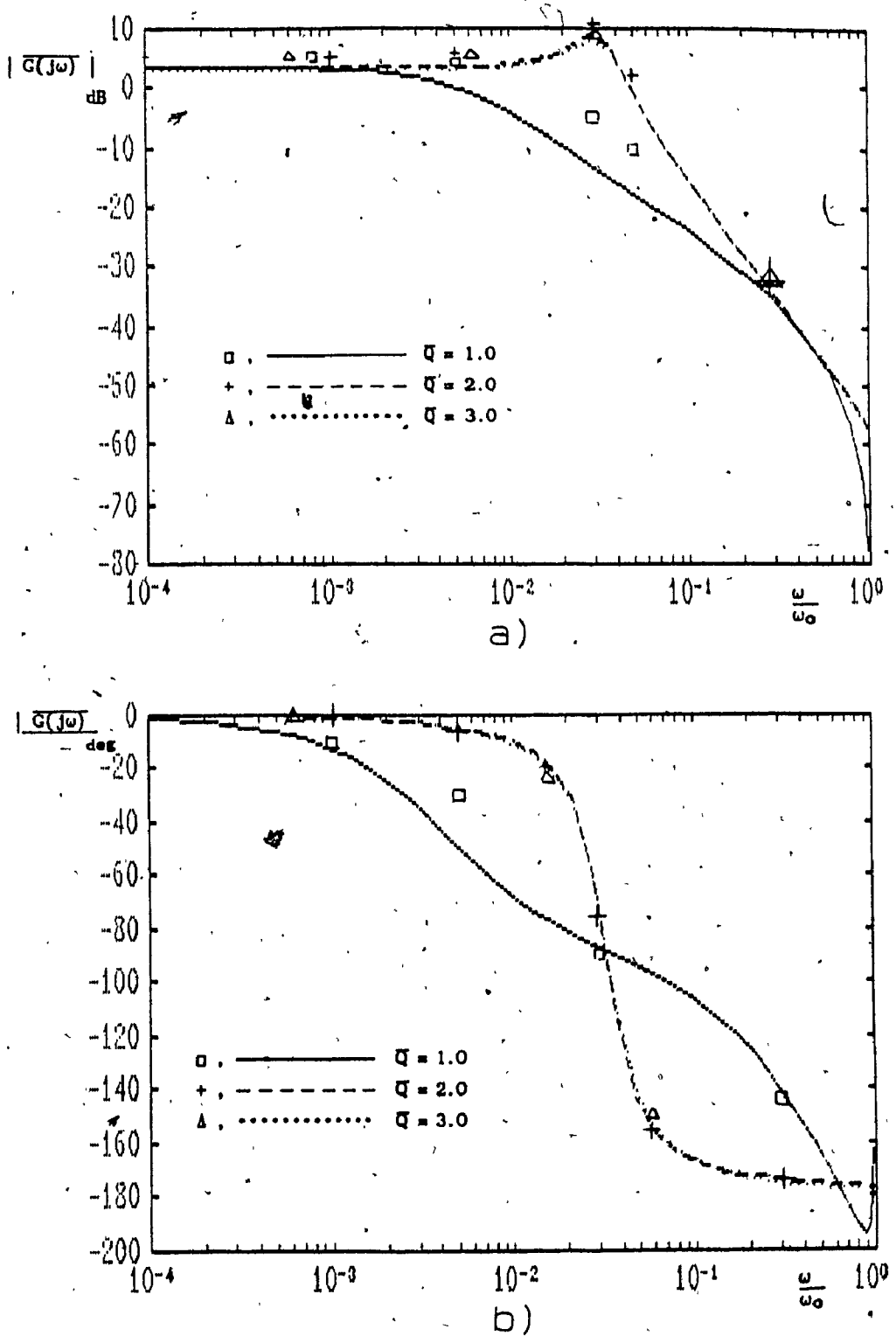

Figure 4-17: Predicted vs Measured Converter Frequency Response for $\overline{Q}$ = 1.0, 2.0, 3.0 and M=0.3.
a) Magnitude
b) Phase

theoretical predictions of Figure 4-16 and 4-17. The input voltage for this test is $120V_{dc}$. The gain scaling factor is therefore

$$\text{Gain Factor} = 20 \log \left[\frac{120V_{dc}}{3} \frac{1}{2.5V} \right] = 24\text{dB} \qquad (4.6\text{-}17)$$

The resonant frequency of the converter is 25Khz, the scaling factor for the frequency is:

$$\text{Frequency Factor} = \frac{1}{25\text{Khz}} = 40\mu s \qquad (4.6\text{-}18)$$

Except for $\bar{Q}$=1, experimental and predicted results agree. For $\bar{Q}$=1, it is seen that around ω_{po} the measured values depart from the prediction. This is due to the fact that the transition between the system with two real poles to the system with a second order resonance happens for a very small variation in $\bar{Q}$. Great accuracy in constructing the test converter would be necessary to obtain matches around ω_{po} for $\bar{Q}$ around 1. This is not necessary as in practice compensation of the voltage error-amplifier is usually designed for a crossover frequency away from the filter resonant frequency.

Although operation in the continuous mode was not retained for in-depth investigation, the theoretical prediction of load independence is verified. To minimize the drop across the mosfet the characteristic impedance of the 200Khz version of the converter is increased. L_r is set at 85μh and C_r at 7.5nF. Voltage transfer ratio is measured for a constant input voltage of 100V. The results are shown in Figure 4-18 for discontinuous mode, $\bar{Q}$=0.333, for the limiting case, $\bar{Q}$=1 and for continuous conduction $\bar{Q}$=3. The voltage variation for a three to one load change in discontinuous conduction between $\bar{Q}$=0.333 and $\bar{Q}$=1 is evident, while the voltage variation for a further three to one load increase to $\bar{Q}$=3 is minimal and mainly due to drops across the MOSFET's.

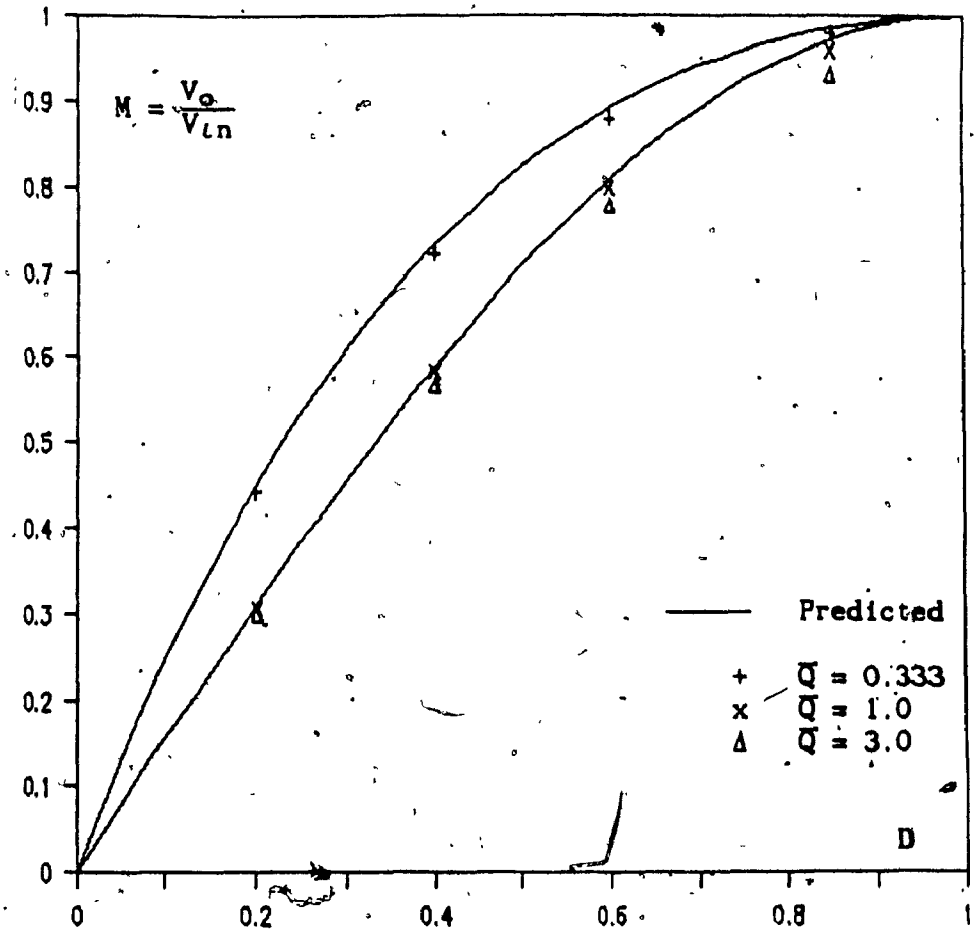

Figure 4-18: Verification of the Load Independance of the Voltage Transfer Ratio in Continuous Mode.

CHAPTER 5: CONCLUSION

In this thesis direct application of fixed frequency pulse-width modulation to the series resonant converter is investigated. The study is limited to operation at the natural resonant frequency of the LC circuit to maximize the control range and enhance power transfer.

Two switching strategies to obtain pulse width modulation are identified and analyzed. For each of the switching strategies, two modes of operation characterized by continuous or discontinuous resonant current are identified. At low load, the converter operates in discontinuous mode while, at higher load, it operates in continuous conduction mode. Steady-state solutions for both switching strategies and both modes are derived. The voltage transfer ratio is calculated for each switching strategy. Stresses for all components are also calculated and normalized to the output power.

Frequency response of the system is analyzed using *Small-Signal Frequency Response Theory* [16,17]. It is found that the response of the system is of the second order. In continuous conduction mode the poles are complex conjugates and the transfer function has a resonant peak at a frequency ω_{po}. ω_{po} is easily expressed in terms of the ratio of the output capacitor impedance to the characteristic impedance of the LC resonant circuit. Damping of this transfer function is expressed in terms of the load. A simple equivalent model is therefore derived. In discontinuous mode the poles, ω_{p1} and ω_{p2}, are real and distinct. It is also found that the product of ω_{p1} by ω_{p2} is always equal to ω_{po}^2. Although, in discontinuous conduction mode, the behavior of the converter is similar to the case of a capacitor in parallel with a resistor fed by a current source, ω_{p1} cannot be simply expressed in terms of the load and output capacitor. Graphs are therefore supplied to calculate ω_{p1}.

After evaluation, the second switching strategy, PSPWM, is found to generally yield lower component stresses. Switching stresses are found to be minimum for PSPWM operation in discontinuous mode. One pair of switches is found to have zero-voltage switching, while the other pair exhibits zero-current switching. Using normalized stress curves the optimal operating point is found to be at the boundary between the two conduction modes.

To verify the analysis, a constant output voltage converter, that theoretically operates over an input voltage range of 2.5 to 1, is designed. The measured voltage transfer ratio approaches the predictions. The difference between the measured and the predicted voltage transfer ratio is due to series drops not accounted for in the theoretical development. The predicted efficiency is also compared to the measured one. The calculated and the measured efficiency are both 90% for the 720W, 48Vdc, 200Khz converter. Frequency response is also measured and is found to, generally, be in agreement with the predictions.

Although discontinuous conduction is preferred in order to minimize switching losses, it is noted that operation in continuous conduction mode yields lower current stress on the devices for a given output power. In particular, it is shown that operation with a characteristic impedance to load resistance ratio of $6/\pi$ ($Q=3$), yields lower rms current without having to pay a heavy penalty on the total VA rating of the resonant capacitor and inductor. It also has to be noted that in PSPWM discontinuous mode, the parasitic capacitance of the switches has to be discharged through the switches causing power loss. For the 200Khz power supply this causes only an efficiency degradation of 1%. But at higher frequency theses losses become much more significant. It has been shown in [22] that these losses would become dominant at 1Mhz.

It is reported in [3], that continuous conduction operation of the converter above resonant frequency, of the frequency modulated

converter, yields a resonant current which is lagging. This property is also retained for operation in pulse-width modulation. The current being negative at the start of the cycle, zero-voltage switching could be achieved for all switching instants. Operation above resonant frequency would therefore offer the possibilty of minimizing the switching losses while operating in continuous conduction.

It is shown in this thesis that the voltage transfer ratio is independent of the load when operated in continuous conduction at resonant frequency. It is pointed out in the Introduction that this much desirable property is lost when operating above resonant frequency. Also, the maximum achievable transfer ratio is different for the various loads. It is also mentioned in the Introduction that current and voltage stress are larger for an operating frequency above resonance. Future work could therefore be devoted evaluating the trade-offs between minimization of switching stresses versus the increase in rms current, peak current, peak voltage and increased volt-seconds when operating above resonant frequency.

REFERENCES

1 - K. Liu, F.C. Lee, "Secondary Side Resonance For High-Frequency Power Conversion", *IEEE Applied Power Electronics Conference Proceedings*, New Orleans, Louisianna, 1986. pp.83-89

2 - P.C. Todd, R.W. Lutz, "Practical Resonant Power Converters Theory and Application, Part 1", *Powertechnics Magazine*, Darnell Research, Garden Grove, California, April 1986. pp. 30-34

3 - R.L. Steigerwald, "High Frequency Resonant Transistor DC-DC Converters", IEEE Transactions on Industrial Electronics, Vol. IE-31, no. 2, May 1984. pp.181-191

4 - R.C. Schwarz, "An Improved Method of Resonant Current Pulse Modulation for Power Converters", *IEEE Power Electronics Specialists Conference Proceedings*, Culver City, California, 1975. pp. 194-204

5 - V. Vorperian, S. Cuk, "A Complete DC Analysis of the Series Resonant Converter", *IEEE Power Electronics Specialists Conference Proceedings*, Cambridge, Massachusetts, 1982. pp.85-100

6 - V. Vorperian, "Small Signal Analysis of Resonant Converters", *IEEE Power Electronics Specialists Conference Proceedings*, Albuquerque, New Mexico, 1983. pp. 269-282.

7 - V. Vorperian, *Analysis of Resonant Converters*, Doctoral Thesis, California Institute of Technology, Pasadena, California, 1984.

8 - F.G. Turnbull, R.E. Tompkins, "Design of a Pulse-Width Modulated Resonant Converter for a High Output Voltage Power Supply", *IEEE Industry Applications Society Conference Record*, Toronto, Ontario 1985. pp. 1145- 1150

9 - S.B. Dewan, A. Straughen, *Power Semiconductor Circuits*, John Wiley & Sons", New York, 1975, p. 408.

10- K.H. Liu, F.C. Lee, "Zero-Voltage Switching Technique in DC/DC Converters", *IEEE Power Electronics Specialists Conference Proceedings*, Vancouver, British Colombia, 1986. pp. 58-70.

11- S. D. Conte, C. De Boor, *Elementary Numerical Ananlysis An Algorithmic Approach*, Third Edition, Mc Graw-Hill, New-York, 1980. pp.78-79.

12- Wima Data Book, *Capacitors for Electronic Equipment, Miniature Type Components*, Wilhelm Westermann, Spezialvertrieb elektronischer Bauelemente, Manheim, Germany. 1987

13- A.E. Fitzgerald, C. Kingsley, A. Kusko, *Electric Machinery*, Third Edition, Mc Graw-Hill, New York, 1971. p. 9.

14- A.R. Brown, R.D. Middlebrook, "Sampled-Data Modeling of Switching Regulators", *IEEE Power Electronics Specialists Conference Proceedings*, Boulder, Colorado, 1981. pp. 349-369.

15- D.J. Short, F.C. Lee, "An Improved Switching Converter Model Using Discrete and Average Techniques", *IEEE Power Electronics Specialists Conference Proceedings*, Cambridge, Massachusetts. pp. 199-212.

16- B.Y. Lau, R.D. Middlebrook, "Small-Signal Frequency Response Theory for Piecewise-Constant Two-Switched-Network DC-to-DC Converter Systems", *IEEE Power Electronics Specialists Conference Proceedings*, Vancouver, British Columbia, 1986. pp. 186-200.

17- B. Y. Lau, *Small-Signal Frequency Response Theory for Ideal DC-to-DC Converter systems*, Ph.D. Thesis, California Institute of Technology, Pasadena, California, 1987.

18- K. H. Liu, R. Oruganti, F.C. Lee, "Resonant Switches - Topologies and Characteristics", *IEEE Power Electronics Specialists Conference Proceedings*, Toulouse, France, 1985. pp. 106-116

19- J.P. Vandelac, P. Ziogas, "A Novel Approach for Minimizing High Frequency Transformer Copper Losses", *IEEE Power Electronics Specialists Conference Proceedings*, Blacksburg, Virginia, 1987. pp. 355-367

20- J.P. Vandelac, P. Ziogas, "A Novel Approach for Minimizing High Frequency Transformer Copper Losses", *IEEE Transactions on Power Electronics*, Vol. 3 no.3, July 1988. pp. 266-277

21- J.P. Vandelac, P. Ziogas, "A DC to DC PWM Series Resonant Converter", *PCI Conference Proceedings*, Boston, Intertec Communications,, Ventura, California, 1986. pp. 17-34.

22- J.P. Vandelac, P. Ziogas, "A DC to DC PWM Series Resonant Converter Operated at Resonant Frequency", *IEEE Transactions on Industrial Electronics*, vol. 35, no. 3, August 1988 pp. 451-460.

23- H. D. Venable, "The K factor: A New Mathematical Tool for Stability Analysis and Synthesis", *Proceedings of Powercon 10*, San Diego, California, Power Concepts inc., Ventura, California, 1983. section H-1 pp. 1-12.

24- Model 250 Frequency Response Analysis System Operator's Manual, Venable Industries, Rancho Palos Verdes, Ca, 1983.

25- G.F. Franklin, J.D. Powell, *Digital Control of Dynamic Systems*, Addison-Wesley, Reading, Massachussets, 1980.

26- D. K. Frederick, A.B. Carlson, *Linear Systems in Communication and Control*, John Wiley and Sons, New York, 1971.

APPENDIX A

HALF-CYCLE SAMPLING PROBLEMATIC

A problem arises from the fact that the state variables are periodic with period $2T_h$ while the sampling of the pulse-width modulator is performed on a half-cycle basis. The nature of the difficulty attributed to this fact is described in section A.1. To overcome this difficulty, the response of the system is found by adding the response of the system found when pulse-width modulator is controlling the t_1's only to the response of the system found when the pulse-width modulator is controlling the t_4's only. This direct application of linear superposition causes an intuitive difficulty. For example although the higher order terms of (3.4.2-3) have been neglected to yield

$$\partial x_1[n] = \partial \mathbb{X}_6[n-1] + (\dot{X}_1^- - \dot{X}_1^+) \cdot \partial t_1[n] , \qquad (A.0-1)$$

the system has a memory, and $\partial \mathbb{X}_6[n-1]$ is a function of $\partial t_4[n-1]$ and therefore so is $\partial x_1[n]$. Intuitively the effect of modulating the t_4's cannot be segregated from the effect of modulating the t_1's. This is true in the large-signal case. But in the small-signal limit this dependence vanishes. This falls directly from (3.4.2-1) and (3.4.2-2). Applying repetitively these two first order (linear) equations demonstrates how the system satisfies the condition for linearity. This is simply verified in section A.2

This splitting of the system into two linearly independent systems causes some notation problems. Although the two systems are linearly independent, the two systems must be referenced to a same timeframe. This is, the state perturbation at any instant is the sum of the state perturbation of each system.

$$\partial x(t) = \partial x_e(t) + \partial x_o(t) \qquad (A.0\text{-}2)$$

Texts on sample data systems generally select the train of sampling impulses such that one of the impulses be coincident with the origin [25]. If this is done with the case under study, only one of the train of impulses can be coincident with the origin. The other train of impulses will be offset from the origin by T_h. In this thesis, neither of the two sampling waves is assumed to have one of its impulses coincident with the origin. The two trains of impulse are assumed to be offset from the origin by $t_1[0]$ and $t_4[0]$ respectively. This fact has an effect in the notation for the description of the pulse-width modulator and in the transform treatment of the two sample data systems. These two subjects are treated in section A.3 and A.4 respectively.

A.1 DESCRIPTION OF THE PROBLEM

The difference equation describing the behavior of the system is given by (3.5.2-8), which is rewritten as:

$$\partial x(m) = \Phi_{sh}\Phi_{fh}\cdot\partial x(m-2) + \Phi_{sh}\cdot T_h k_4 \partial d(m-1) + T_h k_1 \partial d(m) \qquad (A.1\text{-}1)$$

There is nevertheless a restriction on this difference equation. "m"must be an even number for the equation to apply. Usually difference equations describing a system do not contain this restriction. (For this reason (3.5.2-8) has been completed with a twin equation to cover the case for which m is odd.)

Proceeding nevertheless, the following transfer function can be found in the $\mathcal{Z}$ domain.

$$\partial x(z) = T_h \cdot \frac{z^{-1}k_4\Phi_{sh} + k_1}{1 - z^{-2}\Phi_{sh}\Phi_{fh}}\,\partial d(z) \qquad (A.1\text{-}2)$$

Taking the Laplace transform:

$$\partial x^*(s) = T_h \cdot \frac{e^{-sT_h}\Phi_{sh}k_4 + k_1}{I - e^{-2sT_h}\Phi_{sh}\Phi_{fh}} \partial d(s) \qquad (A.1\text{-}3)$$

A discrete transfer function being found, the reconstruction process to obtain a continuous representation is undertook. The Laplace transform of the of the state perturbation is:

$$\delta x(s) = \int_{-\infty}^{+\infty} \delta x(t) \cdot e^{-st}\, \partial t \qquad (A.1\text{-}4)$$

Defining

$$\delta x_{\ell,n}(s) = \int_{\max(t_j,\tau_j)}^{\min(t_{j+1},\tau_{j+1})} \delta x(t) \cdot e^{-st}\, \partial t, \qquad (A.1\text{-}5)$$

summation of all the $\partial x_{\ell,n}(s)$ covers the complete range of the integrand of A.1-4, except during the ∂t_j's. In the interval $\max(t_j,\tau_j) < t < \min(t_{j+1},\tau_{j+1})$, the governing differential equation is

$$\dot{\delta x}(t) = \omega_o A_\ell\, \delta x(t) \; . \qquad (A.1\text{-}6)$$

As is done in section 3.5.3, it is recognized that in the small-signal limit the τ_j's tend toward the t_j's. Subject to the same remark as in section 3.5.3, (A.1-6) is assumed to apply for the interval $t_j < t < t_{j+1}$. Under this approximation (A.1-5) becomes

$$\delta x_{\ell,n}(s) = \int_{t_j}^{t_{j+1}} \delta x(t) \cdot e^{-st}\, \partial t \; . \qquad (A.1\text{-}7)$$

The summation of all the $\delta x_{\ell,n}(s)$ therefore covers the complete range of (A.1-4). Substituting (A.1-6) into (A.1-7) leads to,

$$\omega_o A_\ell \cdot \delta x_{\ell,n}(s) = \int_{t_J}^{t_{J+1}} \dot{\delta x}_{\ell,n}(t) \cdot e^{-st}\, \partial t \ . \qquad \text{(A.1-8)}$$

Integrating by parts,

$$\omega_o A_\ell \cdot \delta x_{\ell,n}(s) = \delta x_{\ell,n}(t) \cdot e^{-st} \Big|_{t_J}^{t_{J+1}} + s \cdot \delta x_{\ell,n}(s)$$

$$[\omega_o A_\ell - sI] \cdot \delta x_{\ell,n}(s) = \delta x_J \cdot e^{-s \cdot t_{J+1}} - \delta x_J \cdot e^{-s \cdot t_J}$$

$$[\omega_o A_\ell - sI] \cdot \delta x_{\ell,n}(s) = e^{-st_J} \{ \Phi_\ell \cdot \delta x_J \cdot e^{-sT_J} - \delta x_J \}$$

$$\delta x_{\ell,n}(s) = e^{-st_J} \cdot [sI - \omega_o A_\ell]^{-1} \cdot \{ I - e^{-sT_\ell} \Phi_\ell \} \cdot \delta x_J$$

$$= e^{-st_\ell[n]} \cdot H_\ell(s) \cdot \delta x_\ell[n] \qquad \text{(A.1-9)}$$

where,

$$H_\ell(s) \equiv [sI - \omega_o A_\ell]^{-1} \cdot \{ I - e^{-sT_\ell} \Phi_\ell \}. \qquad \text{(A.1-10)}$$

Substituting (A.1-9) into (A.1-4) yields

$$\delta x(s) = \sum_n \sum_\ell e^{-st_\ell[n]} H_\ell(s) \cdot \delta x_\ell[n] \qquad \text{(A.1-11)}$$

Summing over the ℓ's yields,

$$\partial x(s) = \sum_n$$

$$\left[e^{-(sT_1+sT_2)} H_3(s) K_3 \Phi_2 K_2 \Phi_1 + e^{-sT_1} H_2(s) K_2 \Phi_1 + H_1(s) \right] \cdot e^{-s2nTh}\, \partial x_1[n]$$

$$+ \left[e^{-(sT_4+sT_5)} H_5(s) K_5 \Phi_5 K_5 \Phi_4 + e^{-sT_4} H_5(s) K_5 \Phi_4 + H_4(s) \right] \cdot e^{-s(2n+1)Th}\, \partial x_4[n]$$

$$\text{(A.1-12)}$$

If the two factors in bracket were the same, then, the following would be true

$$\begin{aligned}\partial x(s) &= \left[\cdots \right] \sum_n \left(e^{-s2nT_h}\, \partial x_1[n] + e^{-s(2n+1)T_h}\, \partial x_4[n] \right) \\ &= \left[\cdots \right] \sum_m e^{-smT_h}\, \partial x(m) \\ &= \left[\cdots \right] \partial x^*(s) \end{aligned} \qquad (A.1\text{-}13)$$

An expression relating $\partial x(s)$ to $\partial x^*(s)$ would therefore be available. The terms in brackets in (A.1-12) not being equal, another mean must be used to find the spectrum of the continuous variable. Linear superposition is therefore used.

A.2 LINEARITY OF THE SYSTEM DESCRIBED BY (3.5.2-9)

(3.5.2-9) is repeated here for convenience.

$$\partial S(\delta x(m), \delta d(m)) \equiv$$

$$\left| \begin{aligned} \delta x(2n) &= \Phi_{sh}\Phi_{fh} \cdot \delta x(2n-2) + \Phi_{sh} \cdot T_h k_4 \cdot \delta d(2n-1) + T_h k_1 \cdot \delta d(2n) \\ \delta x(2n+1) &= \Phi_{fh}\Phi_{sh} \cdot \delta x(2n-1) + \Phi_{fh} \cdot T_h k_1 \cdot \delta d(2n) + T_h k_4 \cdot \delta d(2n+1) \end{aligned} \right. \qquad (3.5.2\text{-}9)$$

Assuming $\partial x(0)$ to be known, the response of the system is found to be

$$S(\delta x(0)), \delta d(m)) =$$

$$\left| \begin{array}{l} \delta x(2n) = (\Phi_{sh}\Phi_{fh})^{n} \cdot \delta x(0) + Th \sum_{i=1}^{n} (\Phi_{sh}\Phi_{fh})^{n-i}(\Phi_{sh} k_4 \delta d(2i-1) + k_1 \delta d(2i)) \\ \delta x(2n+1) = (\Phi_{fh}\Phi_{sh})^{n}\Phi_{fh}\delta x(0) + Th \sum_{i=0}^{n} (\Phi_{fh}\Phi_{sh})^{n-i}(\Phi_{fh} k_1 \delta d(2i) + k_4 \delta d(2i+1)) \end{array} \right. \qquad (A.2\text{-}1)$$

where $\delta d(0)$ is defined to be zero for notational convenience.

From (A.2-1) it can be shown that,

$$S(\alpha\delta x(0), \alpha\delta d(m)) = \alpha \cdot S(\delta x(0)), \delta d(m)), \qquad (A.2\text{-}2)$$

where α is an arbitrary multiplying constant. Homogeneity is therefore satisfied. Next it must be shown that superposition holds, that is:

$$S(0, \delta d_a(m) + \delta d_b(m)) = S(0, \delta d_a(m)) + S(0, \delta d_b(m)) \; . \qquad (A.2\text{-}3)$$

Again this property falls directly from (A.2-1). The system is therefore linear. The property of superposition is illustrated for the case of interest, this is for

$$\delta d_a(m) = \left| \begin{array}{ll} 0 & \text{for m odd} \\ \delta d(m) & \text{for m even} \end{array} \right. \qquad (A.2\text{-}4)$$

and

$$\delta d_b(m) = \left| \begin{array}{ll} \delta d(m) & \text{for m odd} \\ 0 & \text{for m even} \end{array} \right. \; . \qquad (A.2\text{-}5)$$

The substitution of (A.2-4) and (A.2-5) into (A.2-1) leads to the following zero state response,

$$S(0,\delta d_a(m)) = \begin{cases} \delta x(2n) = T_h \sum_{i=1}^{n} (\Phi_{sh}\Phi_{fh})^{n-i} \cdot k_1 \delta d(2i) \\ \delta x(2n+1) = T_h \sum_{i=0}^{n} (\Phi_{fh}\Phi_{sh})^{n-i} \cdot \Phi_{fh} k_1 \delta d(2i) \end{cases} \tag{A.2-6}$$

and

$$S(0,\delta d_b(m)) = \begin{cases} \delta x(2n) = T_h \sum_{i=1}^{n} (\Phi_{sh}\Phi_{fh})^{n-i} \cdot \Phi_{sh} k_4 \delta d(2i-1) \\ \delta x(2n+1) = T_h \sum_{i=0}^{n} (\Phi_{fh}\Phi_{sh})^{n-i} \cdot k_4 \delta d(2i+1) \end{cases} \tag{A.2-7}$$

where $\delta d(0)$ is still identically zero for notational purposes. Adding (A.2-6) to (A.2-7) results into

$$S(0,\delta d_a(m)) + S(0,\delta d_b(m)) =$$

$$\begin{cases} \delta x(2n) = T_h \sum_{i=1}^{n} (\Phi_{sh}\Phi_{fh})^{n-i} (\Phi_{sh} k_4 \delta d(2i-1) + k_1 \delta d(2i)) \\ \delta x(2n+1) = T_h \sum_{i=0}^{n} (\Phi_{fh}\Phi_{sh})^{n-i} (\Phi_{fh} k_1 \delta d(2i) + k_4 \delta d(2i+1)) \end{cases}$$

$$= S(0,\delta d_a(m) + \delta d_b(m)) \tag{A.2-8}$$

which is the zero-state response of the system as described by (A.2-1). Linear superposition is therefore illustrated.

A.3 TIME-SHIFTED PULSE-WIDTH MODULATOR TRANSFER FUNCTION

Consider the ideal sampling wave, $s(t)$, of Figure A-1, where the train of unit impulses is offset from the origin by a time t_{ofs}. The task is to find the Fourier Transform of a function of time, $v_{amp}(t)$, sampled by such a wave. The demonstration follows those steps given in [26] for the case where $t_{ofs}=0$.

The sampling wave being periodic, with period T_s, its Fourier series representation is first derived. The Fourier series coefficients are given by:

$$c_n = \frac{1}{T_s}\int_{T_s} s(t)\, e^{-jn\omega_s t}\, dt$$

$$= \frac{1}{T_s}\int_{-T_s/2}^{+T_s/2} \delta(t-t_{ofs})\, e^{-jn\omega_s t}\, dt$$

$$= \frac{1}{T_s} e^{-jn\omega_s t}\Big|_{t=t_{ofs}}$$

$$= \frac{1}{T_s} e^{-jn\omega_s t_{ofs}} \qquad (A.3\text{-}1)$$

The Fourier series representation for the sampling wave is therefore:

$$s(t) = \sum_{n=-\infty}^{\infty} \frac{1}{T_s} e^{-jn\omega_s t_{ofs}} \cdot e^{jn\omega_s t} \qquad (A.3\text{-}2)$$

The two-sided Laplace transform of the sampled signal is

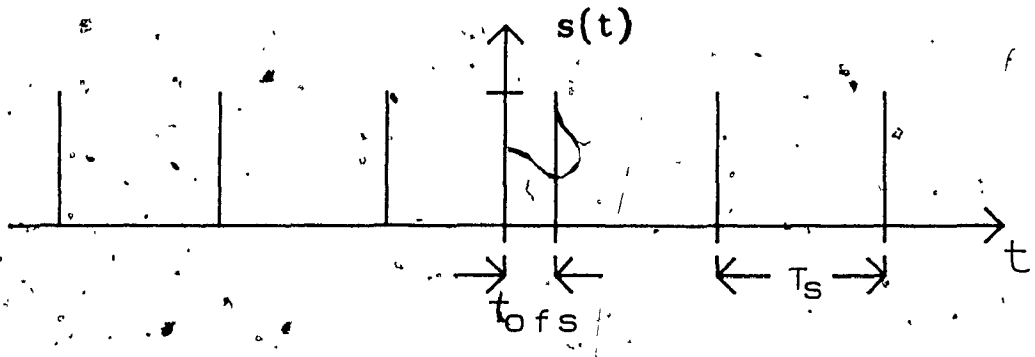

Figure A-1: Sampling Wave Offset from the Origin

$$v^*_{amp}(s) = \int_{-\infty}^{+\infty} v^*_{amp}(t)\ e^{-st}\ dt$$

$$= \int_{-\infty}^{+\infty} v_{amp}(t)\cdot s(t)\ e^{-st}\ dt \quad . \qquad (A.3\text{-}3)$$

At this point, rather than finding the Laplace transform and then later substitute $s=j\omega$, $s=j\omega$ is substituted before the transformation. This yields

$$v^*_{amp}(j\omega) = \int_{-\infty}^{+\infty} v_{amp}(t)\cdot s(t)\ e^{-j\omega t}\ dt \quad . \qquad (A.3\text{-}4)$$

The term on the right hand side is recognized to be the Fourier transform. Since multiplication in the time domain corresponds to convolution in the frequency domain [24],

$$v^*_{amp}(j\omega) = \mathcal{F}(v_{amp}(t)) * \mathcal{F}(s(t)) \qquad (A.3\text{-}5)$$

Where "*" is the convolution operator. Recalling that

$$\mathcal{F}(e^{jn\omega_s t}) = \delta(j\omega - jn\omega_s) \qquad (A.3\text{-}6)$$

[26], the Fourier transform of the sampling wave is

$$\mathcal{F}(s(t)) = s(j\omega) = \frac{1}{T_s} \sum_{n=-\infty}^{\infty} e^{-jn\omega_s t_{ofs}} \cdot \delta(j\omega - jn\omega_s) \quad . \qquad (A.3\text{-}7)$$

Convoluting this impulse train with $v(j\omega)$ yields the sample spectrum.

$$v^*_{amp}(j\omega) = \frac{1}{T_s} \sum_{n=-\infty}^{\infty} e^{-jn\omega_s t_{ofs}} \cdot v_{amp}(j\omega - jn\omega_s) \qquad (A.3\text{-}8)$$

The pulse-width modulator transfer function of is found from (3.5.1-2)

to be

$$PWM(s) \triangleq \frac{\delta d(s)}{\delta v_{amp}(s)} = \frac{K_{pwm} e^{-st_{dpwm}} \cdot \delta v_{amp}^{*}(s)}{\delta v_{amp}(s)} \qquad (A.3\text{-}9)$$

Substituting (A.3-8) yields,

$$PWM(s=j\omega) = K_{pwm}\, e^{-st_{dpwm}} \cdot \frac{\frac{1}{T_s} \sum_{n=-\infty}^{\infty} e^{-jn\omega_s t_{ofs}} \cdot \delta v_{amp}(j\omega - jn\omega_s)}{\delta v_{amp}(j\omega)} \qquad (A.3\text{-}10)$$

This function is difficult to work with. In continuous systems, the transfer function is identical to the impulse response. Letting $\delta v_{amp}(t)$ be an impulse results in a non-converging sum in (A.3-10). This is because the Fourier transform is a constant in the frequency domain. To circumvent the problem, it is noted that in practice, transfer functions are measured by injecting a sinusoidal signal at the input of the modulator and by measuring the disturbance at the output of the converter by using a narrowband meter tuned at the frequency of the injected signal. Letting $\delta v_{amp}(t)$ be a phasor of unity amplitude and of frequency ω_v,

$$\delta v_{amp}(t) = e^{j\omega_v t} . \qquad (A.3\text{-}11)$$

The spectrum of δv_{amp} is

$$\delta v_{amp}(j\omega) = \mathcal{F}(\delta v_{amp}(t)) = \delta(j\omega - j\omega_v) . \qquad (A.3\text{-}12)$$

The spectrum of δv_{amp}^{*} is found to be,

$$\delta v^{*}_{amp}(j\omega) = \frac{1}{T_s} \sum_{n=-\infty}^{\infty} e^{-jn\omega_s t_{ofs}} \cdot \delta v_{amp}(j\omega - jn\omega_s)$$

$$= \frac{1}{T_s} \sum_{n=-\infty}^{\infty} e^{-jn\omega_s t_{ofs}} \cdot \delta(j\omega - jn\omega_s - j\omega_v) \qquad \text{(A.3-13)}$$

(A.3-13) can be rewritten as follows,

$$\delta v^{*}_{amp}(j\omega) = \begin{cases} \frac{1}{T_s} e^{-jn\omega_s t_{ofs}} & \text{for } \omega - n\omega_s = \omega_v \quad n = \ldots -1, 0, 1 \ldots \\ 0 & \text{otherwise} \end{cases} \qquad \text{(A.3-14)}$$

evaluating this at the exciting frequency w_v, or measuring at the exciting frequency as the narrowband voltmeter would, the condition expressed by (A.3-14) is satisfied for n=0 and

$$\delta v^{*}_{amp}(j\omega_v) = \frac{1}{T_s} \qquad \text{(A.3-15)}$$

Since $\delta v_{amp}(j\omega_v)=1$, substituting in (A.3-10) of (A.3-15) gives

$$PWM(s=j\omega_v) = K_{pwm}\, e^{-st_{dpwm}} \cdot \frac{1}{T_s} \Big|_{s=j\omega_v} \qquad \text{(A.3-16)}$$

A.4 SAMPLED-DATA SYSTEM WITH A TIME-SHIFTED SAMPLING WAVE

Consider a sampled-data system where the sampling moment is offset by t_{ofs}. The difference equation governing the behavior of a variable can, in such a system, be expressed as

$$v(nT_s+t_{ofs}) = \sum_{k=1}^{p} a_k \cdot v((n-k)T_s+t_{ofs}) + \sum_{\ell=0}^{q} b_\ell \cdot u((n-\ell)T_s+t_{ofs}) \quad . \tag{A.4-1}$$

Multiplying both sides by z^{-n}.

$$z^{-n}v(nT_s+t_{ofs}) = \sum_{k=1}^{p} z^{-n}a_k \cdot v((n-k)T_s+t_{ofs}) + \sum_{\ell=0}^{q} z^{-n}b_\ell \cdot u((n-\ell)T_s+t_{ofs}) \tag{A.4-2}$$

letting $kk=n-k$ and $\ell\ell=n-\ell$,

$$z^{-n}v(nT_s+t_{ofs}) = \sum_{k=1}^{p} z^{-k} \cdot a_k \cdot v(kk \cdot T_s+t_{ofs})\ z^{-kk} + \sum_{\ell=0}^{q} z^{-\ell} \cdot b_\ell \cdot u(\ell\ell \cdot T_s+t_{ofs})\ z^{-\ell\ell} \tag{A.4-3}$$

Recalling the definition of the $\mathcal{Z}$ transform,

$$\mathcal{Z}w(mT_s+t_{ofs}) = \sum_{m=-\infty}^{\infty} w(mT_s+t_{ofs}) \cdot z^{-n} \quad , \tag{A.4-4}$$

and applying this definition to (A.4-3) yields,

$$z^{-n}v(z) = \sum_{k=1}^{p} a_k \cdot z^{-k} \cdot v(z) + \sum_{\ell=0}^{q} b_\ell \cdot z^{-\ell} \cdot u(z) \quad . \tag{A.4-5}$$

The discrete transfer function is therefore found to be

$$v(z) = \frac{\sum_{\ell=0}^{q} b_\ell \cdot z^{(p-\ell)}}{z^p - \sum_{k=1}^{p} a_k \cdot z^{(p-k)}} \cdot u(z) \quad . \tag{*.4-6}$$

This is the same expression as if the sample moment was not shifted with respect to t=0.

Given the $\mathcal{Z}$ transform of a sample data system variable, the Laplace Transform is found as follows. Consider the function $v^*(t)$ in a sampled data system with a sampling time offset. The Laplace transform of such a function is

$$\mathcal{L}(v^*(t)) = \int_{-\infty}^{+\infty} v^*(t)\, e^{-st}\, dt$$

$$= \int_{-\infty}^{+\infty} \left[\sum_{m=-\infty}^{\infty} v(mT_s+t_{ofs})\cdot\delta(t-mT_s-t_{ofs}) \right] e^{-st}\, dt$$

$$= e^{-st_{ofs}} \sum_{m=-\infty}^{\infty} v(mT_s+t_{ofs})\, e^{-msT_s} \qquad (A.4\text{-}7)$$

Recalling the definition of the $\mathcal{Z}$ transform, (A.4-4) it is seen that

$$v^*(s) = \mathcal{L}(v^*(t)) = e^{-st_{ofs}}\, \mathcal{Z}(v^*(t)) \Big|_{z=\, e^{sT_s}}$$

$$= e^{-st_{ofs}}\, v(z) \Big|_{z=\, e^{sT_s}} . \qquad (A.4\text{-}8)$$